Entropy assisted cathode design for solid-state battery

Chae-Ho Yim

A thesis submitted to the University of Ottawa

in partial fulfillment of the requirements for the

degree of Doctor of Philosophy in Chemical Engineering

Supervised by

Dr. Elena Baranova and Dr. Yaser Abu-Lebdeh

Department of Chemical and Biological Engineering

Faculty of Engineering

University of Ottawa

© Chae-Ho Yim, Ottawa, Canada, 2026

Abstract

The increasing demand for higher energy density and improved safety in electrochemical energy storage has driven significant interest in solid-state battery technologies as successors to conventional lithium-ion batteries. While the replacement of flammable liquid electrolytes with solid electrolytes offers clear safety advantages, practical performance gains remain limited by system-level constraints and materials-level instabilities. In particular, cathode active materials continue to represent the primary bottleneck governing achievable energy density, cost, and long-term stability in both liquid- and solid-state battery systems.

This thesis presents a comprehensive investigation of cathode-driven energy density limitations and introduces a new thermodynamic framework for cathode material design based on entropy change during cycling during electrochemical cycling. First, a cell-level energy density model is developed to evaluate realistic performance limits of all-solid-state batteries under practical design constraints. This analysis demonstrates that widely cited claims of doubling energy density are overly optimistic and establishes that maximizing reversible lithium utilization in the cathode is the most impactful pathway toward meaningful energy density improvements.

Building on this insight, the thesis reframes entropy as a dynamic thermodynamic variable rather than a static material descriptor. Entropy is treated within the framework of mixing entropy, with configurational disorder providing the dominant composition-dependent contribution under solid-solution assumptions. Analytical entropy modeling combined with density functional theory calculations reveals that cathode with moderate entropy, particularly layered oxides containing approximately 65–70% nickel, exhibit minimized entropy change during delithiation, enabling deep reversible lithium extraction while preserving structural stability. These results demonstrate that entropy change during cycling, rather than absolute entropy magnitude or compositional complexity, constitutes a rational design constraint for high-energy cathode materials.

Experimental validation is provided through temperature-dependent open-circuit potential measurements, representing the first systematic comparison of mixing entropy among commercial layered oxide cathodes. The experimentally observed entropy trends are consistent with analytical predictions, confirming entropy change during cycling as a meaningful indicator of cathode stability.

Collectively, this work establishes an entropy-based design paradigm that bridges thermodynamics, electrochemical performance, and system-level battery design, offering clear guidance for the development of stable, high-energy cathode materials and advancing the practical realization of safe, high-performance solid-state batteries.

Résumé

La demande croissante de batteries à l'état solide, capables de remplacer les batteries lithium-ion conventionnelles, a suscité un vif intérêt pour les technologies de batteries à l'état solide. Si le remplacement des électrolytes liquides inflammables par des électrolytes solides offre des avantages indéniables en matière de sécurité, les gains de performance restent limités par des contraintes système et l'instabilité des matériaux. En particulier, les matériaux actifs de la cathode constituent le principal facteur limitant la densité énergétique, le coût et la stabilité à long terme des batteries, qu'elles soient à l'état liquide ou solide.

Cette thèse présente une étude approfondie des limitations de densité énergétique liées à la cathode et introduit un nouveau cadre thermodynamique pour la conception des matériaux de cathode, basé sur la variation d'entropie lors des cycles électrochimiques. Un modèle de densité énergétique à l'échelle de la cellule est d'abord développé afin d'évaluer les limites de performance réalistes des batteries tout-solide, compte tenu des contraintes de conception. Cette analyse démontre que les affirmations, souvent citées, d'un doublement de la densité énergétique sont excessivement optimistes et établit que maximiser l'utilisation réversible du lithium dans la cathode est la voie la plus efficace pour obtenir des améliorations significatives de la densité énergétique.

S'appuyant sur cette observation, la thèse repense l'entropie comme une variable thermodynamique dynamique plutôt que comme un descripteur statique du matériau. L'entropie est traitée dans le cadre de l'entropie de mélange, le désordre configurationnel constituant la contribution dominante, dépendante de la composition, dans l'hypothèse d'une solution solide. La modélisation analytique de l'entropie, combinée à des calculs de la théorie de la fonctionnelle de la densité, révèle que les cathodes à entropie modérée, en particulier les oxydes stratifiés contenant environ 65 à 70 % de nickel, présentent une variation d'entropie minimale lors de la délithiation, permettant une extraction réversible importante du lithium tout en préservant la stabilité structurale. Ces résultats démontrent que la variation d'entropie au cours des cycles, plutôt que l'amplitude absolue de

l'entropie ou la complexité de la composition, constitue une contrainte de conception rationnelle pour les matériaux de cathode à haute énergie. La validation expérimentale repose sur des mesures de potentiel en circuit ouvert en fonction de la température, constituant la première comparaison systématique de l'entropie de mélange entre des cathodes commerciales à base d'oxydes stratifiés. Les tendances d'entropie observées expérimentalement concordent avec les prédictions analytiques, confirmant que la variation d'entropie lors des cycles est un indicateur pertinent de la stabilité de la cathode.

Ce travail établit ainsi un paradigme de conception basé sur l'entropie, reliant thermodynamique, performances électrochimiques et conception de batteries à l'échelle du système. Il offre des orientations claires pour le développement de matériaux de cathode stables et à haute énergie, et favorise la réalisation pratique de batteries à l'état solide sûres et performantes.

Statement of contributions

This thesis presents original research conducted by the author, Chae-Ho Yim, under the supervision of Dr. Elena Baranova and Dr. Yaser Abu-Lebdeh. Except where explicitly stated, the work presented herein represents the independent intellectual and experimental contributions of the author. Chapters that include published or collaborative work are detailed below to clearly delineate individual contributions.

Chapter 3 is based on the published article: *Yim, C.-H., et al., "Understanding key limiting factors for the development of all-solid-state batteries," Chemical Engineering Journal Advances*, 2023, 13, 100436. The author developed the cell-level energy density model, performed all calculations and parametric analyses, interpreted the results, and prepared the original manuscript. Co-authors contributed through technical discussion, supervision, and manuscript review but did not directly perform modeling or analysis.

Chapter 4 presents original work conducted solely by the author. The author developed the entropy-based thermodynamic framework for cathode active material design, formulated and implemented analytical mixing entropy models, performed density functional theory calculations, analyzed and interpreted all results, and prepared all figures and text. This chapter represents an original conceptual contribution to the thesis.

Chapter 5 reports experimental work conducted collaboratively. The author designed the experimental methodology for entropy measurements, performed electrochemical testing and temperature-dependent open-circuit potential measurements, analyzed and interpreted the data, and prepared the manuscript. Co-authors contributed to experimental setup support, technical discussion, and manuscript review.

Throughout the thesis, the supervisors provided guidance on research direction, interpretation, and presentation but did not directly perform calculations or experiments unless explicitly stated. The author is responsible for the overall conceptualization, execution, and integration of the research presented in this thesis.

Acknowledgements

I would like to express my sincere gratitude to my supervisors, Dr. Elena Baranova and Dr. Yaser Abu-Lebdeh, for their guidance, mentorship, and continuous support throughout my doctoral studies. Their scientific insight, constructive criticism, and encouragement were instrumental in shaping this research and in my development as an independent researcher. I am deeply appreciative of the intellectual freedom, patience, and trust they provided, which allowed this work to evolve into a meaningful and original contribution.

I would also like to acknowledge my colleagues and collaborators at the National Research Council of Canada (NRC) for their support, technical assistance, and valuable discussions. The collaborative research environment at NRC provided access to expertise, facilities, and a stimulating scientific community that greatly enriched this work. I am grateful to all colleagues who contributed directly or indirectly through experimental support, technical advice, and constructive exchanges.

Finally, I would like to express my deepest gratitude to my family. Above all, I thank my lovely wife, Claire Kong, for her unwavering love, patience, and understanding throughout this journey. Her constant encouragement and support made it possible for me to persevere through the challenges of doctoral research. I am also profoundly grateful to my son, Francis Yim, whose presence brought joy, motivation, and perspective to my life. This thesis is dedicated to my family, whose love and support have been my greatest source of strength.

Table of Contents

Abstract ii

Résumé iii

Statement of contributions v

Acknowledgements vi

Table of Figures xi

List of Abbreviation xiv

Chapter 1: Introduction 1

1.1 Background and Motivation 1

1.2 Solid-State Batteries: Promise and Practical Limitations 1

1.3 Cathodes as the Central Bottleneck in Lithium Based Batteries 2

1.4 Entropy Beyond High-Entropy Materials: An Original Design Paradigm for Active Battery Materials 3

1.5 Research Gap and Central Hypothesis 4

1.6 Research Objectives and Scope 5

1.6.1 Scope of the Thesis 7

1.7 Structure of the Thesis 7

1.8 References 8

Chapter 2: Literature Review 10

2.1 Scope, Methodology, and Critical Framework of the Literature Review 10

2.1.1 Battery Testing 16

2.2 Solid-State Batteries: System-Level Constraints and Cathode-Driven Limitations 11

2.2.1 Basic components (cathode, anode, electrolytes). 11

2.2.2 Solid-state battery (SSB) and solid-state electrolyte (SE) 18

2.2.3 Recommendation and Implication for Cathode Design: 21

2.3 Cathode Active Materials for Solid-State Batteries 21
2.3.1 Layered Oxide Cathodes (LCO, NMC, NCA): Performance and Degradation Mechanisms 22
2.3.2 Olivine-Type Cathodes: Two-Phase Stability and Energy Density Limitations 23
2.3.3 Spinel Type Cathodes: High Voltage Operation and Electrolyte Compatibility 24
2.3.4 Cathode–Electrolyte Interactions as a Central Design Constraint 24
2.3.5 Solid–Solid Interphases and Cathode Driven Energy Density Limitations 25
2.4 Entropy in Battery Cathode Materials: Static Descriptors versus Dynamic Entropy change during cycling 26
2.4.1 Thermodynamic Characteristics of High-Nickel Cathodes: Phase Transitions and Free-Energy Changes 26
2.4.2 Thermodynamic Characteristics of Mid-Nickel Cathodes: Solid-Solution Behavior and Smooth Free-Energy Landscapes 28
2.4.3 Limitations of Entropy-Based Design Approaches for Battery Cathodes 29
2.5 Experimental and Thermodynamic Approaches to Probing Entropy in Battery Cathodes 31
2.6 Summary of Literature Review and Identified Research Gaps 33
2.7 References 35
Chapter 3: Understanding key limiting factors for the development of all-solid-state batteries 39
3.1 Abstract 39
3.2 Introduction 40
3.3 Results and Discussion 45
3.4 Conclusion 51
3.5 References 52
Chapter 4: Leveraging Entropy for Enhanced Energy Density in Cathode-Active Materials for Li-ion Batteries 55

4.1 Abstract: 55
4.2 Introduction 56
4.3 Methods 62
4.3.1 Mixing entropy 62
4.3.2 Computational method 64
4.4 Results 65
4.5 Discussion 74
4.6 Conclusion 78
4.7 References 78
Chapter 5: Measuring mixed entropy to assess the effect of the configurational entropy on layered oxide cathode active materials in Li-ion batteries 80
5.1 Abstract 80
5.2 Introduction 81
5.3 Experimental 84
5.4 Results 85
5.4.1 Electrochemical Performance 85
5.4.2 Entropy measurements 86
5.5 Discussion 88
5.6 Conclusion 90
5.7 References 91
Chapter 6: Conclusion and Future work 93
6.1 Overall Conclusions 93
6.2 Implications for Cathode and Solid-state Battery Design 94
6.3 Future Work 95
6.4 Concluding Remarks 96

Chapter 7: Appendix 97
7.1 Appendix form chapter 4 97
7.1.1 Jupyter notebook coding for analysis 97
7.1.2 Jupyter code to create VASP input files 121
7.1.3 Jupyter code to dope 122
7.1.4 Examples of VASP input files 122
7.2 Appendix for chapter 5 127
7.2.1 SEM images of the commercial electrodes 127
7.2.2 XRD results of the commercial electrodes 129

Table of Figures

Figure 2-1 Schematic illustration of a lithium-ion battery, showing lithium-ion and electron transport during charge and discharge[52] 12
Figure 2-2 Image and schematic of the 2325 coin-cell 16
Figure 2-3. Comparison of (a) stability window and (b) ionic conductivity of different electrolyte systems[7] 20
Figure 3-1 Schematic of stacked electrodes and separator/solid-state electrolyte 43
Figure 3-2 a) Percent improvement of the stack energy density as N/P changes, b) thickness of anode with N/P c) percent improvement of stack energy density as cathode thickness changes, d) percent improvement of stack energy density as cathode active material volume changes 46
Figure 3-3 Performance improvement on cathode thickness and active material volume on three SE thicknesses a) 20 μm, b) 50 μm, and c) 100 μm, N/P ratio = 1. 49
Figure 3-4 Performance improvement on cathode thickness and N/P ratio on three SE thicknesses a) 20 μm, b) 50 μm, and c) 100 μm, cathode thickness = 70 μm 50
Figure 4-1 Optimized crystal structures of (a) fully lithiated $LiNiO_2$ and (b) 50% delithiated $Li_{0.5}NiO_2$ obtained from density functional theory (DFT) calculations. Lithium, oxygen, and nickel atoms are shown in green, red, and gray, respectively. These structures serve as reference frameworks for evaluating the effect of lithium removal and transition-metal substitution on configurational entropy and energetic stability in layered oxide cathodes. 65
Figure 4-2 mixing entropy of commercial layered oxide cathodes evaluated at the fully lithiated (0% SOC) and fully charged (100% SOC) states, together with their corresponding practical discharge capacities. While low-nickel cathodes exhibit higher absolute mixing entropy, high-nickel cathodes achieve greater lithium utilization with smaller entropy changes, highlighting the decoupling between entropy magnitude and reversible capacity. 67
Figure 4-3 Evolution of mixing entropy as a function of lithium content (x) for commercial cathode materials Li_xTMsO_2. Blue arrows indicate the lithium composition at which maximum configurational entropy occurs, while red arrows denote the experimentally accessible end-of-charge state. The shift of entropy maxima toward higher lithium content with increasing

nickel concentration demonstrates how compositional tuning governs entropy change during cycling during delithiation. 69
Figure 4-4 Calculated mixing entropy profiles for layered oxide cathodes with varying nickel content, illustrating the shift in entropy maxima as a function of lithium composition. As nickel concentration increases, the maximum entropy shifts toward higher lithium fractions, indicating a reduced entropy change during cycling during deep delithiation for nickel-rich compositions... 70
Figure 4-5 Comparison of mixing entropy change during cycling across cathodes with different nickel contents plotted on a common scale. Although cathodes with approximately 33% nickel exhibit the highest absolute entropy, the total entropy change during cycling during lithiation and delithiation decreases systematically with increasing nickel content, emphasizing the importance of entropy change rather than entropy magnitude. 71
Figure 4-6 (a) Maximum mixing entropy change from the fully lithiated state to the end-of-charge state as a function of nickel content under different delithiation limits. (b) Entropy changes as a function of lithiation depth for fixed nickel compositions. Cathodes containing approximately 70% nickel exhibit minimized entropy change during cycling while enabling deep delithiation, identifying a thermodynamically favorable compositional window for high reversible energy density. 73
Figure 4-7 DFT-calculated energetic changes associated with lithiation and delithiation of layered oxide cathodes with varying nickel content. Shown are the total energy and formation energy differences between fully lithiated and 50% delithiated states. The composition near 67–70% nickel exhibits the smallest energetic penalty upon lithium removal, corroborating entropy-based predictions of enhanced thermodynamic stability and reversible lithium utilization. 74
Figure 5-1 (a) Galvanostatic charge–discharge voltage profiles and (b) corresponding differential capacity (dQ/dV) curves of commercial layered oxide cathodes (LCO, NMC111, NMC532, and NMC811) measured in Li half-cells. Increasing nickel content leads to higher specific capacity, while the emergence of multiple dQ/dV peaks in NMC811 indicates phase transitions associated with deep delithiation. Lower nickel cathodes exhibit smoother voltage profiles consistent with solid-solution behavior and enhanced structural reversibility. 86
Figure 5-2 Open-circuit potential (OCP) measurements as a function of temperature and state of charge for (a) LCO, (b) NMC811, (c) NMC532, and (d) NMC111 measured in half-cells against lithium metal. The temperature-dependent shift in equilibrium potential (dE/dT) provides direct

experimental access to entropy changes associated with lithium insertion and extraction. Nickel-rich cathodes exhibit smaller temperature-induced potential variations, indicating reduced entropy change during cycling during cycling. 87
Figure 5-3 Thermodynamic quantities derived from temperature-dependent OCP measurements for commercial layered oxide cathodes: (a) entropy change (ΔS), (b) Gibbs free energy change (ΔG), and (c) enthalpy change (ΔH) as a function of cell potential. LCO exhibits substantially larger entropy values compared to NMC-type cathodes, reflecting significant electronic and vibrational contributions, while NMC811 shows minimal entropy change during cycling across the operating voltage range. The relatively constant ΔH and smooth ΔG evolution for NMC cathodes indicate that entropy change, rather than enthalpy, governs thermodynamic stability during delithiation. 88
Figure 7-1LiCoO2 electrodes 127
Figure 7-2 NMC111 127
Figure 7-3 NMC532 128
Figure 7-4 NMC811 128
Figure 7-5 XRD of the commercial electrodes 129

List of Abbreviation

ASSB	All-Solid-State Battery
CAM	Cathode Active Material
CE	Coulombic Efficiency
CPE	Composite Polymer Electrolyte
DRX	Disordered Rock salt
EC	Ethylene Carbonate
EMC	Ethyl-methyl Carbonate
EV	Electric Vehicle
ΔG	Gibbs free energy
ΔH	Enthalpy
ISE	Inorganic Solid Electrolyte
LCO	$LiCoO_2$,
LE	Liquid Electrolyte
LFP	$LiFePO_4$
LIB	Lithium-ion Battery
LLO	Lithium-rich Layered Oxide
LLTO	$Li_{3x}La_{2/3-x}TiO_3$
LLZO	$Li_7La_3Zr_2O_{12}$
LMNO	$LiMn_{1.5}Ni_{0.5}O_4$
LMO	$LiMn_2O_4$
LNO	$LiNiO_2$
NCA	$LiNi_xCo_yAl_zO_2$, x+y+z=1

NMC	Nickel-Manganese-Cobalt (NMC) cathodes
NMC111	$LiNi_{0.33}Mn_{0.33}Co_{0.33}O_2$
NMC532	$LiNi_{0.5}Mn_{0.3}Co_{0.2}O_2$
NMC622	$LiNi_{0.6}Mn_{0.2}Co_{0.2}O_2$
NMC811	$LiNi_{0.8}Mn_{0.1}Co_{0.1}O_2$
N/P	Anode electrode capacity/Cathode electrode capacity ratio
OCP	Open-Circuit Potential
OEM	Original Equipment Manufacturers
PEO	Poly Eethylene Oxide
SE	Solid Electrolyte
SOC	State of Charge
SPE	Solid Polymer Electrolyte
SSB	Solid-State Battery
ΔS	Entropy
TM	Transition-Metal

Chapter 1: Introduction

1.1 Background and Motivation

Electrochemical energy storage technologies underpin modern society, enabling portable electronics, large-scale renewable energy integration, and the ongoing electrification of transportation.[1-6] Among available battery chemistries, lithium-ion batteries (LIBs) have emerged as the dominant technology due to their high gravimetric and volumetric energy densities, long cycle life, and steadily decreasing cost. Since their commercialization in the early 1990s, LIBs have undergone continuous improvement, resulting in approximately a twofold increase in energy density and nearly a 90% reduction in cost over the past three decades.[7, 8]

Despite these advances, the rapid electrification of the transportation sector has exposed fundamental limitations of current LIB technology. Transportation accounts for approximately 17% of global greenhouse gas emissions, motivating governments worldwide to accelerate the adoption of electric vehicles (EVs). However, widespread EV deployment remains constrained by two persistent challenges**:** range anxiety, driven by insufficient energy density at the battery pack level, and safety concerns, particularly those associated with thermal runaway in high-energy cells. Projections indicate that global demand for lithium-ion batteries will increase by nearly fourfold by 2030, intensifying pressure on battery performance, cost, and material sustainability.[1, 2, 9]

As LIB energy density increases, safety becomes an increasingly critical concern. Conventional LIBs rely on flammable organic liquid electrolytes, which can ignite at temperatures as low as ~60 °C. Under abusive conditions, oxygen release from layered oxide cathodes can further exacerbate thermal runaway, leading to catastrophic cell failure. These safety risks pose significant challenges for large format batteries used in electric vehicles and grid-scale storage.[1, 2, 9]

1.2 Solid-State Batteries: Promise and Practical Limitations

Solid-state batteries (SSBs) have emerged as a promising next-generation energy storage technology capable of addressing both energy density and safety limitations of conventional LIBs. By replacing the flammable liquid electrolyte with a solid electrolyte, SSBs offer substantially improved thermal stability and the potential to enable lithium-metal anodes or anode-free configurations. In principle, these advances could yield up to a 100% increase in cell-level energy density compared to state-of-the-art LIBs.[10-15]

However, despite intense academic and industrial interest, practical implementation of all-solid-state batteries (ASSBs) remains elusive.[11, 16-19] The replacement of liquid electrolytes with solid materials introduces a complex network of solid–solid interfaces that fundamentally alter ion transport, electrochemical kinetics, and mechanical behavior within the cell. Recent analyses have identified more than a dozen distinct interfaces in ASSBs, with the majority located within the cathode composite.[17] These interfaces give rise to high interfacial resistance, mechanical degradation, chemical instability, and constrained electrode architecture.

Critically, many claims regarding the transformative energy density potential of ASSBs fail to account for realistic constraints imposed by solid electrolyte thickness, cathode formulation, inactive material volume, and anode excess. [20, 21] As a result, there exists a growing discrepancy between the theoretical promise of ASSBs and their achievable near-term performance.

1.3 Cathodes as the Central Bottleneck in Lithium Based Batteries

Across both conventional LIBs and ASSBs, the cathode active material (CAM) represents the principal bottleneck to further increases in energy density. Cathodes account for more than 50% of the total cell cost and possess significantly lower specific capacity than anode materials such as graphite, silicon, or lithium metal. [1, 8] Consequently, improving cathode performance is the most direct and impactful strategy for enhancing overall battery energy density.

Commercial LIB cathodes are dominated by layered oxide materials, particularly $LiNi_xMn_yCo_zO_2$ (NMC) and $LiNi_xMn_yAl_zO_2$ (NCA). Increasing nickel content within these materials has proven effective in boosting specific capacity and reducing reliance on cobalt, a critical and geopolitically sensitive element. However, high nickel cathodes suffer from pronounced structural instability, phase transitions, oxygen release, and capacity fade during cycling—issues that are further exacerbated in solid-state battery environments.[8, 22-24]

In ASSBs, the challenges associated with cathodes are amplified by the need to incorporate solid electrolytes within the electrode composite, reducing the fraction of electrochemically active material and limiting achievable energy density. Furthermore, the constrained ionic transport pathways in solid composites demand cathode materials that remain structurally stable and kinetically accessible over extended states of lithiation and delithiation.

1.4 Entropy Beyond High-Entropy Materials: An Original Design Paradigm for Active Battery Materials

Recent advances in materials science have focused on the design and synthesis of high-entropy materials, which incorporate multiple principal elements in near-equimolar ratios to maximize configurational entropy (>1.6R, typically corresponding to five equimolar elements) and stabilize single-phase structures. This strategy has been successfully applied to metallic alloys, ceramics, and electrochemical materials, where entropy primarily serves as a thermodynamic stabilizer of the as-synthesized phase.[25-30]

However, this high-entropy framework is fundamentally rooted in materials that are intended to operate under quasi-equilibrium or structurally static conditions. In such systems, the objective is to prevent phase separation or decomposition by maximizing entropy at a fixed composition. While this philosophy has yielded important insights, it is not inherently suited to electrochemically active materials, such as lithium-ion battery electrodes, that undergo continuous compositional, structural, and electronic changes during operation.

In lithium-ion batteries, cathode active materials are not static solids. During charge and discharge, lithium ions are repeatedly inserted into and extracted from the host lattice, continuously altering site occupancies, local environments, and thermodynamic state variables. Under these dynamic conditions, the absolute value of configurational entropy at a single composition is insufficient to describe material stability or reversibility. Instead, the change in entropy associated with lithiation and delithiation should be more critical, yet largely unexplored, parameter governing electrochemical performance.

This thesis introduces an original entropy-based design concept that is fundamentally distinct from conventional high-entropy material design. Rather than maximizing entropy through equimolar compositional complexity, this work proposes that minimizing entropy change during electrochemical cycling is a key requirement for achieving both high energy density and structural stability in layered oxide cathodes. In this framework, entropy is treated not as a static descriptor of material complexity, but as a dynamic thermodynamic variable that evolves during battery operation. To the author’s knowledge, no prior cathode design framework has explicitly used entropy change during cycling as a quantitative design constraint for layered oxide cathodes.

The central premise of this approach is that large entropy changes during lithium intercalation are indicative of significant rearrangements in local order, phase behavior, or electronic structure, which can drive irreversible transformations, mechanical strain, and capacity fade. Conversely, cathode materials that accommodate lithium insertion and extraction with minimal entropy change are more likely to preserve solid-solution behavior, suppress phase transitions, and maintain electrochemical reversibility—even at high degrees of delithiation.

Importantly, this concept does not advocate for high-entropy cathodes in the traditional sense. Instead, it suggests that moderate-entropy compositions, judiciously engineered to limit entropy fluctuations during use, may offer superior performance compared to both low-entropy (highly ordered) and high-entropy (over-disordered) systems. This perspective provides a new lens through which to interpret the observed trade-off between energy density and stability in high nickel layered oxides and offers a rational pathway for designing next-generation cathode materials.

By explicitly focusing on entropy change during operation, rather than entropy magnitude at synthesis, this thesis establishes a new thermodynamic design principle for active materials—one that is particularly relevant to lithium-ion batteries and other energy storage systems in which materials are required to function far from equilibrium and under repeated compositional cycling.

1.5 Research Gap and Central Hypothesis

Despite extensive research on layered oxide cathodes and the rapid expansion of high-entropy materials literature, a fundamental gap remains in the thermodynamic understanding of materials that undergo repeated compositional changes during use. Existing cathode design strategies predominantly rely on static metrics—such as average composition, crystal structure, or absolute configurational entropy—evaluated at the fully lithiated or as-synthesized state.[30-35] These approaches implicitly assume that material stability and electrochemical performance can be inferred from equilibrium properties alone.

However, lithium-ion battery cathodes operate under conditions far removed from equilibrium. During cycling, lithium insertion and extraction continuously modify thermodynamic landscape of the material. Under these circumstances, performance is governed not only by the initial thermodynamic state, but by how key variables, particularly entropy and Gibbs free energy, evolve

throughout lithiation and delithiation. To date, the role of entropy change during electrochemical cycling has not been systematically quantified or incorporated into cathode material design.

This limitation is particularly evident in high-nickel layered oxide cathodes. Increasing nickel content enhances energy density by enabling deeper delithiation and higher redox activity, yet it simultaneously exacerbates phase transitions, oxygen release, and capacity fade. While these trade-offs are well documented experimentally, they remain inadequately explained by compositional trends or absolute entropy values alone. A quantitative thermodynamic metric capable of rationalizing this balance between energy density and stability is currently lacking.

The central hypothesis of this thesis is that the magnitude of entropy changes during lithiation and delithiation, rather than the absolute value of configurational entropy, is a critical determinant of cathode stability and reversible energy density. It is proposed that cathode materials capable of accommodating lithium insertion and extraction with minimal entropy change during cycling are more likely to maintain solid-solution behavior, suppress irreversible phase transformations, and sustain high reversible capacity, even at high states of charge.

By reframing entropy as a dynamic thermodynamic variable, this work introduces an original framework for cathode material design that moves beyond conventional high-entropy paradigms. This approach enables the identification of optimized, moderate-entropy compositions that balance redox activity and thermodynamic stability, offering a rational pathway to overcome the long-standing tradeoff between energy density and durability in layered oxide cathodes.

1.6 Research Objectives and Scope

Guided by the hypothesis that entropy change during electrochemical cycling governs cathode stability and performance, the overarching objective of this thesis is to establish entropy change during cycling as a quantitative design principle for layered oxide cathode materials in lithium-based batteries. This objective is pursued through a combination of cell level modeling, thermodynamic analysis, computational methods, and experimental validation.

To achieve this goal, the research is structured around the following specific objectives:

Objective 1: Evaluate realistic energy density limits in all-solid-state batteries and identify cathode-level constraints.

A cell-level energy density model is developed to critically assess the often-cited performance advantages of all-solid-state batteries. This analysis identifies key architectural and materials level parameters, including solid electrolyte thickness, cathode active material fraction, catholyte content, and anode excess, that limit achievable energy density. The results establish the practical importance of maximizing reversible lithium utilization in cathode materials and motivate the need for thermodynamically stable cathode designs.

Objective 2: Develop a thermodynamic framework that captures entropy change during cycling in dynamically active cathodes.

Configurational entropy is analytically evaluated for layered oxide cathodes as a function of lithium content and transition-metal composition. Unlike traditional approaches that emphasize static entropy values, this objective explicitly quantifies entropy change across states of charge, enabling direct correlation between entropy change during cycling, structural reversibility, and electrochemical behavior.

Objective 3: Identify cathode compositions that minimize entropy change while maintaining high energy density.

By systematically varying nickel content and compositional complexity within the NMC family, this objective seeks to identify moderate-entropy cathode compositions capable of deep delithiation with minimal entropy change during cycling. Density functional theory (DFT) calculations are employed to assess energetic stability at different lithiation states and to support entropy-based design rules for layered oxide cathodes.

Objective 4: Experimentally validate entropy-based design principles through potentiometric measurements.

Temperature-dependent open-circuit potential measurements are used to experimentally quantify entropy changes in commercial layered oxide cathodes. These measurements provide direct validation of the proposed framework by linking entropy change during cycling, Gibbs free energy, and electrochemical performance across different states of charge.

1.6.1 Scope of the Thesis

This thesis focuses on lithium-based battery systems, with primary emphasis on layered oxide cathode active materials. While anode materials and electrolytes are discussed where necessary to contextualize system level performance, particularly for all-solid-state batteries, the central contribution of this work lies in establishing entropy-based design principles for dynamically active cathode materials.

1.7 Structure of the Thesis

This thesis is organized into six chapters addressing cathode-driven energy density limitations and entropy-based design principles for lithium-based batteries, with particular emphasis on solid-state battery systems.

Chapter 1 introduces the research motivation, objectives, and central hypothesis, highlighting the need for improved energy density and safety and proposing entropy change during cycling as a guiding thermodynamic concept for cathode design.

Chapter 2 provides a critical review of solid-state batteries, cathode materials, and entropy-related design strategies, identifying key gaps that motivate a dynamic thermodynamic framework focused on entropy change during cycling during cycling.

Chapter 3 evaluates system level energy density limitations in all-solid-state batteries using a cell-level modeling approach, demonstrating that cathode utilization represents the dominant bottleneck for practical energy density improvements.

Chapter 4 develops an entropy-based thermodynamic framework for cathode active material design. Mixing entropy is treated as a dynamic variable, and analytical modeling combined with density functional theory calculations is used to show that minimizing entropy change during cycling enables deep reversible lithium extraction, identifying an optimal compositional window near 65–70% nickel.

Chapter 5 experimentally validates the proposed framework through temperature-dependent open-circuit potential measurements, providing the first systematic comparison of mixing entropy among commercial layered oxide cathodes and confirming entropy change during cycling as a meaningful stability indicator.

Chapter 6 summarizes the key findings, discusses implications for cathode and solid-state battery design, and outlines future research directions.

1.8 References

1. Houache, M.S.E., et al., *On the Current and Future Outlook of Battery Chemistries for Electric Vehicles—Mini Review.* Batteries, 2022. **8**(7): p. 70.
2. Chen, Y., et al., *A review of lithium-ion battery safety concerns: The issues, strategies, and testing standards.* Journal of Energy Chemistry, 2021. **59**: p. 83-99.
3. Kim, J.G., et al., *A review of lithium and non-lithium based solid state batteries.* Journal of Power Sources, 2015. **282**: p. 299-322.
4. Nasajpour-Esfahani, N., et al., *Comprehensive review of lithium-ion battery materials and development challenges.* Renewable and Sustainable Energy Reviews, 2024. **203**: p. 114783.
5. Park, S.H., et al., *Toward high-performance anodeless batteries based on controlled lithium metal deposition: a review.* Journal of Materials Chemistry A, 2021. **9**(26): p. 14656-14681.
6. Xi, Z., et al., *Modification strategies of high-energy Li-rich Mn-based cathodes for Li-ion batteries: A Review.* Molecules, 2024. **29**(5): p. 1064.
7. Nazri, G.-A. and G. Pistoia, *Lithium batteries: science and technology*. 2008: Springer Science & Business Media.
8. Choi, J.U., et al., *Recent Progress and Perspective of Advanced High-Energy Co-Less Ni-Rich Cathodes for Li-Ion Batteries: Yesterday, Today, and Tomorrow.* Advanced Energy Materials, 2020. **10**(42): p. 2002027.
9. Park, O.K., et al., *Who will drive electric vehicles, olivine or spinel?* Energy & Environmental Science, 2011. **4**(5): p. 1621-1633.
10. Abouali, S., et al., *Garnet-Based Solid-State Li Batteries: From Materials Design to Battery Architecture.* ACS Energy Letters, 2021. **6**(5): p. 1920-1941.
11. Janek, J. and W.G. Zeier, *Challenges in speeding up solid-state battery development.* Nature Energy, 2023. **8**(3): p. 230-240.
12. Lu, Y., et al., *Dry electrode technology, the rising star in solid-state battery industrialization.* Matter, 2022. **5**(3): p. 876-898.
13. Peres, J.P., F. Weill, and C. Delmas, *Lithium/vacancy ordering in the monoclinic LixNiO2 (0.50 ≤x ≤ 0.75) solid solution.* Solid State Ionics, 1999. **116**(1): p. 19-27.
14. Yim, C.-H., et al., *Understanding key limiting factors for the development of all-solid-state-batteries.* Chemical Engineering Journal Advances, 2023. **13**: p. 100436.
15. Yu, X., et al., *Battery Safety: From Lithium-Ion to Solid-State Batteries.* Engineering, 2023. **21**: p. 9-14.
16. Bachman, J.C., et al., *Inorganic Solid-State Electrolytes for Lithium Batteries: Mechanisms and Properties Governing Ion Conduction.* Chemical Reviews, 2016. **116**(1): p. 140-162.
17. Liang, Y., et al., *Challenges, interface engineering, and processing strategies toward practical sulfide-based all-solid-state lithium batteries.* InfoMat, 2022. **4**(5): p. e12292.
18. Schmaltz, T., et al., *A Roadmap for Solid-State Batteries.* Advanced Energy Materials, 2023. **13**(43): p. 2301886.
19. Yan, S., et al., *Perovskite Solid-State Electrolytes for Lithium Metal Batteries.* Batteries, 2021. **7**(4): p. 75.
20. Zheng, H., et al., *A comprehensive understanding of electrode thickness effects on the electrochemical performances of Li-ion battery cathodes.* Electrochimica Acta, 2012. **71**: p. 258-265.

21. Wu, J., et al., *Reducing the thickness of solid-state electrolyte membranes for high-energy lithium batteries.* Energy and Environmental Science, 2021. **14**(1): p. 12-36.
22. Park, K.-J., G.W. Nam, and Y.-K. Sun. *Capacity Fading Mechanism of Ni-Rich NCA Cathode for Lithium-Ion Batteries*. in *Electrochemical Society Meeting Abstracts 236*. 2019. The Electrochemical Society, Inc.
23. Li, W., E.M. Erickson, and A. Manthiram, *High-nickel layered oxide cathodes for lithium-based automotive batteries.* Nature Energy, 2020. **5**(1): p. 26-34.
24. Zhuang, D. and M.Z. Bazant, *Theory of layered-oxide cathode degradation in Li-ion batteries by oxidation-induced cation disorder.* Journal of The Electrochemical Society, 2022. **169**(10): p. 100536.
25. Ouyang, B. and Y. Zeng, *The rise of high-entropy battery materials.* Nature Communications, 2024. **15**(1): p. 973.
26. Murty, B.S., et al., *2 - High-entropy alloys: basic concepts*, in *High-Entropy Alloys (Second Edition)*, B.S. Murty, et al., Editors. 2019, Elsevier. p. 13-30.
27. Baek, S.W., et al., *Thermodynamic Analysis and Interpretative Guide to Entropic Potential Measurements of Lithium-Ion Battery Electrodes.* The Journal of Physical Chemistry C, 2022. **126**(14): p. 6096-6110.
28. Sarkar, A., et al., *High-Entropy Oxides: Fundamental Aspects and Electrochemical Properties.* Advanced Materials, 2019. **31**(26): p. 1806236.
29. Zeng, Y., et al., *High-entropy mechanism to boost ionic conductivity.* Science, 2022. **378**(6626): p. 1320-1324.
30. Sturman, J., et al., *Communication—Design of LiNi0.2Mn0.2Co0.2Fe0.2Ti0.2O2 as a High-Entropy Cathode for Lithium-Ion Batteries Guided by Machine Learning.* Journal of The Electrochemical Society, 2021. **168**(5): p. 050541.
31. Arunkumar, T.A. and A. Manthiram, *Influence of chromium doping on the electrochemical performance of the 5 v spinel cathode LiMn1.5Ni0.5O4.* Electrochimica Acta, 2005. **50**(28): p. 5568-5572.
32. Li, B., et al., *Anion doping in LiCoO2 cathode materials for Li-ion batteries: a first-principles study.* Journal of Solid State Electrochemistry, 2022. **26**(12): p. 2743-2748.
33. Mao, G., et al., *Improved cycling stability of high nickel cathode material for lithium ion battery through Al- and Ti-based dual modification.* Nanoscale, 2021. **13**(44): p. 18741-18753.
34. Park, S.B., et al., *Electrochemical properties of LiNi0.5Mn1.5O4 cathode after Cr doping.* Journal of Power Sources, 2006. **159**(1 SPEC. ISS.): p. 679-684.
35. Sun, H.H., et al., *Beyond Doping and Coating: Prospective Strategies for Stable High-Capacity Layered Ni-Rich Cathodes.* ACS Energy Letters, 2020. **5**(4): p. 1136-1146.

Chapter 2: Literature Review

2.1 Scope, Methodology, and Critical Framework of the Literature Review

The development of next-generation lithium-based batteries has motivated extensive research into solid-state battery architectures, advanced cathode materials, and emerging materials design strategies.[1-6] This chapter provides a critical synthesis of the literature relevant to these areas, with particular emphasis on identifying conceptual and thermodynamic gaps that motivate the entropy-based design framework developed in this thesis.

While substantial progress has been made in improving ionic conductivity, interfacial stability, and electrochemical performance through materials innovation, much of the existing literature remains grounded in static design principles. Cathode materials are typically evaluated based on equilibrium properties, such as crystal structure, average composition, or absolute thermodynamic descriptors, measured at a single state of charge or in the as-synthesized condition.[7-19] These approaches implicitly assume that material stability and performance can be inferred from static metrics alone.

However, lithium-ion battery cathodes operate under fundamentally dynamic conditions, undergoing repeated lithium insertion and extraction during charge and discharge.[20-23] Under such conditions, the thermodynamic state of the material continuously evolves, and performance is governed not only by equilibrium stability, but by how the material responds to changes in composition and local order during use. This distinction between static and dynamic behavior is particularly critical for layered oxide cathodes, where phase transitions, oxygen release, and structural degradation are closely coupled to the degree of lithiation.

Recent trends in materials science, most notably the rise of high entropy materials, have introduced entropy as a stabilizing design parameter.[24-31] In these systems, configurational entropy is maximized through equimolar multi-element compositions to suppress phase separation and stabilize single-phase structures. While effective for structurally static materials, this strategy does not directly address the requirements of electrochemically active materials, where excessive disorder or large entropy fluctuations during cycling may hinder lithium transport and reversibility. As a result, the applicability of high-entropy design principles to layered oxide cathodes remains an open and unresolved question.

Within the context of lithium-ion batteries, increasing nickel content in layered oxide cathodes has emerged as the dominant strategy for improving energy density and reducing cobalt dependence. Although this approach has yielded significant gains in specific capacity, it has also intensified challenges related to structural instability, phase transitions, and capacity fade, issues that are magnified in solid-state battery configurations. While these trade-offs are well documented, the underlying thermodynamic mechanisms that govern them are not yet fully understood.[32-36]

This literature review is therefore structured to highlight the limitations of existing cathode design paradigms and to identify the need for a dynamic thermodynamic framework capable of capturing material behavior during electrochemical cycling. In particular, it emphasizes the absence of systematic studies that quantify entropy change during cycling during lithiation and delithiation and examines how this gap limits current understanding of cathode stability and energy density.

The chapter is organized into three main thematic sections. First, the fundamental architecture and performance constraints of solid-state batteries are reviewed, with emphasis on cathode-level limitations and interfacial challenges. Second, existing cathode materials, layered oxides, olivine phosphates, and spinel oxides, are critically examined in terms of their electrochemical behavior, stability, and suitability for solid-state systems. Third, entropy-related concepts in battery materials are reviewed, including high-entropy materials and experimental methods for entropy measurement, to establish the context and limitations of current approaches.

By critically analyzing the literature through the lens of dynamic material behavior, this chapter establishes the conceptual foundation for the entropy-change-based design framework developed in subsequent chapters. Rather than treating entropy as a static descriptor of material complexity, this review motivates its reinterpretation as a thermodynamic variable that evolves during battery operation, thereby justifying the central hypothesis and research objectives of this thesis.

2.2 Solid-State Batteries: System-Level Constraints and Cathode-Driven Limitations

2.2.1 Basic components (cathode, anode, electrolytes).

Lithium-ion batteries consist of three essential components: a cathode, an anode, and an electrolyte. [20-23] Together, these components govern lithium transport, electrochemical reactions, and overall cell performance. Figure 2-1 schematically illustrates the operation of a

lithium-ion battery, highlighting the coupled transport of lithium ions through the electrolyte and electrons through the external circuit during charge and discharge.

In conventional lithium-ion batteries, lithium cobalt oxide ($LiCoO_2$, LCO) and graphite are commonly employed as cathode and anode, respectively. The cathode acts as the lithium reservoir, hosting lithium ions within a layered oxide framework, while the anode accommodates lithium through intercalation or alloying reactions. The electrolyte, typically a solution of lithium salt dissolved in organic carbonate solvents, provides ionic conductivity between electrodes while remaining electronically insulating. During charging, lithium ions are extracted from the cathode and inserted into the anode; the process reverses during discharge.

While this architecture has enabled the widespread commercialization of lithium-ion batteries, replacing the liquid electrolyte with a solid electrolyte fundamentally alters transport pathways, interfacial chemistry, and mechanical constraints within the cell.[2, 37-39] These changes impose stricter requirements on all components, particularly the cathode, which must maintain structural integrity and electrochemical accessibility under constrained solid–solid interfaces.

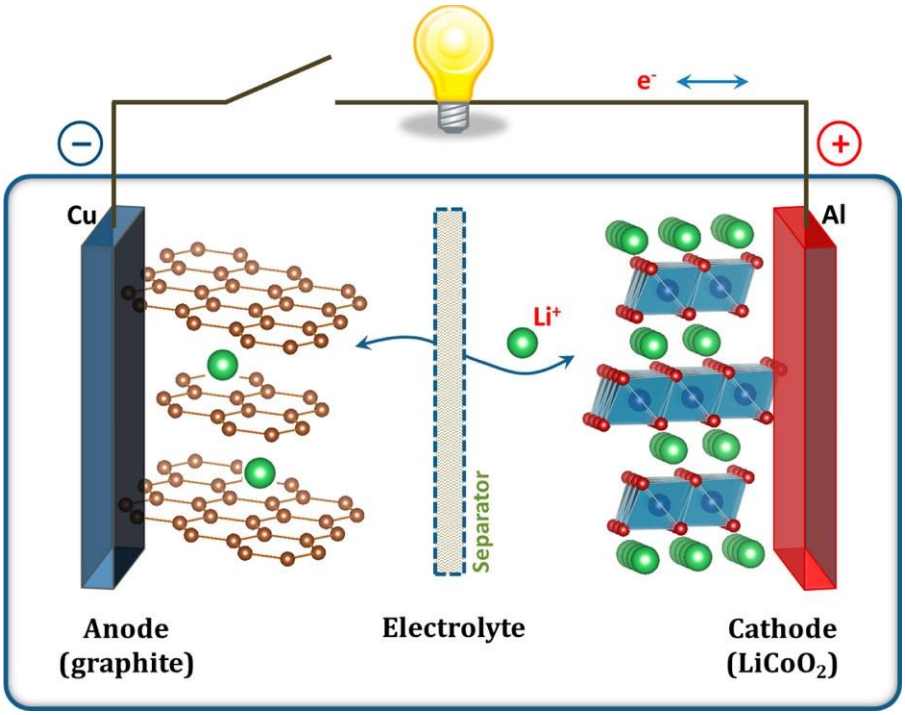


Figure 2-1 Schematic illustration of a lithium-ion battery, showing lithium-ion and electron transport during charge and discharge[40]

2.2.1.1 Cathode

The cathode is the most critical and cost-intensive component of lithium-ion batteries, accounting for more than 50% of the total cell cost and largely determining the achievable energy density and power capability of the cell [9]. Since the introduction of $LiCoO_2$ by Goodenough in 1980 [41], layered oxide cathodes have dominated commercial battery technologies due to their favorable combination of high operating voltage, reasonable specific capacity, and structural reversibility.

However, the reliance on cobalt presents significant economic, environmental, and geopolitical challenges, particularly in the context of large-scale electric vehicle deployment. As a result, substantial research efforts have focused on reducing cobalt content by partially substituting cobalt with more abundant transition metals such as nickel and manganese. This has led to the development of three major classes of cobalt-reduced cathode materials: layered oxides, spinel oxides, and olivine phosphates.

Among these, layered oxide cathodes remain the most widely used and extensively studied. Modern layered oxides are typically based on the general formula $LiNi_xMn_yCo_zO_2$ (NMC, $x + y + z = 1$), with progressive generations increasing nickel content to enhance specific capacity and reduce cobalt usage. Early NMC compositions employed near-equimolar ratios (NMC111), while later generations evolved toward nickel-rich formulations such as NMC532, NMC622, and NMC811. A similar design philosophy underpins $LiNiCoAlO_2$ (NCA), which is widely used in commercial electric vehicles.

Increasing nickel content improves energy density by enabling deeper delithiation and higher redox activity. However, this strategy introduces significant structural challenges. In layered oxides, only approximately 50% of the lithium can be reversibly extracted without inducing irreversible structural changes. Although nickel-rich compositions such as NMC622 and NMC811 allow higher lithium utilization, they suffer from pronounced lattice expansion and contraction during cycling, leading to microcracking, phase transitions, oxygen release, and accelerated capacity fade [35, 42-45]. Consequently, extensive efforts have been devoted to mitigating degradation through doping, surface coatings, and microstructural control, underscoring the intrinsic trade-off between energy density and structural stability in layered oxide cathodes.

Spinel oxides represent an alternative cathode class capable of delivering higher average operating voltages. $LiMn_{1.5}Ni_{0.5}O_2$ (LMNO), a representative spinel cathode, operates near 5.0 V versus Li/Li^+—approximately 0.8 V higher than layered oxides—and can achieve higher lithium utilization due to its three-dimensional lithium diffusion network [46]. Additionally, spinel cathodes eliminate the need for cobalt, reducing material cost. However, their high operating voltage exceeds the stability window of most liquid and solid electrolytes, severely limiting practical implementation and market adoption.

Olivine-type cathodes, most notably $LiFePO_4$ (LFP), offer exceptional thermal and structural stability, low cost, and environmental benignity [47]. Their two-phase reaction mechanism provides outstanding cycle life and safety, making them attractive for large-scale and cost-sensitive applications. Nevertheless, the relatively low operating voltage (~3.4–3.6 V vs. Li/Li^+) constrains achievable energy density, which has historically limited their adoption in long-range electric vehicles despite recent resurgence driven by supply-chain considerations.

Collectively, these cathode classes illustrate a fundamental challenge in battery design: materials that offer high energy density tend to suffer from structural instability under deep delithiation, while highly stable materials sacrifice energy density. This trade-off becomes even more pronounced in solid-state batteries, where constrained ionic transport and rigid interfaces amplify cathode degradation mechanisms.

2.2.1.2 Anode

Anode materials store lithium during charging and release it during discharge, and therefore must combine high specific capacity, excellent reversibility, and a low average operating potential versus Li/Li^+. Graphite remains the dominant commercial anode material due to its well-defined intercalation mechanism, high reversibility, and relatively low operating potential (~0.1 V vs. Li/Li^+), corresponding to a theoretical capacity of 372 mAh g^{-1} [48, 49].

Although lithium metal offers an order-of-magnitude higher theoretical capacity (3860 mAh g^{-1}) and the lowest possible operating potential, its practical use in liquid-electrolyte batteries is hindered by dendrite formation, low Coulombic efficiency, and severe safety risks [50].These limitations have renewed interest in lithium metal anodes for solid-state batteries, where

mechanically robust solid electrolytes may suppress dendrite growth and enable substantially higher energy density [26–30].

Silicon and other alloy-type anodes have also been explored due to their extremely high theoretical capacities. However, the large volume changes associated with lithiation and delithiation result in mechanical degradation and unstable solid–electrolyte interphases, limiting long-term performance despite extensive mitigation strategies [13–25].

While anode optimization is critical for achieving high energy density in solid-state batteries, the cathode ultimately dictates the upper bound of reversible lithium inventory and operating voltage. As a result, cathode stability remains the dominant factor limiting practical energy density gains in solid-state battery systems.

2.2.1.3 Electrolyte

The electrolyte provides ionic conductivity between the cathode and anode while electronically isolating the two electrodes. Conventional liquid electrolytes based on organic carbonate solvents offer high ionic conductivity and good electrode wetting but suffer from low thermal stability and flammability, with flash points as low as ~60 °C [31,32]. These limitations pose significant safety concerns as battery energy density increases.

Solid electrolytes offer a promising alternative by providing improved thermal stability, mechanical robustness, and compatibility with lithium metal anodes [33]. Broadly, solid electrolytes can be classified into inorganic, polymer, and composite (hybrid) systems [34–37]. Inorganic solid electrolytes exhibit high mechanical strength and can be fabricated as thin membranes, but often suffer from brittleness, limited electrochemical stability windows, and high interfacial resistance with electrodes [38–50]. Polymer electrolytes offer improved interfacial contact and processability but typically exhibit low ionic conductivity at room temperature [51–57]. Composite electrolytes attempt to combine the advantages of both systems but introduce additional fabrication and interfacial challenges [58–61].

Importantly, the properties of the solid electrolyte impose stringent constraints on cathode design. Limited electrochemical stability windows, mechanical mismatch, and interfacial reactivity restrict the choice of cathode materials and exacerbate degradation under high-voltage and

deep-delithiation conditions. Consequently, solid-state battery performance is strongly coupled to cathode stability, reinforcing the cathode-driven nature of system-level limitations.

2.2.2 Cell Testing of the Active materials

Most electrochemical testing in this work is conducted using the 2325 coin cell, developed and patented by the National Research Council of Canada (NRC). A schematic and image of the cell are shown in Figure 2-2. This coin cell configuration is designed for evaluating research-scale electrochemical materials, where the anode and cathode are tightly compressed to ensure uniform contact and reproducible electrochemical behavior.

In typical laboratory studies, lithium metal is used as the anode, counter electrode, and/or reference electrode. When lithium metal serves as a counter electrode, the configuration is referred to as a half-cell, as it isolates the electrochemical performance of the working electrode (either cathode or anode). In contrast, full-cell configurations consist of both cathode and anode materials without lithium metal as a counter electrode. Common full-cell systems include lithium metal oxide cathodes paired with graphite anodes.

For solid-state battery systems, lithium metal is often employed as the anode in full-cell configurations. In these cases, the amount of lithium is carefully controlled and minimized to improve practical relevance and energy density, distinguishing these systems from conventional lithium metal half-cells.

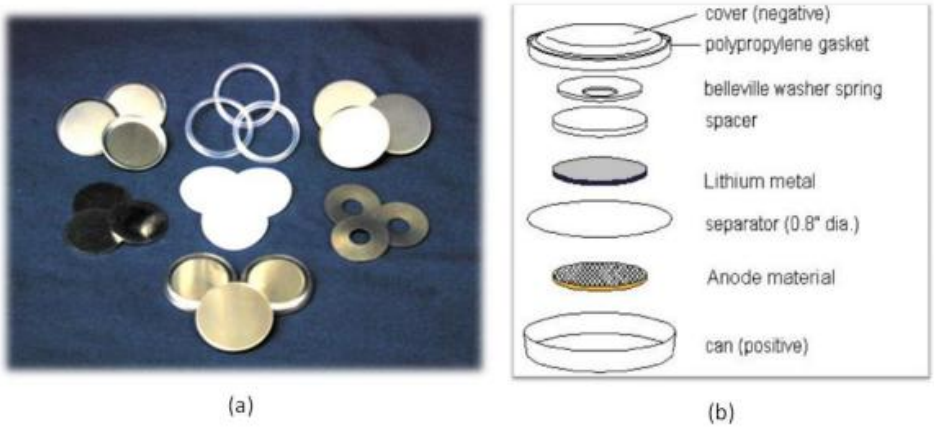


Figure 2-2 Image and schematic of the 2325 coin-cell

The electrochemical performance of battery materials is evaluated using assembled coin cells through galvanostatic testing. In galvanostatic measurements, a constant current is applied while

the resulting potential is recorded as a function of time. This technique is primarily used to determine specific capacity, coulombic efficiency, and cycling stability.

Galvanostatic charge–discharge testing is typically performed within a defined voltage window, depending on the electrode material. For example, voltage ranges of 2.5–4.5 V are commonly used for cathode materials, while 5 mV–1.5 V is used for anode materials. The applied current is defined using the C-rate, which determines the time required for a full charge or discharge process.

The C-rate is defined as:

$$\mathrm{C-rate} = \frac{SpC \times m_{active\ material}}{t}$$

SpC: the practical or theoretical specific capacity of the active material (mAh/g or Ah/g)

$m_{\text{active materialm}}$: the mass of active material in the cell (g)

t: the charge/discharge time (h)

For example, a C/10 rate corresponds to a charge or discharge duration of 10 hours. The use of C-rate normalizes current across cells with different active material loadings, enabling direct comparison of electrochemical performance.

In addition to standard galvanostatic cycling, polarization behavior is analyzed using charge–discharge voltage profiles plotted as voltage versus capacity. These profiles, often referred to as polarization curves, provide insight into the electrochemical behavior and internal losses within the cell during operation.

Polarization is evaluated by comparing the charge and discharge curves at a given current density. The voltage difference between the charge and discharge profiles at the same capacity represents the degree of polarization in the system. A larger voltage gap indicates increased internal resistance and kinetic limitations, which may arise from factors such as ionic transport resistance, charge transfer resistance at electrode–electrolyte interfaces, and electrode polarization effects.

The shape and slope of the voltage–capacity curves also provide important information. Flat voltage plateaus typically correspond to phase transitions or well-defined redox reactions, whereas

sloped profiles may indicate solid-solution behavior or increased polarization. Changes in these profiles over cycling can reveal performance degradation, such as increased impedance, loss of active material, or interfacial instability.

Furthermore, differential capacity analysis (dQ/dV) is employed to characterize redox processes and phase transitions in the electrode materials. The dQ/dV curves are obtained by differentiating the charge–discharge capacity with respect to voltage. Peaks in dQ/dV profiles correspond to electrochemical reactions occurring at specific potentials and provide detailed information on reaction mechanisms, reversibility, and structural stability.

Changes in peak position, intensity, or shape over cycling can reveal degradation mechanisms such as loss of active material, increased polarization, or structural transformations. In particular, peak broadening or shifting is often associated with increased internal resistance or kinetic limitations, while peak disappearance may indicate irreversible reactions.

The combined use of galvanostatic cycling, polarization analysis, and dQ/dV characterization provides a comprehensive evaluation of electrochemical performance, including capacity retention, rate capability, reaction kinetics, and long-term stability.

Detailed experimental conditions, including electrode composition, cell assembly procedures, and testing parameters, are provided in the corresponding manuscript and final report.

2.2.3 Solid-state battery (SSB) and solid-state electrolyte (SE)

Solid-state batteries (SSBs) replace the flammable liquid electrolyte and polymer separator used in conventional lithium-ion batteries with a solid electrolyte (SE) that simultaneously conducts lithium ions and blocks electronic transport.[2, 37-39] This fundamental architectural change offers two primary advantages: enhanced safety due to the intrinsic thermal stability of solid electrolytes and the potential to significantly increase energy density through the use of lithium metal anodes. In contrast to liquid electrolytes, which typically exhibit flash points near 60 °C and contribute to thermal runaway under abusive conditions, most solid electrolytes are thermally stable at temperatures exceeding 1000 °C, thereby reducing the risk of fire and explosion in high-energy battery systems.

Beyond safety, the mechanical rigidity of solid electrolytes enables the use of lithium metal anodes, which are impractical in liquid-electrolyte cells due to dendrite growth and

short-circuiting. In principle, this configuration can yield substantial gains in gravimetric and volumetric energy density. As a result, replacing liquid electrolytes with solid electrolytes is widely regarded as a necessary step toward next-generation battery technologies for electric vehicle applications.

Despite these advantages, solid electrolytes introduce a distinct set of system-level challenges that fundamentally constrain SSB performance. Compared to liquid electrolytes, most solid electrolytes exhibit lower ionic conductivity at room temperature, narrower electrochemical stability windows, and limited chemical compatibility with lithium metal and high-voltage cathodes.[1] These constraints are not isolated material issues; rather, they directly influence electrode architecture, interfacial resistance, and achievable depth of delithiation in cathode materials.

Solid electrolytes can be broadly classified into three categories: inorganic solid electrolytes (ISEs), solid polymer electrolytes (SPEs), and composite or hybrid solid electrolytes (CSEs).[51] Inorganic solid electrolytes—such as garnet-, perovskite-, and sulfide-based materials—generally offer superior mechanical strength and higher ionic conductivity than polymer electrolytes.[1, 6, 7, 52-55] However, their brittleness, high interfacial resistance, and chemical instability in the presence of lithium metal, air, or moisture have significantly hindered large-scale implementation in all-solid-state batteries.

Solid polymer electrolytes, typically based on high-molecular-weight polymers such as poly(ethylene oxide) (PEO), offer improved interfacial contact and manufacturability, particularly for roll-to-roll processing.[51, 56, 57] Nevertheless, their ionic conductivity at room temperature remains several orders of magnitude lower than that of liquid electrolytes (10^{-6}–10^{-8} S cm^{-1}), restricting their applicability to elevated-temperature or low-power applications. Attempts to enhance polymer electrolyte conductivity through plasticizers or additives often compromise mechanical strength and thermal stability.

Composite solid electrolytes have been proposed as a compromise, combining inorganic fillers with polymer matrices to balance ionic conductivity, mechanical compliance, and interfacial contact. [51, 56-58] While promising, composite electrolytes introduce additional fabrication complexity and remain challenging to process thin, defect-free membranes suitable for

high-energy battery stacks. Moreover, lithium reactivity with both inorganic and polymer components continue to pose challenges for long-term stability.

Figure 2-3 compares the electrochemical stability windows and ionic conductivities of representative solid electrolytes relative to liquid electrolytes. Although many solid electrolytes operate within the nominal voltage range of lithium-ion batteries (2.5–4.2 V), the effective electrochemical window experienced at electrode interfaces—referenced to Li/Li^+—is often substantially narrower. This limitation becomes particularly critical for high-voltage and nickel-rich cathodes, which demand both wide stability windows and low interfacial resistance to enable deep delithiation.

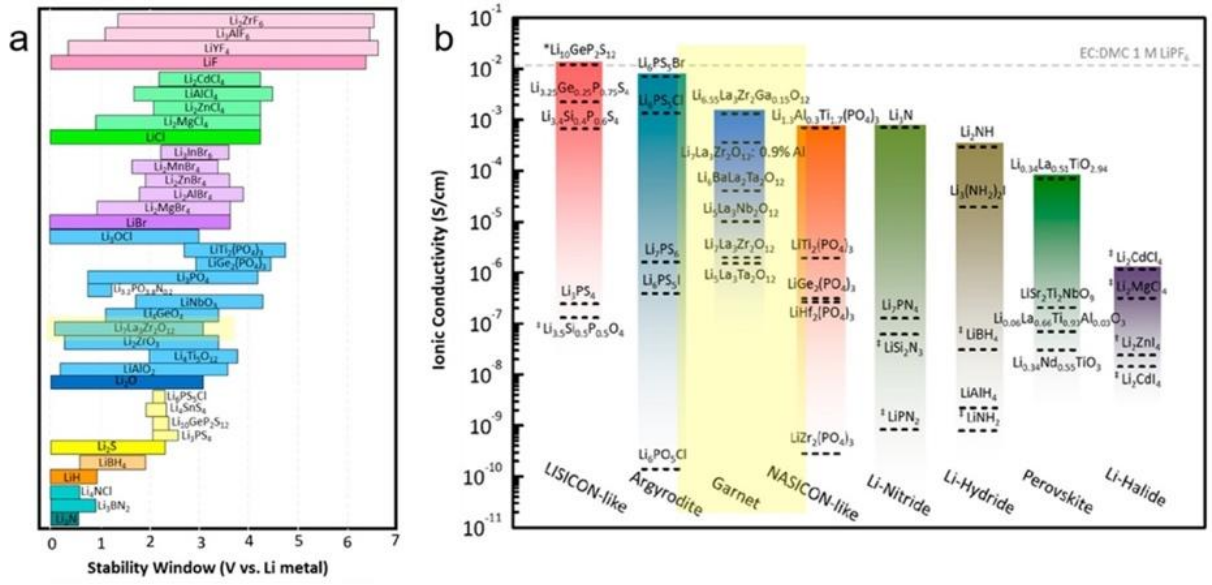


Figure 2-3. Comparison of (a) stability window and (b) ionic conductivity of different electrolyte systems[7]

Among inorganic solid electrolytes, garnet-type materials such as $Li_7La_3Zr_2O_{12}$ (LLZO) have attracted significant attention due to their relatively high room-temperature ionic conductivity (>10^{-4} S cm^{-1}) and chemical stability against lithium metal.[1, 17, 57-60] However, stabilizing the highly conductive cubic phase typically requires high-temperature sintering (1000–1500 °C), which can induce secondary phase formation and degrade ionic transport. Perovskite-type electrolytes such as $Li_{3x}La_{2/3-x}TiO_3$ (LLTO) offer even higher bulk ionic conductivity but suffer from poor interfacial stability with lithium metal and significant grain-boundary resistance. [6, 14, 51, 52] Sulfide-based electrolytes exhibit liquid-like ionic conductivities (up to 10^{-2} S cm^{-1}) and excellent interfacial contact, yet their sensitivity to air and moisture, along with limited

electrochemical stability against oxide cathodes, restricts their practical operating voltage.[4, 53, 55]

Collectively, these constraints reveal a critical system-level insight: the performance of solid-state batteries is not limited solely by electrolyte conductivity, but by the coupled interaction between the solid electrolyte and the cathode under deep delithiation conditions. Narrow electrochemical windows, interfacial instability, and mechanical mismatch impose severe restrictions on cathode utilization, making cathode stability the dominant factor governing achievable energy density in SSBs.

2.2.4 Recommendation and Implication for Cathode Design:

The limitations of solid electrolytes impose stringent requirements on cathode materials, particularly under high-voltage and deep-delithiation conditions. Rather than viewing solid electrolytes as a standalone solution for achieving higher energy density, future SSB development must prioritize cathode designs that remain structurally and thermodynamically stable within the constrained electrochemical environment imposed by solid electrolytes. This necessity motivates the exploration of alternative cathode design principles—beyond conventional compositional tuning—capable of accommodating lithium insertion and extraction with minimal structural and thermodynamic disruption. In this context, entropy-based design strategies that explicitly consider entropy change during cycling during electrochemical cycling emerge as a promising framework for addressing cathode-driven limitations in solid-state batteries.

The constraints imposed by solid electrolytes—particularly limited electrochemical stability windows, interfacial resistance, and mechanical mismatch—ultimately restrict the degree of reversible lithium extraction achievable at the cathode. As a result, the cathode active material becomes the dominant bottleneck governing both energy density and long-term stability in solid-state batteries. The following section therefore focuses on cathode materials for solid-state batteries, with emphasis on their structural behavior, degradation mechanisms, and suitability under deep-delithiation conditions.

2.3 Cathode Active Materials for Solid-State Batteries

Commercial lithium ion batteries primarily employ three classes of cathode active materials: layered oxides, olivine phosphates, and spinel oxides.[20, 22] Each cathode class presents distinct advantages and limitations in terms of energy density, structural stability, cost, and compatibility

with solid electrolytes. Importantly, not all cathode chemistries developed for liquid-electrolyte batteries are directly transferable to solid-state battery (SSB) systems. The following subsections critically review these cathode families with emphasis on their performance, degradation mechanisms, and suitability for operation under the electrochemical and mechanical constraints imposed by solid electrolytes.

2.3.1 Layered Oxide Cathodes (LCO, NMC, NCA): Performance and Degradation Mechanisms

Layered oxide cathodes remain the dominant cathode materials in both commercial lithium-ion batteries and near-term solid-state battery concepts due to their high operating voltage, relatively high specific capacity, and mature manufacturing infrastructure. $LiCoO_2$ (LCO), first commercialized by Sony, established the layered oxide framework but suffers from high cost and ethical concerns associated with cobalt mining [6]. These limitations motivated the development of mixed transition-metal layered oxides, most notably $LiNi_xMn_yCo_zO_2$ (NMC) and $LiNi_xCo_yAl_zO_2$ (NCA), which reduce cobalt content while enhancing energy density.

Progressive generations of NMC cathodes have systematically increased nickel content, evolving from NMC111 to NMC532, NMC622, and ultimately NMC811 to increase capacity while reducing reliance on costly cobalt. As nickel content rises, both specific capacity and gravimetric energy density improve because of the high redox activity of the Ni^{2+}/Ni^{4+} couple. For example, NMC811 and NCA can deliver capacities approaching 200 mAh g^{-1} [7,8]. However, these performance gains come at the expense of structural stability. High-nickel layered oxides undergo significant lattice expansion and contraction during lithium extraction and insertion, which promotes microcracking, cation mixing, oxygen release, and detrimental phase transformations that accelerate capacity fade and reduce cycle life [4–8].

Despite these durability challenges, high-nickel cathodes remain attractive because the increase in energy density and reduction in cobalt content generally outweigh the associated degradation-related costs, particularly for electric vehicle applications where maximizing driving range and lowering material costs are key objectives. Consequently, NMC811 and related high-nickel compositions have become leading commercial candidates. Current research therefore focuses primarily on mitigating the stability limitations of high-nickel cathodes through compositional

engineering, surface coatings, particle design, and other strategies aimed at improving long-term cycling performance.

A fundamental limitation of layered oxides is the incomplete utilization of lithium. In most compositions, delithiating more than ~50% of the lithium leads to irreversible structural changes. Although nickel-rich cathodes permit deeper delithiation, the resulting structural instability significantly shortens cycle life. Considerable efforts, including elemental doping, surface coatings, and particle-level engineering, have been devoted to mitigating these degradation pathways. Nevertheless, these strategies address symptoms rather than the underlying thermodynamic drivers of instability.

In solid-state batteries, the challenges of layered oxides are further amplified. Most solid electrolytes exhibit narrower electrochemical stability windows than liquid electrolytes, often below 3.7 V versus Li/Li^+, and are chemically unstable against highly delithiated cathode surfaces. As a result, interfacial reactions between layered oxides and solid electrolytes become a dominant degradation mechanism. To suppress these reactions, protective coating layers such as $LiNbO_3$ or $LiNbO_2$ are frequently employed, increasing interfacial complexity and reducing effective energy density [9,10]. Despite these challenges, nickel-rich layered oxides, particularly NMC811 remain the most viable candidates for high-energy solid-state batteries due to their unmatched energy density and industrial maturity.

2.3.2 Olivine-Type Cathodes: Two-Phase Stability and Energy Density Limitations

Olivine-type cathodes, represented by $LiMPO_4$ (M = Fe, Mn, Co), exhibit an orthorhombic structure (space group *Pnma*) and are distinguished by their exceptional thermal and structural stability [12–15]. $LiFePO_4$ (LFP) is the most widely adopted olivine cathode due to its low cost, environmental benignity, and long cycle life [16]. The two-phase reaction mechanism between $LiFePO_4$ and $FePO_4$ produces a flat voltage plateau near 3.4 V versus Li/Li^+ and minimizes structural strain during cycling.

Despite these advantages, the relatively low operating voltage and moderate capacity (~170 mAh g^{-1}) limit the achievable energy density of olivine cathodes compared to layered oxides. Early development was further hindered by low intrinsic electronic and ionic conductivity, which was later mitigated through carbon coating and particle downsizing. In solid-state battery

contexts, LFP exhibits excellent compatibility with many solid electrolytes due to its low operating potential and chemical stability, making it attractive for safe and durable SSBs.

However, the two-phase nature of olivine cathodes inherently constrains deep delithiation and limits energy density. Efforts to increase voltage and capacity through substitution of Fe with Mn or Ni have demonstrated partial success [19], but these modifications often introduce new phase instability or kinetic limitations. Consequently, olivine cathodes are well suited for safety critical and long-life applications but remain suboptimal for high-energy solid-state batteries.

2.3.3 Spinel Type Cathodes: High Voltage Operation and Electrolyte Compatibility

Spinel cathodes, typified by $LiMn_2O_4$ (LMO), offer three-dimensional lithium diffusion pathways and higher operating voltages (~4.0 V vs Li/Li^+) compared to olivine cathodes [21]. Manganese-based spinel are attractive due to their low cost and reduced toxicity; however, they suffer from severe capacity fade caused by Jahn–Teller distortion associated with Mn^{3+} [22–28].

Partial substitution of manganese with other transition metals (e.g., Ni, Co, Cr) suppresses Jahn–Teller distortion and enhances structural stability. $LiMn_{1.5}Ni_{0.5}O_4$ (LMNO) is a prominent example, delivering operating voltages near 4.7 V versus Li/Li^+ through the Ni^{2+}/Ni^{4+} redox couple [29]. In principle, such high voltage could significantly increase energy density in solid-state batteries.

In practice, however, the electrochemical stability window of most solid electrolytes is insufficient to support spinel cathodes operating above 4 V. Interfacial decomposition, high resistance, and chemical incompatibility severely limit practical implementation. As with layered oxides, surface coatings and doping strategies have been proposed to mitigate these issues [9,10], but electrolyte compatibility remains the dominant obstacle for high-voltage spinel cathodes in SSBs.

2.3.4 Cathode–Electrolyte Interactions as a Central Design Constraint

In all-solid-state batteries, cathode performance is inseparably linked to cathode–electrolyte interfacial behavior. Xu *et al.* defined the "interphase" as a complex region encompassing chemical reactions, defect formation, contact loss, and electronic structure modification at electrode–electrolyte interfaces [4]. In composite cathodes, additional interparticle interfaces further complicate lithium transport.

Liang *et al.* identified up to 13 distinct interfaces in sulfide based SSBs, with more than half located within the cathode composite [16]. These interfaces dominate cell resistance, impede lithium-ion transport, and accelerate degradation during cycling. Unlike liquid electrolytes, which conformally wet electrode surfaces, solid electrolytes impose rigid contact constraints that exacerbate interfacial impedance and mechanical stress [61, 62].

2.3.5 Solid–Solid Interphases and Cathode Driven Energy Density Limitations

Although solid-state batteries promise enhanced safety and higher energy density, their practical performance is limited by solid–solid interphases, particularly at the cathode. High-energy cathodes require deep delithiation and high operating voltage, both of which strain the electrochemical and mechanical stability of solid electrolytes. Moreover, the necessity of incorporating solid electrolyte within the cathode composite reduces active material volume fraction, further lowering energy density relative to liquid-electrolyte systems [3,5].

The constrained lithium-ion transport pathways in solid composites impose additional kinetic penalties, making cathode architecture and interfacial design critical. While polymer or composite electrolytes can partially mitigate contact issues, many interfacial challenges remain unresolved. Surface coatings, catholyte optimization, and microstructural engineering have been explored, but these approaches increase complexity and introduce new tradeoffs.

Collectively, these limitations underscore a central conclusion: the cathode, rather than the solid electrolyte, is likely to represent the primary bottleneck in achieving both high energy density and long-term stability in solid-state batteries. Addressing this challenge requires cathode design strategies that extend beyond conventional compositional optimization and explicitly consider thermodynamic stability under deep delithiation, thereby motivating the entropy-based framework developed in the subsequent chapters.

It is important to note that solid electrolytes continue to face significant challenges, including achieving high ionic conductivity, enabling cost-effective large-scale manufacturing, and mitigating interfacial reactions with lithium metal in certain electrolyte systems. Continued advances in solid electrolyte design remain essential for the commercialization of solid-state batteries. However, even if these electrolyte-related challenges are successfully resolved, the cathode will remain the critical limiting component. The same electrolyte materials that function effectively as solid electrolytes must also be compatible with the cathode as part of the catholyte

composite, where stringent requirements for electrochemical stability, mechanical integrity, ionic transport, and high-voltage operation must be simultaneously satisfied.

As a result, the development of cathode materials and cathode architectures represents the most significant barrier to realizing high-performance solid-state batteries with both practical energy density and long-term cycling stability. Consequently, cathode design serves as the primary focus of this thesis.

2.4 Entropy in Battery Cathode Materials: Static Descriptors versus Dynamic Entropy change during cycling

Entropy has increasingly been discussed in the context of battery materials, most prominently through the emergence of high entropy materials, where configurational entropy is maximized by incorporating multiple principal elements in near-equimolar ratios.[24-31, 63] In these systems, entropy is typically treated as a static thermodynamic descriptor, evaluated at a fixed composition to rationalize phase stability, suppression of ordering, or resistance to phase separation. While this framework has proven effective for structurally static or equilibrium materials, its applicability to electrochemically active cathodes remain fundamentally limited.

In lithium-ion battery cathodes, entropy contributes to the Gibbs free energy alongside enthalpic, electronic, and elastic terms. However, unlike conventional high-entropy systems, cathode materials do not operate at a single equilibrium composition. Instead, they continuously traverse a range of lithium concentrations during charge and discharge, altering site occupancies, oxidation states, and local structural order.[20-23] Under these conditions, the evolution of entropy during lithiation and delithiation, rather than its absolute magnitude becomes a critical thermodynamic variable governing stability and reversibility.

2.4.1 Thermodynamic Characteristics of High-Nickel Cathodes: Phase Transitions and Free-Energy Changes

High-nickel layered oxide cathodes are widely pursued due to their high redox activity and large achievable specific capacities. However, extensive experimental and computational studies have shown that these materials undergo Cy!1030 deep delithiation. In compositions with high nickel content (≥80% Ni), lithium extraction is accompanied by a sequence of discrete phase

transformations commonly described as H1 → H2 → H3—which are associated with abrupt changes in lattice parameters, particularly along the crystallographic *c*-axis.[32-36, 64]

From a thermodynamic perspective, these phase transitions reflect large changes in Gibbs free energy as a function of lithium content, indicating that the system moves between distinct free-energy minima rather than evolving smoothly along a single solid-solution pathway. The steep free-energy gradients associated with these transformations give rise to mechanical stress, interfacial instability, and irreversible structural rearrangements, especially at high states of charge.

The large free-energy changes accompanying phase transitions in high-nickel cathodes are closely linked to transition-metal redox saturation and the onset of oxygen participation in charge compensation.[65-67] As lithium extraction progresses beyond the stable solid-solution regime, destabilization of the metal–oxygen framework leads to oxygen lattice distortion, oxygen release, and surface reconstruction. These processes further modify the free-energy landscape, promoting irreversible reactions at the cathode–electrolyte interface.

In solid-state batteries, the consequences of these free-energy-driven phase transitions are amplified. Rigid solid electrolytes limit mechanical accommodation of lattice strain, while narrow electrochemical stability windows exacerbate interfacial decomposition at highly delithiated cathode surfaces. As a result, the thermodynamic instability inherent to high-nickel cathodes manifest as rapid impedance growth, loss of interfacial contact, and accelerated capacity fade in solid-state configurations.

Importantly, while high-nickel cathodes may offer high theoretical energy density, their electrochemical behavior is dominated by discontinuous phase evolution and large Gibbs free energy changes during cycling, which fundamentally constrain reversibility and long-term stability. These characteristics distinguish high-nickel systems from compositions that maintain solid-solution-like behavior over broader lithiation ranges and motivate closer examination of alternative compositional regimes.

2.4.2 Thermodynamic Characteristics of Mid-Nickel Cathodes: Solid-Solution Behavior and Smooth Free-Energy Landscapes

Mid-nickel layered oxide cathodes, typically containing approximately 60–70% nickel, exhibit thermodynamic behavior that is distinct from both high-nickel and low-nickel compositions. Numerous experimental studies have shown that these materials maintain extended over a broad range of lithium contents, with delayed or suppressed phase transitions compared to high-nickel cathodes. [34, 64] This behavior is reflected in smoother voltage profiles, reduced lattice parameter discontinuities, and improved electrochemical reversibility during cycling.

From a thermodynamic standpoint, solid-solution behavior indicates that the system evolves along a continuous Gibbs free-energy surface as a function of lithium content, rather than transitioning between discrete free-energy minima associated with first-order phase transformations.[20, 21] In mid-nickel cathodes, lithium extraction proceeds with gradual changes in local coordination environments and transition-metal oxidation states, minimizing abrupt free-energy changes that would otherwise drive mechanical and interfacial instability.[34, 64]

The presence of manganese and cobalt in mid-nickel compositions play a stabilizing role by moderating nickel redox activity and distributing charge compensation more evenly across the transition-metal sublattice.[32, 33, 36, 64, 68, 69] This compositional balance suppresses excessive lattice distortion and delays the onset of oxygen participation in charge compensation. As a result, mid-nickel cathodes exhibit reduced structural reconstruction and improved resistance to oxygen lattice destabilization at high states of charge compared to high-nickel systems.

In solid-state battery configurations, the thermodynamic advantages of mid-nickel cathodes become particularly important. The rigid nature of solid electrolytes imposes mechanical constraints that amplify the consequences of abrupt free-energy changes and phase transitions. Cathodes that evolve smoothly along a continuous free-energy landscape are therefore inherently better suited to operate under solid-state conditions, as they generate lower internal stress and maintain more stable cathode–electrolyte interfaces during cycling.

Although mid-nickel cathodes offer slightly lower theoretical capacities than their high-nickel counterparts, their improved thermodynamic stability enables higher practical lithium utilization over extended cycling, especially in environments with limited interfacial tolerance. This trade-off suggests that practical energy density in solid-state batteries is not determined solely by maximum

capacity, but by the ability of the cathode to undergo lithium insertion and extraction without triggering discontinuous thermodynamic or structural responses.[70]

Importantly, while the smoother free-energy evolution of mid-nickel cathodes is widely observed experimentally, the underlying thermodynamic descriptors that govern this behavior remain insufficiently quantified. In particular, existing studies rarely examine how thermodynamic quantities evolve continuously with lithium content across different compositions. This limitation prevents a unified comparison between cathodes that undergo abrupt phase transitions and those that maintain solid-solution-like behavior.

These observations highlight the need for a framework capable of quantitatively describing thermodynamic evolution during lithiation and delithiation, rather than relying on static material descriptors. The following chapter addresses this gap by developing analytical and experimental approaches to evaluate how key thermodynamic variables evolve with lithium content, providing a basis for rational cathode design across different nickel regimes.

2.4.3 Limitations of Entropy-Based Design Approaches for Battery Cathodes

Entropy-based design concepts have gained increasing attention in materials science, particularly through the development of high-entropy alloys and ceramics, where configurational entropy is deliberately maximized to stabilize single-phase structures.[24-31] In these systems, entropy is commonly treated as a static thermodynamic quantity evaluated at a fixed composition and temperature. While this approach has proven effective for equilibrium or quasi-static materials, its direct application to battery cathodes presents fundamental limitations.

Most entropy-assisted cathode studies focus on absolute configurational entropy, often calculated for the fully lithiated or as-synthesized state. Such analyses implicitly assume that higher entropy correlates with improved phase stability and electrochemical performance. However, lithium-ion battery cathodes do not operate at a single composition; instead, they continuously traverse a wide range of lithium contents during charge and discharge.[20-23] Under these conditions, static entropy descriptors fail to capture the thermodynamic response of the material as it evolves during cycling.

Moreover, many entropy-based design strategies emphasize compositional complexity without explicitly considering phase behavior and free-energy continuity. In layered oxide cathodes,

electrochemical instability is often associated with first-order phase transitions and abrupt changes in Gibbs free energy during deep delithiation.[20] These phenomena are well documented experimentally, yet they are not adequately addressed by static entropy calculations performed at a single lithium concentration. As a result, high-entropy or compositionally complex cathodes may still experience severe degradation if they undergo discontinuous phase evolution during cycling.[29, 66, 67]

Another limitation of existing entropy-based approaches is the lack of distinction between structural disorder that stabilizes a phase and thermodynamic disorder that emerges during electrochemical operation. In battery cathodes, disorder introduced during cycling, such as cation migration, oxygen lattice distortion, or surface[35, 71, 72] reconstruction, is often detrimental, even though it may increase local configurational entropy.[66, 67] Consequently, maximizing entropy without regard to its origin or evolution can obscure the mechanisms responsible for irreversible degradation.

Experimental studies capable of probing thermodynamic quantities in battery materials, such as temperature-dependent open-circuit potential measurements, demonstrate that entropy contributes measurably to electrode behavior.[73, 74] However, these measurements are typically restricted to limited state-of-charge ranges or single compositions and are rarely used to systematically compare cathodes across different nickel contents or phase-transition regimes. As a result, entropy remains underutilized as a comparative thermodynamic metric for cathode design.

Collectively, these limitations indicate that current entropy-based design paradigms are insufficient for describing electrochemically active cathodes in which lithium insertion and extraction induce continuous changes in composition, structure, and free energy. A meaningful entropy-informed design framework for battery cathodes must therefore move beyond static descriptors and account for how thermodynamic quantities evolve as a function of lithium content.

This gap motivates the approach taken in this thesis. Rather than maximizing absolute entropy or compositional disorder, the following chapter develops a framework that examines thermodynamic evolution during lithiation and delithiation, with particular emphasis on how cathodes traverse their free-energy landscape during cycling. By focusing on the continuity or discontinuity of thermodynamic changes across different compositions, this approach provides a

more physically grounded basis for comparing cathode stability and guiding rational material design.

2.5 Experimental and Thermodynamic Approaches to Probing Entropy in Battery Cathodes

Quantifying thermodynamic quantities in electrochemically active materials presents unique challenges due to their dynamic nature and non-equilibrium operation. While structural and electrochemical characterization techniques, such as X-ray diffraction, electron microscopy, and voltage profiling, provide valuable insight into phase evolution and degradation mechanisms, they do not directly resolve the thermodynamic variables that govern cathode stability during lithiation and delithiation. As a result, experimental approaches capable of probing Gibbs free energy and its constituent terms are essential for developing a rigorous thermodynamic understanding of battery cathodes.

Among available techniques, temperature-dependent electrochemical measurements offer a direct route to accessing thermodynamic information in battery materials.[73, 74] The equilibrium cell potential is related to the Gibbs free energy change of the electrochemical reaction, and its temperature dependence provides access to the entropy contribution through fundamental thermodynamic relations. Specifically, measurements of the open-circuit potential (OCP) as a function of temperature allow separation of enthalpic and entropic contributions to the free energy of lithium insertion and extraction.

In practice, the measured OCP may deviate from the true thermodynamic equilibrium potential due to factors such as incomplete electrochemical equilibration, lithium concentration gradients, diffusion limitations within electrode particles, interfacial polarization, side reactions, and temperature variations. To minimize these effects, the 2325 coin cell developed by the National Research Council of Canada was employed. The cell design minimizes the separation distance between the working and counter electrodes, with the gap primarily limited by the separator thickness of less than 15 μm. Furthermore, sufficient electrolyte was added to ensure complete wetting of both the electrodes and separator, thereby promoting uniform ionic transport and reducing concentration polarization. Long relaxation periods following each electrochemical step were also used to allow the cell to approach thermodynamic equilibrium before OCP

measurements were recorded. Collectively, these experimental considerations reduce deviations from equilibrium and improve the accuracy of calculated Gibbs free energy and entropy values.

Potentiometric entropy measurements, typically performed by monitoring the change in equilibrium potential with temperature at a fixed state of charge, have been applied to a range of electrode materials. Prior studies have demonstrated that entropy contributions can reveal phase transitions, order–disorder behavior, and changes in reaction mechanism that are not readily apparent from voltage profiles alone.[73] In particular, sharp features in entropy-related quantities have been associated with first-order phase transitions, while smoother responses are characteristic of solid-solution behavior.

Despite their potential, entropy measurements in cathode materials remain relatively sparse and fragmented in the literature. Many reported studies focus on narrow state-of-charge windows, single compositions, or model systems, limiting their applicability for comparative cathode design.[74] Moreover, entropy measurements are often interpreted qualitatively rather than integrated into a broader thermodynamic framework that links free-energy evolution to structural stability and electrochemical performance.

Another limitation of existing experimental studies is the lack of systematic comparison across cathode compositions with differing phase behavior, particularly across the nickel-content spectrum in layered oxides. While high-nickel cathodes are known to undergo abrupt phase transitions and mid-nickel cathodes often exhibit extended solid-solution behavior, few studies directly examine how these differences manifest in experimentally accessible thermodynamic quantities. Consequently, the relationship between phase evolution, free-energy changes, and measurable entropy-related responses remains insufficiently established.

In the context of solid-state batteries, this gap is particularly significant. Rigid solid electrolytes amplify the consequences of thermodynamic instability at the cathode, making subtle differences in free-energy evolution highly consequential for interfacial stability and cycle life. Experimental approaches capable of resolving thermodynamic signatures across lithiation and delithiation therefore provide a critical link between fundamental materials behavior and practical battery performance.

These limitations highlight the need for systematic, composition-dependent thermodynamic measurements that track how cathode materials evolve across a wide range of lithium contents. Such measurements enable direct comparison between cathodes that undergo discontinuous phase transitions and those that maintain solid-solution-like behavior, offering insight into the thermodynamic origins of stability and degradation. Chapter 6 addresses this need by employing temperature-dependent electrochemical measurements to experimentally probe thermodynamic evolution in layered oxide cathodes, providing an experimental foundation for the entropy-based design framework developed in this thesis.

2.6 Summary of Literature Review and Identified Research Gaps

This chapter has critically reviewed the current state of solid-state battery research with emphasis on cathode active materials, system level constraints, degradation mechanisms under deep delithiation, and thermodynamic design concepts. While significant progress has been made in developing solid electrolytes and high energy cathode materials, the literature reveals persistent limitations that prevent solid-state batteries from achieving their theoretical performance advantages.

At the system level, solid electrolytes provide clear benefits in safety and enable lithium-metal anodes; however, their limited ionic conductivity, narrow electrochemical stability windows, and rigid mechanical properties impose stringent constraints on cathode operation. These constraints disproportionately affect the cathode, where high operating voltage, deep delithiation, and structural reversibility must be simultaneously maintained. As a result, cathode utilization and interfacial stability emerge as the dominant factors limiting achievable energy density in solid-state batteries.

The review of cathode active materials highlights a fundamental trade-off between energy density and stability. High-nickel layered oxide cathodes offer the highest theoretical capacities but undergo pronounced phase transitions, large lattice distortions, and oxygen lattice instability during deep delithiation, leading to severe chemo-mechanical degradation—particularly under solid-state conditions[32, 33, 35, 66]. In contrast, mid-nickel cathodes exhibit extended solid-solution behavior, smoother structural evolution, and improved interfacial compatibility, enabling higher practical lithium utilization despite slightly lower theoretical capacity.[34, 64]

These observations indicate that maximizing nickel content does not necessarily maximize practical energy density in solid-state batteries.

Cathode failure mechanisms under deep delithiation are shown to arise from the coupled effects of phase transitions, free-energy discontinuities, oxygen instability, and mechanical stress accumulation.[35, 66, 71, 72] While these mechanisms are well documented experimentally, existing mitigation strategies—such as surface coatings, doping, and microstructural engineering—primarily address symptoms rather than the underlying thermodynamic drivers of instability. Moreover, the presence of multiple solid–solid interfaces in composite cathodes further amplifies degradation, underscoring the cathode-driven nature of solid-state battery limitations.

Entropy-based design concepts have been explored in the literature, particularly through high-entropy materials; however, their application to battery cathodes remains limited. Most studies rely on static descriptors such as absolute configurational entropy evaluated at fixed compositions, which are insufficient to describe electrochemically active materials that continuously evolve during cycling. Importantly, existing entropy-based approaches do not adequately capture the thermodynamic evolution associated with lithium insertion and extraction, nor do they systematically distinguish between cathodes exhibiting discontinuous phase transitions and those maintaining solid-solution behavior.

Experimental techniques capable of probing thermodynamic quantities, such as temperature-dependent open-circuit potential measurements, offer a pathway to bridging this gap. Although prior studies demonstrate that thermodynamic measurements can reveal phase behavior and reaction mechanisms, such approaches have rarely been applied systematically across cathode compositions or integrated into a cathode design framework relevant to solid-state batteries.

Collectively, the literature reveals a critical gap: there is no unified framework that quantitatively links cathode composition, thermodynamic evolution during cycling, and practical energy density in solid-state batteries. In particular, the role of thermodynamic continuity versus discontinuity during lithiation and delithiation remains insufficiently understood, despite its clear relevance to structural stability and interfacial degradation.

Addressing this gap requires moving beyond static material descriptors toward design principles that explicitly consider how cathodes traverse their thermodynamic landscape during operation.

The following chapters address this need by (i) evaluating realistic energy density limits in solid-state batteries at the cell level, (ii) developing a thermodynamic framework to analyze cathode evolution during lithiation and delithiation, and (iii) experimentally probing thermodynamic signatures in layered oxide cathodes. Together, these approaches establish a basis for rational cathode design that balances energy density and stability in solid-state batteries.

2.7 References

1. Abouali, S., et al., *Garnet-Based Solid-State Li Batteries: From Materials Design to Battery Architecture.* ACS Energy Letters, 2021. **6**(5): p. 1920-1941.
2. Janek, J. and W.G. Zeier, *Challenges in speeding up solid-state battery development.* Nature Energy, 2023. **8**(3): p. 230-240.
3. Lee, Y.G., et al., *Publisher Correction: High-energy long-cycling all-solid-state lithium metal batteries enabled by silver–carbon composite anodes (Nature Energy, (2020), 5, 4, (299-308), 10.1038/s41560-020-0575-z).* Nature Energy, 2020. **5**(4): p. 348.
4. Liang, Y., et al., *Challenges, interface engineering, and processing strategies toward practical sulfide-based all-solid-state lithium batteries.* InfoMat, 2022. **4**(5): p. e12292.
5. Schmaltz, T., et al., *A Roadmap for Solid-State Batteries.* Advanced Energy Materials, 2023. **13**(43): p. 2301886.
6. Yan, S., et al., *Perovskite Solid-State Electrolytes for Lithium Metal Batteries.* Batteries, 2021. **7**(4): p. 75.
7. Bachman, J.C., et al., *Inorganic Solid-State Electrolytes for Lithium Batteries: Mechanisms and Properties Governing Ion Conduction.* Chemical Reviews, 2016. **116**(1): p. 140-162.
8. Chen, Y., et al., *A review of lithium-ion battery safety concerns: The issues, strategies, and testing standards.* Journal of Energy Chemistry, 2021. **59**: p. 83-99.
9. Houache, M.S.E., et al., *On the Current and Future Outlook of Battery Chemistries for Electric Vehicles—Mini Review.* Batteries, 2022. **8**(7): p. 70.
10. Kim, J.G., et al., *A review of lithium and non-lithium based solid state batteries.* Journal of Power Sources, 2015. **282**: p. 299-322.
11. Masquelier, C. and L. Croguennec, *Polyanionic (Phosphates, Silicates, Sulfates) Frameworks as Electrode Materials for Rechargeable Li (or Na) Batteries.* Chemical Reviews, 2013. **113**(8): p. 6552-6591.
12. Muralidharan, N., et al., *Next-Generation Cobalt-Free Cathodes – A Prospective Solution to the Battery Industry's Cobalt Problem.* Advanced Energy Materials, 2022. **12**(9): p. 2103050.
13. Nasajpour-Esfahani, N., et al., *Comprehensive review of lithium-ion battery materials and development challenges.* Renewable and Sustainable Energy Reviews, 2024. **203**: p. 114783.
14. Pang, Y., et al., *Electrolyte/Electrode Interfaces in All-Solid-State Lithium Batteries: A Review.* Electrochemical Energy Reviews, 2021. **4**(2): p. 169-193.
15. Park, S.H., et al., *Toward high-performance anodeless batteries based on controlled lithium metal deposition: a review.* Journal of Materials Chemistry A, 2021. **9**(26): p. 14656-14681.
16. Sim, Y.B., B.K. Park, and K.J. Kim, *Reasonable design of thick electrodes in lithium-ion batteries.* Frontiers in Batteries and Electrochemistry, 2023. **2**.

17. Wang, C., et al., *Garnet-Type Solid-State Electrolytes: Materials, Interfaces, and Batteries.* Chemical Reviews, 2020. **120**(10): p. 4257-4300.
18. Wang, Y., et al., *Ice-Templated Method to Promote Electrochemical Energy Storage and Conversion: A Review.* Energies, 2023. **16**(9): p. 3865.
19. Xi, Z., et al., *Modification strategies of high-energy Li-rich Mn-based cathodes for Li-ion batteries: A Review.* Molecules, 2024. **29**(5): p. 1064.
20. Nazri, G.-A. and G. Pistoia, *Lithium batteries: science and technology*. 2008: Springer Science & Business Media.
21. Huggins, R.A., *Advanced batteries : materials science aspects*. 2009, New York ;: Springer.
22. Yoshio, M., R.J. Brodd, and A. Kozawa, *Lithium-ion batteries : science and technologies*. 1st 2009. ed. 2009, New York: Springer.
23. Schalkwijk, W.A.v. and B. Scrosati, *Advances in lithium-ion batteries*. 2002, New York, NY: Kluwer Academic/Plenum Publishers.
24. Murty, B.S., et al., *2 - High-entropy alloys: basic concepts*, in *High-Entropy Alloys (Second Edition)*, B.S. Murty, et al., Editors. 2019, Elsevier. p. 13-30.
25. Otto, F., et al., *Relative effects of enthalpy and entropy on the phase stability of equiatomic high-entropy alloys.* Acta Materialia, 2013. **61**(7): p. 2628-2638.
26. Ouyang, B. and Y. Zeng, *The rise of high-entropy battery materials.* Nature Communications, 2024. **15**(1): p. 973.
27. Sarkar, A., et al., *High-Entropy Oxides: Fundamental Aspects and Electrochemical Properties.* Advanced Materials, 2019. **31**(26): p. 1806236.
28. Shin, D., et al., *Rational engineering of high-entropy oxides for Li-ion battery anodes with finely tuned combustion syntheses.* NPG Asia Materials, 2023. **15**(1): p. 54.
29. Sturman, J., et al., *Communication—Design of LiNi0.2Mn0.2Co0.2Fe0.2Ti0.2O2 as a High-Entropy Cathode for Lithium-Ion Batteries Guided by Machine Learning.* Journal of The Electrochemical Society, 2021. **168**(5): p. 050541.
30. Xiao, B., et al., *High-entropy oxides as advanced anode materials for long-life lithium-ion Batteries.* Nano Energy, 2022. **95**: p. 106962.
31. Zeng, Y., et al., *High-entropy mechanism to boost ionic conductivity.* Science, 2022. **378**(6626): p. 1320-1324.
32. Kim, H., et al., *Controlling the Microstructure of Cobalt-Free, High-Nickel Cathode Materials with Dopant Solubility for Lithium-Ion Batteries.* ACS Applied Materials & Interfaces, 2023. **15**(22): p. 26585-26592.
33. Li, W., E.M. Erickson, and A. Manthiram, *High-nickel layered oxide cathodes for lithium-based automotive batteries.* Nature Energy, 2020. **5**(1): p. 26-34.
34. Loghavi, M.M., et al., *Electrochemical evaluation of LiNi0.5Mn0.3Co0.2O2, LiNi0.6Mn0.2Co0.2O2, and LiNi0.8Mn0.1Co0.1O2 cathode materials for lithium-ion batteries: from half-coin cell to pouch cell.* Monatshefte für Chemie - Chemical Monthly, 2022. **153**(12): p. 1197-1212.
35. Mao, G., et al., *Improved cycling stability of high nickel cathode material for lithium ion battery through Al- and Ti-based dual modification.* Nanoscale, 2021. **13**(44): p. 18741-18753.
36. You, Y., et al., *Modified High-Nickel Cathodes with Stable Surface Chemistry Against Ambient Air for Lithium-Ion Batteries.* Angewandte Chemie International Edition, 2018. **57**(22): p. 6480-6485.
37. Lu, Y., et al., *Dry electrode technology, the rising star in solid-state battery industrialization.* Matter, 2022. **5**(3): p. 876-898.
38. Yim, C.-H., et al., *Understanding key limiting factors for the development of all-solid-state-batteries.* Chemical Engineering Journal Advances, 2023. **13**: p. 100436.
39. Yu, X., et al., *Battery Safety: From Lithium-Ion to Solid-State Batteries.* Engineering, 2023. **21**: p. 9-14.

40. Goodenough, J.B. and K.-S. Park, *The Li-Ion Rechargeable Battery: A Perspective.* Journal of the American Chemical Society, 2013. **135**(4): p. 1167-1176.
41. Mizushima, K., et al., *LixCoO2 (0<x<-1): A new cathode material for batteries of high energy density.* Materials Research Bulletin, 1980. **15**(6): p. 783-789.
42. Kim, Y.S., et al., *Evolution of a Radially Aligned Microstructure in Boron-Doped Li[Ni0.95Co0.04Al0.01]O2 Cathode Particles.* ACS Applied Materials & Interfaces, 2022. **14**(15): p. 17500-17508.
43. Kim, U.-H., et al., *High-Energy-Density Li-Ion Battery Reaching Full Charge in 12 min.* ACS Energy Letters, 2022. **7**(11): p. 3880-3888.
44. Goonetilleke, D., et al., *Structural Evolution and High-Voltage Structural Stability of Li(NixMnyCoz)O2 Electrodes.* Chemistry of Materials, 2019. **31**(2): p. 376-386.
45. Ryu, H.-H., et al., *Microstrain Alleviation in High-Energy Ni-Rich NCMA Cathode for Long Battery Life.* ACS Energy Letters, 2021. **6**(1): p. 216-223.
46. Niketic, S., et al., *Influence of Ti Substitution on Electrochemical Performance and Evolution of LiMn1.5−x Ni0.5TixO4 (x = 0.05, 0.1, 0.3) as a High Voltage Cathode Material with a Very Long Cycle Life.* Inorganics, 2022. **10**(1): p. 10.
47. Yim, C.-H., et al., *Highly ordered LiFePO4 cathode material for Li-ion batteries templated by surfactant-modified polystyrene colloidal crystals.* Journal of Power Sources, 2012. **205**: p. 414-419.
48. Chan, C.K., et al., *High-performance lithium battery anodes using silicon nanowires.* Nature Nanotechnology, 2008. **3**(1): p. 31-35.
49. Larcher, D., et al., *Recent findings and prospects in the field of pure metals as negative electrodes for Li-ion batteries.* Journal of Materials Chemistry, 2007. **17**(36): p. 3759-3772.
50. Kasavajjula, U., C. Wang, and A.J. Appleby, *Nano- and bulk-silicon-based insertion anodes for lithium-ion secondary cells.* Journal of Power Sources, 2007. **163**(2): p. 1003-1039.
51. Al-Salih, H., et al., *A Polymer-Rich Quaternary Composite Solid Electrolyte for Lithium Batteries.* Journal of the Electrochemical Society, 2020. **167**(7).
52. Cho, Y.H., et al., *Mechanical properties of the solid Li-ion conducting electrolyte: Li 0.33 La 0.57 TiO 3.* Journal of Materials Science, 2012. **47**(16): p. 5970-5977.
53. Ma, Z., H.G. Xue, and S.P. Guo, *Recent achievements on sulfide-type solid electrolytes: crystal structures and electrochemical performance.* Journal of Materials Science, 2018. **53**(6): p. 3927-3938.
54. Sharafi, A., et al., *Surface Chemistry Mechanism of Ultra-Low Interfacial Resistance in the Solid-State Electrolyte Li7La3Zr2O12.* Chemistry of Materials, 2017. **29**(18): p. 7961-7968.
55. Zhang, Q., et al., *Sulfide-Based Solid-State Electrolytes: Synthesis, Stability, and Potential for All-Solid-State Batteries.* Advanced Materials, 2019. **31**(44).
56. An, H., et al., *Coupling two-dimensional fillers with polymer chains in solid polymer electrolyte for room-temperature dendrite-free lithium-metal batteries.* Energy Storage Materials, 2021. **43**: p. 358-364.
57. Chen, L., et al., *PEO/garnet composite electrolytes for solid-state lithium batteries: From "ceramic-in-polymer" to "polymer-in-ceramic"*. Nano Energy, 2018. **46**: p. 176-184.
58. Bag, S., et al., *LiF modified stable flexible PVDF-garnet hybrid electrolyte for high performance all-solid-state Li–S batteries.* Energy Storage Materials, 2020. **24**: p. 198-207.
59. Nolan, A.M., E.D. Wachsman, and Y. Mo, *Computation-guided discovery of coating materials to stabilize the interface between lithium garnet solid electrolyte and high-energy cathodes for all-solid-state lithium batteries.* Energy Storage Materials, 2021. **41**: p. 571-580.
60. Zhang, Y., et al., *Garnet-Based Solid-State Lithium Fluoride Conversion Batteries Benefiting from Eutectic Interlayer of Superior Wettability.* ACS Energy Letters, 2020. **5**(4): p. 1167-1176.

61. Famprikis, T., et al., *Fundamentals of inorganic solid-state electrolytes for batteries.* Nature Materials, 2019. **18**(12): p. 1278-1291.
62. Ahmad, Z. and C.-D. Yeo, *Contact Mechanics of Solid-State Batteries.* Journal of Electrochemical Energy Conversion and Storage, 2026. **23**(2).
63. Radha, A.V., et al., *Understanding the stability of fluorosulfate Li-ion battery cathode materials: a thermochemical study of LiFe1−xMnxSO4F (0 ≤ x ≤ 1) polymorphs.* Journal of Materials Chemistry, 2012. **22**(46): p. 24446-24452.
64. Sim, R., L. Su, and A. Manthiram, *A High Energy-Density, Cobalt-Free, Low-Nickel LiNi0.7Mn0.25Al0.05O2 Cathode with a High-Voltage Electrolyte for Lithium-Metal Batteries.* Advanced Energy Materials, 2023. **13**(21): p. 2300096.
65. Liu, Q., et al., *Ni Migration Arising from Inter-transition Metal Charge Transfer in the NCM811 System.* The Journal of Physical Chemistry C, 2023. **127**(22): p. 10853-10860.
66. Zhao, G., et al., *Exploring Degradation Mechanisms and Recent Developments in High-Nickel Layered Cathodes for Lithium Batteries.* Electrochemical Energy Reviews, 2025. **8**(1): p. 21.
67. Li, Q., et al., *A comprehensive understanding on the anionic redox chemistry of high-voltage cathode materials for high-energy-density lithium-ion batteries.* Chemical Society Reviews, 2025. **54**(7): p. 3441-3474.
68. Arunkumar, T.A. and A. Manthiram, *Influence of chromium doping on the electrochemical performance of the 5 v spinel cathode LiMn1.5Ni0.5O4.* Electrochimica Acta, 2005. **50**(28): p. 5568-5572.
69. Manthiram, A. and J.B. Goodenough, *Lithium insertion into Fe2(MO4)3 frameworks: Comparison of M = W with M = Mo.* Journal of Solid State Chemistry, 1987. **71**(2): p. 349-360.
70. Lee, D., et al., *Alleviating kinetical delamination induced by localized cathode contact via electrochemo-mechanical modeling in all-solid-state batteries.* Joule, 2025. **9**(8): p. 102046.
71. Zhuang, D. and M.Z. Bazant, *Theory of layered-oxide cathode degradation in Li-ion batteries by oxidation-induced cation disorder.* Journal of The Electrochemical Society, 2022. **169**(10): p. 100536.
72. Liu, H., et al., *Spatially resolved surface valence gradient and structural transformation of lithium transition metal oxides in lithium-ion batteries.* Physical Chemistry Chemical Physics, 2016. **18**(42): p. 29064-29075.
73. Swiderska-Mocek, A., E. Rudnicka, and A. Lewandowski, *Temperature coefficients of Li-ion battery single electrode potentials and related entropy changes – revisited.* Physical Chemistry Chemical Physics, 2019. **21**(4): p. 2115-2120.
74. Baek, S.W., et al., *Thermodynamic Analysis and Interpretative Guide to Entropic Potential Measurements of Lithium-Ion Battery Electrodes.* The Journal of Physical Chemistry C, 2022. **126**(14): p. 6096-6110.

Chapter 3: Understanding key limiting factors for the development of all-solid-state batteries

This chapter has been adapted from a research paper published in Chemical Engineering Journal Advances (doi.org/10.1016/j.ceja.2022.100436).

The preceding chapters established that solid-state batteries, while promising substantial gains in safety and theoretical energy density, face persistent practical limitations rooted at both the system and materials levels. In particular, the literature review highlighted that cathode active materials represent the dominant bottleneck constraining achievable energy density, especially under the architectural and interfacial constraints imposed by solid electrolytes. However, beyond qualitative discussions, a quantitative and realistic assessment of how individual cell parameters influence system-level energy density remains necessary.

In this context, Chapter 3 adopts a bottom-up cell-level modeling approach to critically evaluate the extent to which all-solid-state batteries can realistically outperform conventional lithium-ion batteries. By systematically examining the influence of solid electrolyte thickness, cathode composition, active material fraction, electrode thickness, and anode configuration, this chapter establishes practical performance limits and identifies cathode utilization as the most impactful lever for near-term energy density improvement. These findings provide a quantitative foundation that motivates the thermodynamic investigation of cathode behavior developed in the subsequent chapters.

3.1 Abstract

The All-Solid-State-Battery (ASSB) is projected to offer higher energy density and enhanced safety compared to the current commercial Li-ion battery. In this study, we have used a simple model to evaluate the effect of different cell components on the battery's overall performance. We critically examine the promised 100% increase (vs. a standard Li-ion battery) in the overall energy density of an ASSB— a claim often made in both the literature and industry. Through a survey of cell parameters possible with current technology, we were able to evaluate optimum parameters that can be expected in future ASSBs. Herein, we identify three critical parameters required to reach the promised energy density: (1) minimize the thickness of the solid electrolyte to less than 20 μm; (2) modify the cathode formulation to minimize the amount of catholyte and optimize the

electrode thickness; and (3) minimize the N/P ratio by developing cells that are anode-free or utilize ultrathin lithium anodes. In conclusion, we believe that the often-cited 100% improvement in energy density for ASSBs is overly optimistic. Instead, a 30% improvement is a more reasonable target for the near future.

3.2 Introduction

All-solid-state batteries (ASSBs) use solid electrolytes (SEs) to replace flammable liquid electrolytes (LE) resulting in safer batteries with increased energy density enabled by the lithium metal anode. Despite the breakthroughs at the material and cell level, there are still various challenges to overcome besides the grand challenge of manufacturing these types of batteries without altering current manufacturing processes at lower costs (< 100$/KWh). The electric vehicle market continues to drive the research on ASSBs and there has been a major push to introduce the technology into the market through partnerships between ASSB developers and major original equipment manufacturers (OEM) with ambitious Start of Production goals before 2025.

The promised increase in energy density of ASSBs is often quoted at 100% in volumetric and gravimetric values compared to Li-ion batteries (200 Wh/Kg or 400 Wh/l) when ultra-thin lithium is used. [1] For this to happen it is important to investigate all the changes that need to be made at the material and cell level compared to what is used in Li-ion cells (used herein as a baseline). This work focuses on the following limiting parameters: the thickness of the SE, anode and cathode mate-rials; N/P ratio; and amount of cathode active materials. In general, a SE has 10 to 100 times lower ionic conductivity (10^{-4} to 10^{-3} S/cm) compared to a LE (10^{-2} S/cm). The commercial battery uses a 20 μm separator with a LE, and to perform the same for ASSBs the thickness of the SE needs to be less than 20 μm if the remaining components in the battery stay the same (which is also a major challenge depending on the class of the SE). There are three classes of SEs: inorganic, polymer, and composite (hybrid) solid electrolytes. [2-5] Inorganic solid electrolytes (ISEs) generally have a lower ionic conductivity than LEs and re-searchers have explored ISEs comparable to or higher than LEs. [6-10] ISEs have excellent mechanical properties and can be made thinner than 20 μm. However, their brittleness, interface resistance, and chemical instability in air, moisture, and lithium have hindered their application in ASSBs. [11-18] Solid polymer electrolytes (SPEs) are another type that use a high molecular weight polymer that can solvate a

lithium salt. [2, 5, 19] The electrolyte Poly-ethylene-oxide (PEO) was first introduced by Michel Armand as a suitable electrolyte for the early generation of Li-ion batteries. [20-22] PEO electrolyte is easy to mass produce as a film and easy to utilize in roll-to-roll processes. In addition, it has better electrode/electrolyte interfacial resistance compared to the ISE. [23] Nevertheless, even though it is currently used in commercial batteries produced by Blue solutions in Canada and France for niche applications, its mass-market penetration is heavily hindered by the low conductivity (10^{-6} - 10^{-8} S cm^{-1}) at room temperature. [24, 25] To improve the conductivity at room temperature, additives such as succinonitriles have been studied. However, the increase in conductivity with the additives gives rise to poor mechanical and thermal properties. [19] As a result, composite (or hybrid) polymer electrolytes (CPEs) are suggested to maximize the advantages and minimize the disadvantages of ISEs and SPEs [2, 5, 16, 26-28]. Nevertheless, the fabrication of thin SEs is difficult. [29] Moreover, the reactivity of lithium towards ISEs and SPEs is another challenge that needs to be overcome. [26]

The projected 100% increase in energy density of ASSBs depends on the use of a lithium metal anode. However, the traditional assumption that dendrites will have more difficulty penetrating through the SE upon cycling is not entirely correct. [1, 30, 31] Nevertheless, lithium is a light metal with a high specific capacity (3.8 Ah/g) that is 10 times higher than that of the commercial graphite anode. Park et al. claim that using 190% excess Li metal as an anode decreases the volumetric energy density below that of a graphite anode. Therefore the benefits of high energy density are offset when using excess Li metal. [32] In principle, the lithium that shuttles between cathode and anode originates from the cathode, which suggests that any amount of lithium in the lithium metal anode will always be in excess. One approach to reduce the dead-weight associated with excess lithium is the use of an ultra-thin lithium anode with a thickness of less than 50 μm. [33] Moreover, the N/P ratio (capacity ratio of negative to positive) needs to be optimized for the lithium metal anode with the consideration of Coulombic efficiency, 99% [34], to maximize the energy density and durability. Another approach is an anode-free, “anode-less”, Li-ion battery [32, 35-37] that uses no or very thin layer of anode materials where N/P is close to 0, which can maximize the energy density. Lee et al. [37]. succeeded to use a Ag-C layer to control the lithium plating and stripping for 1000 cycles. The thickness of the Ag-C layer was 10 μm which is smaller than the cathode capacity used in the studies that result in lithium plating and stripping during cycling. Yan

et al. have also shown an anode-free concept by coating the copper electrode with a 2D boron nitride layer that results in lithium dendrites-free cycling. [38]

The ASSB cathode has only 60 to 85 wt% of cathode active material (CAM) due to the addition of SE to aid ionic conductivity. [2, 5, 37, 39, 40] The addition of SE in the cathode electrode increases the inactive material volume and mass, which lowers the energy density and is one of the limiting factors to improving the energy density. [41] The amount of CAM in a commercial battery range from 95 to 98% to maximize the energy density of the cell. The only way to compensate for the lower CAM in ASSBs is thicker electrodes, however, the study by Du et al. [42]. has shown that thick electrodes show lower power densities due to the limitation of the lithium diffusion in LEs. However, considering the lower ionic conductivity of most SEs, the cathode thickness would have a more severe effect on the power density.

The limiting factors studied in this work are (1) SE thickness, (2) N/P ratio that also corresponds to (2a) lithium metal thickness, (2b) cathode thickness, and (2c) cathode active material volume. Figure 3-1 shows the schematic of the battery and is used as the basis for evaluating the stack energy density using Eq. 3-1 from our previous work. [43] The energy of an active material is evaluated by multiplying the capacity by the voltage. However, the battery also contains inactive materials such as the casing, electrodes and separator. To find the influence of the inactive materials on the overall density of the battery, Obrovac et al. [44]. derived an equation for the stack energy density using the thickness of the cathode, anode, separator and current collector. The equation summarizes the dilution of the energy density due to the inactive materials. Their study concentrated on the effect of the average voltage and the capacity of the anode, while the rest of the parameters were held constant (such as the cathode thickness and the type of materials). In our previous work, we have applied the equation to study the effect of the changes in the silicon composite with changing the materials of the cathode to optimize the overall stack energy density. [43] The parameters optimized in our previous study were irreversible capacity, the energy density of the cathode, and the composition of the anode. In this study, we used the equation to study the change of all parameters except the thickness of the current collector to identify the limiting factors that influence the solid-state battery performance. The parameters are as described below and Table 3-1 shows the parameters used for the studies unless it is the factors of interest. The percent improvements are compared to the stack energy density when NMC and graphite are used and

parameters are also shown in Table 3-1. Eq. 3-1 does not include the thickness of the anode since it depends on the N/P ratio and the thickness of the cathode. Eq. 3-2 shows the volumetric reversible capacity of the electrode that depends on the percentage of the active material volume in the electrodes. Due to the limitation of the equation, the type of the solid electrolyte is not discussed in this work. Only the thickness dependency of the solid electrolyte is discussed. Furthermore, due to the focus of this theoretical work on the energy density, the cycle life and reversibility is assumed to be similar with the commercial battery.

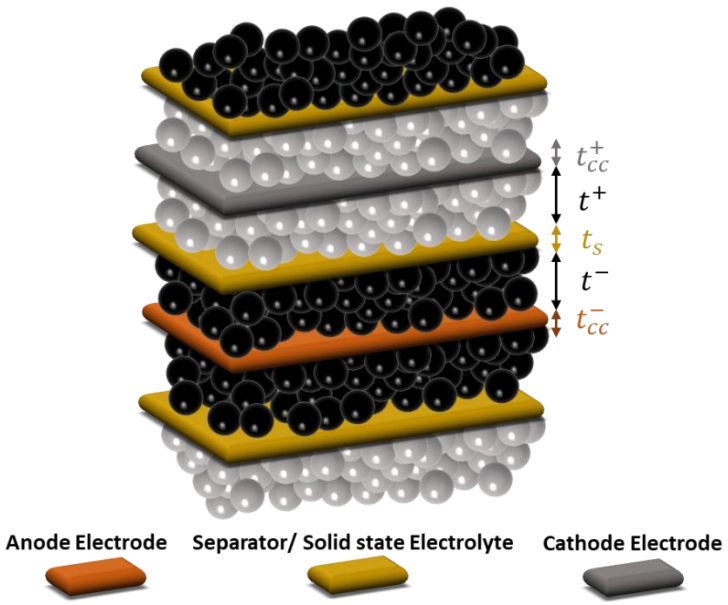


Figure 3-1 Schematic of stacked electrodes and separator/solid-state electrolyte

$$\breve{U}_R = \frac{2\tilde{q}_R^+ t^+}{t_{cc}^+ + t_{cc}^- + 2t_s + 2t^+\left[1 + \frac{\tilde{q}_R^+ \varphi_0^-}{\tilde{q}_R^- \varphi_0^+}\left(\frac{N}{P}\right)\right]}\left(V_{avg}^+ - V_{avg}^-\right) \quad \text{Eq. 3-1}$$

Where:

Constants

$t_{cc}^+ \; and \; t_{cc}^-$: Thickness of anode and cathode current collector

Parameters

t^+: Thickness of cathode

t_s: Thickness of separator

$\tilde{q}_R^+$ and $\tilde{q}_R^-$: Volumetric reversible capacity of anode and cathode

$\varphi_0^+ \; and \; \varphi_0^-$: Initial Coulombic efficiency of anode and cathode

N/P: Negative to positive capacity ratio

$V_{avg}^+ \; and \; V_{avg}^-$: Average voltage of anode and cathode

$$\tilde{q}_R = \rho_{AM} \times RC \times V_{AM} \qquad \text{Eq. 3-2}$$

$\tilde{q}_R$: Volumetric reversible capacity of the anode or cathode

RC: Reversible capacity of the anode or cathode

V_{AM}: Percent volume of active material in the anode or cathode

Table 3-1 Parameters used for the simulation

Electrode	*NMC with catholyte*	*Commercial NMC electrodes*	*Li anode*	*Graphite*
Active Material Density (g/mL)	4.77	4.77	0.53	2.26
$V_{average}$ *(V)*	3.7	3.7	0	0.125
Specific Gravimetric Capacity (mAh/g)	163	163	3860	350
Percentage of initial irreversible capacity (%)	6.0	6.0	6.0	6.0
Active material volume (%)	60	80	100	60
Thickness of coating (μm)	70	70	18	81
Thickness of current collector(μm)	15	15	15	15
N/P	-	-	1	1.1
Stack Energy Density (Wh/L)	-	-	1326[1]	729[2]

[1]Based on NMC/Li with 20 μm SE

[2]Based on NMC/Graphite with 20 um SE

3.3 Results and Discussion

Figure 3-2a shows the percent improvement of the stack energy density as N/P changes with different thicknesses of SE. All performances were compared with the NMC cathode and graphite anode. Three different thicknesses of SE were considered: 20, 50, and 100 μm to study the change in percent improvement compared to an NMC cathode and a graphite anode. Even though ionic conductivity is an important factor in SE performance, it was not considered in the evaluation since the energy density is a function of the materials' capacity and potential. As a result, we have assumed the ionic conductivity of the SE to be similar to LEs. 20 μm is the thickness of the separator in a commercial battery, where the target of the SE should be to match or surpass the performance of the LE batteries. 50 μm is the thickness where a SE can be prepared as a free-standing film using tape casting. It is likely a thinner electrolyte could be produced with process optimization, but 50 μm was selected for comparison to see what improvements we could observe. Finally, 100 μm is compared since the minimum possible thickness of the SE could be prepared by cutting a disc from films/pellets that are currently tested in lab-scale batteries for proof-of-concept. The highest percent improvement was achieved with an N/P ratio of 0 for all three SE thicknesses. A maximum percent improvement of 130% was achieved with a thickness of 20 μm. This improvement is very optimistic and also not realistic for three reasons. The commercial battery has an N/P ratio of 1.1 because of the initial irreversible capacity of the graphite anode. [45, 46] As discussed, when lithium metal is used, the lithium metal acts as a reservoir of lithium ions in the cell. [47] Theoretically, it is possible to omit lithium completely. However, when the Coulombic efficiency of lithium metal is considered the cell would need the excess lithium but not as much as N/P to 1.0. [32]

Figure 3-2b shows the thickness of the lithium as a function of the N/P ratio when 70 μm and 60% cathode active material thickness and volume are used. As shown, due to the high energy density of the lithium, 3.8Ah/g, the thickness of the anode is thin. When N/P is 1 the thickness of the lithium becomes 20 μm. This suggests the need for an ultrathin lithium anode, probably less than 50 μm to limit excess lithium to below 190%. [32] The result also emphasizes the need for an anode-free battery to improve energy density. Nevertheless, the anode-free battery also has a lot of challenges ahead. The stability of SEI formation for long cycle life is necessary, which mostly forms during the first cycle. The additive materials to form SEI need to be carefully chosen for ASSBs. Many research was performed on the LE batteries for lithium anode, [47-50] however,

most of the salt and solvents will not be required for ASSB. As a result, an additive for in-situ solid-electrolyte interphase formation could be considered to withhold the full cycling life of the battery as in LE, which can also improve the Coulombic efficiency of the lithium metal anode. [51] Optimization of the stack pressure applied to the cell during lithium plating and stripping for high CE is another factor since maintaining high pressure will require additional structural support at the pack level. Furthermore, the anode-free battery will experience close to 20 μm of added lithium plating which is close to a 20% expansion of the total thickness during charging to 2mAh/cm2, which is another concern for EV manufacturers. As a result, dense and porous bi or tri-layer solid electrolytes are studied. [52, 53]

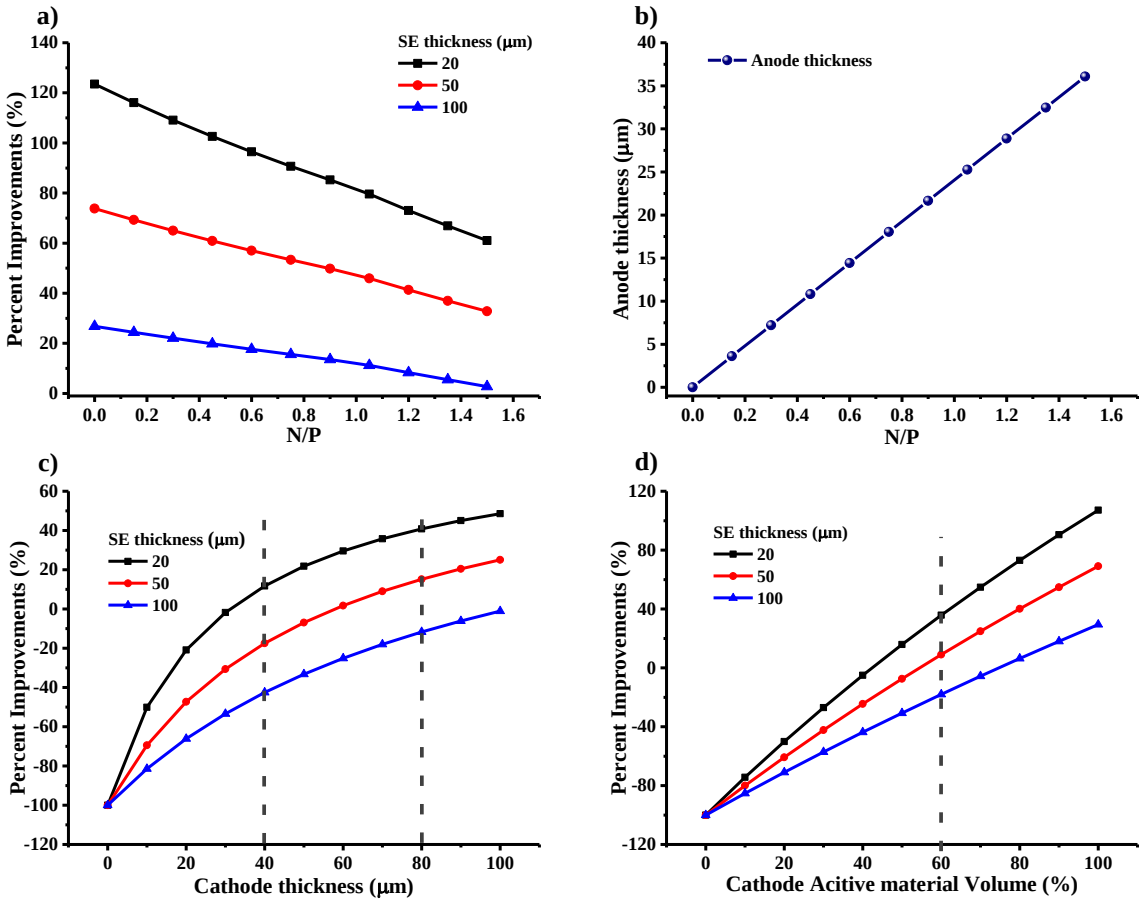


Figure 3-2 a) Percent improvement of the stack energy density as N/P changes, b) thickness of anode with N/P c) percent improvement of stack energy density as cathode thickness changes, d) percent improvement of stack energy density as cathode active material volume changes

Silicon anodes are also considered for next-generation anodes for Li-ion batteries. [54] It has 3.5 Ah/g of practical capacity and there are already some commercial batteries with small amounts of

silicon. The silicon anode for ASSBs has several benefits besides the high energy density. However, it still has well-known challenges such as a high-volume expansion when lithiated, which results in pulverization with repeated charging and discharging. The repeated volume expansion and contraction also exposes a new surface to the silicon particle that creates solid electrolyte interfaces and result in irreversible capacity when the LE is used. Using solid electrolytes, the SEI formation on the silicon can be minimized due to the solid-solid interaction which can also result in better durability for the silicon anode. [54] Two possible implementations of the silicon can be considered. Silicon as an anode that can result in a 25 μm thick anode or interfacial materials for the anode-free ASSB. The high specific capacity of the silicon is preferred for SSB compared to graphite anode, but not to the lithium anode since the lithium can be used with a lower N/P ratio. The silicon can act as an interfacial layer between the solid electrolyte and the current collector to protect the solid electrolyte and also improve interface resistance. The application can also lower the N/P ratio, increase overall ASSB energy density and compete with the ultra-thin lithium anode. Furthermore, silicon is abundant and less sensitive to air and moisture which is much easier to process, resulting in lower manufacturing costs.

Figure 3-2c shows the change of percent improvement as cathode thickness changes at different SE thicknesses. The results assume the cathode electrodes include SE resulting in 60% active material volume in CAM with an N/P ratio equal to 1. As shown when 100 μm SE is used no improvements can be achieved. It is also important to note, that commercial cathode thickness range from 40 to 80 μm, depending on the high-energy or high-power application purpose. As mentioned before thick cathodes hinder the power density in the LE [42] and SE will have a more profound effect due to the lower ionic conductivity. This suggests that the thinner the SE the higher the energy density. However, due to the challenge of scaling up the process to produce 20 μm SE, it becomes important to improve active material volume in the cathode and optimize N/P by reducing the amount of lithium used as an anode. It should also be pointed out that the SE also requires improvement of the interphases with the cathode and anode, which can also increase the thickness of the SE layers.

Figure 3-2d shows improvement in stack energy density as the cathode active material volume changes while the thickness of the cathode is fixed at 70 μm. As shown the improvements are highest when the thickness of the electrolyte is 20 μm. The commercial battery has 95 to 98% of

active material in the cathode which represents 80 to 95% active material volume (AV). This represents a 90% improvement with 95% AV and 20 μm SE thickness. However, most of the ASSB battery adds 20wt% SSE to the cathode electrode to provide ionic conductivity that results in 60% AV. With 60% AV, the thickness of the SE needs to be lower than 50 μm to obtain improvement in the stack energy density. The result also shows improving the AV for the cathode provides better performance improvement compared to the thickness of the cathode electrodes.

Figure 3-3 shows the percent improvement of the stack energy density when the cathode thickness and active material volume change at three SE thicknesses, 20, 50 and 100 μm. At 100 μm SE thickness the improvements can be 50% when the cathode thickness is 100 μm, but the study from Du et al. [42]. suggests that going over 60 μm will lower the power density due to the diffusion limitation. Also, the active material volume cannot be 100% on the ASSB due to the SE, carbon additives, and binders on the cathode. Devaux et al. [55]. studied a 54 μm thick SE and the maximum cathode thickness without impairing the battery power performance is 48 μm. The needs for the interphase layer on the SE are another important factor. The interfacial layer on the SE lowers interphase resistance and improves the contact between the anode and cathode. Also depending on the SE material, the interfacial layer can protect the SE from lithium metal. The thickness of the layer has not been studied, but based on our studies, the thickness should be part of the SE, which can reduce the actual SE layer to thinner than 20 or 50 μm. This imposes a very difficult challenge to the production of SE. In Fig. 3b, where SE thickness is 50 μm, the energy density starts improving when cathode thickness and CAM volumes are 40 μm and 60% respectively. The limitation of cathode thickness can only be overcome by a decrease in the SE thickness and/or an increase in CAM volume for significant improvement in the energy density. The result implies the importance of catholyte development. Many SE battery includes 10 to 40 wt% of SE in the CAM which corresponds to less than 50% CAM volume. The catholyte in the CAM has many challenges. The amount of catholyte will impact the thickness of the cathode to optimize the energy and power density. The catholyte also needs to have good ionic conductivity to deliver lithium ions to and from the SE. It also needs to have a good interface coating to minimize the interface resistance to lower the overall impedance. Another possible solution to improve the overall energy density can be using the high voltage (5 V) spinel cathode, $LiMn_{1.5}Ni_{0.5}O_4$, LMNO, instead of the conventional $LiNi_{0.33}Mn_{0.33}Co_{0.33}O_2$, NMC 111, and its variants. Based on the calculation when all parameters are the same, due to the higher working

potential, 4.7 V, the stack energy density can be improved by up to 82%, which is 20% higher than NMC which is used to evaluate the energy density in this work. However, due to the instability of most SE at high potential, it is difficult to find compatible materials that can last and perform in the battery. Currently, NMC is still challenging due to the instability of the SE over 3.7 V, and many studies are performed using $LiFePO_4$ which has a much lower average voltage of 3.4 V.

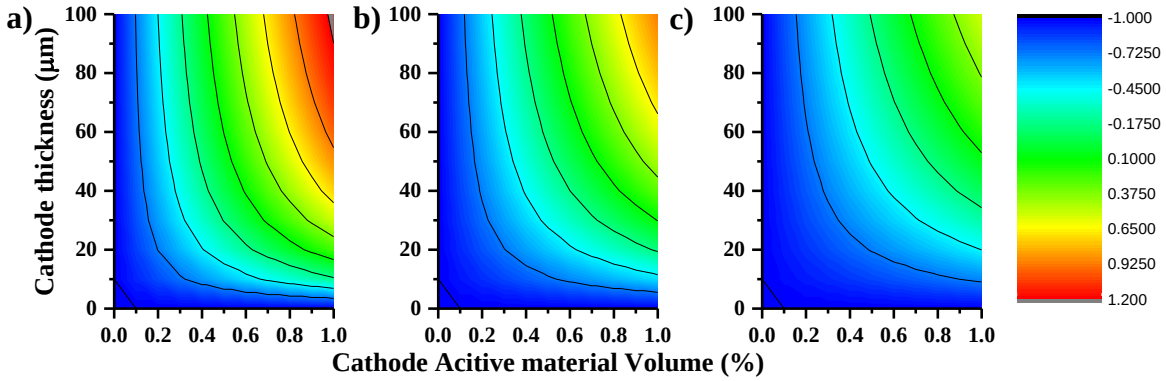


Figure 3-3 Performance improvement on cathode thickness and active material volume on three SE thicknesses a) 20 µm, b) 50 µm, and c) 100 µm, N/P ratio = 1.

Figure 3-4 shows the performance improvement as a function of N/P and CAM volume at different SE thicknesses of 20, 50, and 100 µm. Lowest N/P, high CAM volume, and thin SE will provide the biggest improvement as shown in Figure 3-4a. However, CAM volume cannot be higher than 95%, due to the carbon additives and polymer binders, especially when the SE is added to the cathode. May researcher use 50 to 85 wt% CAM which corresponds to 40 - 75% CAM by volume. This implies that with 100 µm SE thickness, the ASSB will not achieve any improvement in energy density when a 70 µm thick cathode is used. The SE should be at least 50 µm to see the improvement in the energy density. The N/P ratio has a minor effect compared to CAM volume. N/P should be less than 1 to benefit from the high energy density of ASSB and it is only possible when lithium metal is used. To get lower than 1 the manufacturing process needs to be improved since the thickness of the lithium anode becomes less than 25 µm.

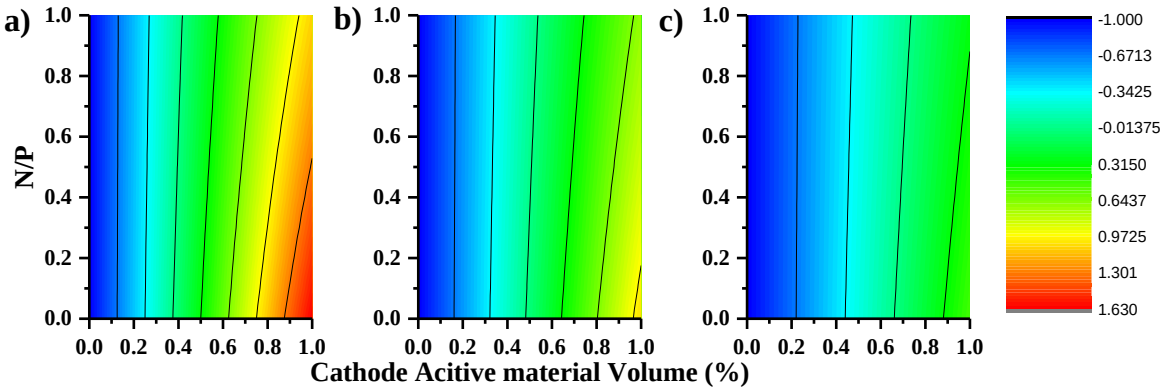


Figure 3-4 Performance improvement on cathode thickness and N/P ratio on three SE thicknesses a) 20 μm, b) 50 μm, and c) 100 μm, cathode thickness = 70 μm

Table 3-2 shows the possible generation of ASSB. Generation 1, GEN 1, can be the current state of the ASSB where the active material in volume, N/P ratio and thickness of SE are set to 60%, 1, and 100 μm, respectively. This results in no improvements, but poor performance. This generation would be better described as a proof of concept only. Generation 2, GEN 2, can be the next ASSB where the active material in volume, N/P ratio and thickness of SE are set to 70%, 0.5, and 50 μm, respectively. These factors were determined by considering improvement on the cathode formulation to increase the active material in the cathode, minimizing the amount of lithium in the anode, and thinner fabrication of SE. GEN 2 could be the next commercial ASSB that can be introduced in the near future. This would be the best target with the most recent technological development to achieve 30% higher energy density compared to the current commercial Li-ion battery. With these improvements, it is possible to obtain a 33% increase in the stack energy density. Improving stack energy density does not have equal improvement to the energy storage system as it was shown by Lobberding et al. [56]. that the energy density of the whole system is 60% of that of the cell. When the estimation is considered the energy density improvement for the whole system can be 23%. The final concept generation 3, GEN 3, would be the maximum active material volume in the cathode, anode-free battery, and 20 μm SE same thickness as the commercial separator. This improvement results in 110% and 77% improvement in the stacking and the system energies, respectively. GEN 3 would be the holy grail for the ASSB that can achieve

close to a 100% energy density increase. To achieve the GEN 3 battery following parameters should be met and also the challenges would need to be solved.

Table 3-2 Possible strategic target for SSB energy density

	GEN 1	GEN 2	GEN 3
ACTIVE MATERIAL VOLUME IN CATHODE	60%	70%	80%
N/P RATIO	1	0.5	0
THICKNESS OF SE	100 μm	50 μm	20 μm
PERCENT IMPROVEMENTS IN STACK ENERGY DENSITY	-18%	33%	110%
PERCENT IMPROVEMENT TO THE SYSTEM	N/A	23%	77%

3.4 Conclusion

In this study, we have calculated the energy densities of ASSBs using a different set of parameters and compared energy improvements to a baseline of current lithium-ion batteries under different scenarios. By assuming the ionic conductivity of the SE to be the same as the LE, the influence of certain limiting factors (SE thickness, cathode thickness, cathode active material volume, N/P ratio and lithium metal thickness) on the energy density was evaluated. From this study, we found that the SE thickness must be 20 um or less to achieve the highest possible energy improvements. Also, we found that thicker cathodes can provide higher energy density reaching 50% when the cathode thickness is 100 um, but this will have a negative impact on power density. We found that the active material volume in the cathode must reach 80 % which corresponds to the maximum 95% active material weight at the optimized SE and cathode thicknesses, 20 um and 100 um, respectively. However, this target is hard to achieve because of the need for a critical volume of catholyte that is currently way higher than 20% of the cathode formulations. As for the N/P ratio we found that it must be close to 0 that can only be achieved by the use of anode-free or ultrathin lithium anodes. This study demonstrates that are still ongoing challenges that are yet to be overcome before the successful commercialization of All-Solid State Batteries.

3.5 References

1. Randau, S., et al., *Benchmarking the performance of all-solid-state lithium batteries.* Nature Energy, 2020. **5**(3): p. 259-270.
2. Al-Salih, H., et al., *A Polymer-Rich Quaternary Composite Solid Electrolyte for Lithium Batteries.* Journal of the Electrochemical Society, 2020. **167**(7).
3. Abouali, S., et al., *Garnet-Based Solid-State Li Batteries: From Materials Design to Battery Architecture.* ACS Energy Letters, 2021. **6**(5): p. 1920-1941.
4. Wang, C., et al., *Garnet-Type Solid-State Electrolytes: Materials, Interfaces, and Batteries.* Chemical Reviews, 2020. **120**(10): p. 4257-4300.
5. Chen, L., et al., *PEO/garnet composite electrolytes for solid-state lithium batteries: From "ceramic-in-polymer" to "polymer-in-ceramic".* Nano Energy, 2018. **46**: p. 176-184.
6. Bachman, J.C., et al., *Inorganic Solid-State Electrolytes for Lithium Batteries: Mechanisms and Properties Governing Ion Conduction.* Chemical Reviews, 2016. **116**(1): p. 140-162.
7. Ma, Z., H.G. Xue, and S.P. Guo, *Recent achievements on sulfide-type solid electrolytes: crystal structures and electrochemical performance.* Journal of Materials Science, 2018. **53**(6): p. 3927-3938.
8. Varzi, A., et al., *Challenges and prospects of the role of solid electrolytes in the revitalization of lithium metal batteries.* Journal of Materials Chemistry A, 2016. **4**(44): p. 17251-17259.
9. Zhang, Y., et al., *Garnet-Based Solid-State Lithium Fluoride Conversion Batteries Benefiting from Eutectic Interlayer of Superior Wettability.* ACS Energy Letters, 2020. **5**(4): p. 1167-1176.
10. Yang, L., et al., *Rapid sintering method for highly conductive Li7La3Zr2O12 ceramic electrolyte.* Ceramics International, 2020. **46**(8): p. 10917-10924.
11. Pang, Y., et al., *Electrolyte/Electrode Interfaces in All-Solid-State Lithium Batteries: A Review.* Electrochemical Energy Reviews, 2021. **4**(2): p. 169-193.
12. Chen, C.H. and K. Amine, *Ionic conductivity, lithium insertion and extraction of lanthanum lithium titanate.* Solid State Ionics, 2001. **144**(1-2): p. 51-57.
13. Cho, Y.H., et al., *Mechanical properties of the solid Li-ion conducting electrolyte: Li 0.33 La 0.57 TiO 3.* Journal of Materials Science, 2012. **47**(16): p. 5970-5977.
14. Wang, M. and J. Sakamoto, *Correlating the interface resistance and surface adhesion of the Li metal-solid electrolyte interface.* Journal of Power Sources, 2018. **377**: p. 7-11.
15. Schmaltz, T., et al., *A Roadmap for Solid-State Batteries.* Advanced Energy Materials, 2023. **13**(43): p. 2301886.
16. Keller, M., A. Varzi, and S. Passerini, *Hybrid electrolytes for lithium metal batteries.* Journal of Power Sources, 2018. **392**: p. 206-225.
17. Zhang, Q., et al., *Sulfide-Based Solid-State Electrolytes: Synthesis, Stability, and Potential for All-Solid-State Batteries.* Advanced Materials, 2019. **31**(44).
18. Sharafi, A., et al., *Surface Chemistry Mechanism of Ultra-Low Interfacial Resistance in the Solid-State Electrolyte Li7La3Zr2O12.* Chemistry of Materials, 2017. **29**(18): p. 7961-7968.
19. Echeverri, M., N. Kim, and T. Kyu, *Ionic conductivity in relation to ternary phase diagram of poly(ethylene oxide), succinonitrile, and lithium bis(trifluoromethane)sulfonimide blends.* Macromolecules, 2012. **45**(15): p. 6068-6077.
20. Armand, M. and M. Duclot, *Composition composite de matériau d'électrode et d'un matériau élastomère à conduction ionique et électrode formée à partir de cette composition.* French Pat, 1978.
21. Armand, M.B., J.M. Chabagno, and M. Duclot, 1978.
22. Armand, M.B., J.M. Chabagno, and M.J. Duclot, 1979: p. 131-136.

23. Sun, C., et al., *Recent advances in all-solid-state rechargeable lithium batteries.* Nano Energy, 2017. **33**: p. 363-386.
24. Fullerton-Shirey, S.K. and J.K. Maranas, *Effect of LiClO 4 on the structure and mobility of PEO-based solid polymer electrolytes.* Macromolecules, 2009. **42**(6): p. 2142-2156.
25. Kim, J.G., et al., *A review of lithium and non-lithium based solid state batteries.* Journal of Power Sources, 2015. **282**: p. 299-322.
26. Bag, S., et al., *LiF modified stable flexible PVDF-garnet hybrid electrolyte for high performance all-solid-state Li–S batteries.* Energy Storage Materials, 2020. **24**: p. 198-207.
27. Hu, J., et al., *Unlocking solid-state conversion batteries reinforced by hierarchical microsphere stacked polymer electrolyte.* Science Bulletin, 2021. **66**(7): p. 694-707.
28. An, H., et al., *Coupling two-dimensional fillers with polymer chains in solid polymer electrolyte for room-temperature dendrite-free lithium-metal batteries.* Energy Storage Materials, 2021. **43**: p. 358-364.
29. Wu, J., et al., *Reducing the thickness of solid-state electrolyte membranes for high-energy lithium batteries.* Energy and Environmental Science, 2021. **14**(1): p. 12-36.
30. LePage, W.S., et al., *Lithium Mechanics: Roles of Strain Rate and Temperature and Implications for Lithium Metal Batteries.* Journal of The Electrochemical Society, 2019. **166**(2): p. A89.
31. Liu, J., et al., *Unlocking the Failure Mechanism of Solid State Lithium Metal Batteries.* Advanced Energy Materials, 2022. **12**(4): p. 2100748.
32. Park, S.H., et al., *Toward high-performance anodeless batteries based on controlled lithium metal deposition: a review.* Journal of Materials Chemistry A, 2021. **9**(26): p. 14656-14681.
33. Li, T., et al., *Dendrite-free sandwiched ultrathin lithium metal anode with even lithium plating and stripping behavior.* Nano Research, 2019. **12**(9): p. 2224-2229.
34. Adams, B.D., et al., *Accurate Determination of Coulombic Efficiency for Lithium Metal Anodes and Lithium Metal Batteries.* Advanced Energy Materials, 2018. **8**(7): p. 1702097.
35. Weber, R., et al., *Long cycle life and dendrite-free lithium morphology in anode-free lithium pouch cells enabled by a dual-salt liquid electrolyte.* Nature Energy, 2019. **4**(8): p. 683-689.
36. Louli, A.J., et al., *Diagnosing and correcting anode-free cell failure via electrolyte and morphological analysis.* Nature Energy, 2020. **5**(9): p. 693-702.
37. Lee, Y.G., et al., *Publisher Correction: High-energy long-cycling all-solid-state lithium metal batteries enabled by silver–carbon composite anodes (Nature Energy, (2020), 5, 4, (299-308), 10.1038/s41560-020-0575-z).* Nature Energy, 2020. **5**(4): p. 348.
38. Yan, K., et al., *Ultrathin Two-Dimensional Atomic Crystals as Stable Interfacial Layer for Improvement of Lithium Metal Anode.* Nano Letters, 2014. **14**(10): p. 6016-6022.
39. Zhang, B., et al., *Solid-state lithium metal batteries enabled with high loading composite cathode materials and ceramic-based composite electrolytes.* Journal of Power Sources, 2019. **442**: p. 227230.
40. Ohta, S., et al., *All-solid-state lithium ion battery using garnet-type oxide and Li3BO3 solid electrolytes fabricated by screen-printing.* Journal of Power Sources, 2013. **238**: p. 53-56.
41. Al-Salih, H., et al., *Composite Cathodes for Solid-State Lithium Batteries:"Catholytes" the Underrated Giants.* Advanced Energy and Sustainability Research, 2022. **3**(8): p. 2200032.
42. Du, Z., et al., *Understanding limiting factors in thick electrode performance as applied to high energy density Li-ion batteries.* Journal of Applied Electrochemistry, 2017. **47**(3): p. 405-415.
43. Yim, C.-H., et al., *Towards Improving the Practical Energy Density of Li-Ion Batteries: Optimization and Evaluation of Silicon:Graphite Composites in Full Cells.* Journal of The Electrochemical Society, 2017. **164**(1): p. A6294.
44. Obrovac, M.N. and V.L. Chevrier, *Alloy Negative Electrodes for Li-Ion Batteries.* Chemical Reviews, 2014. **114**(23): p. 11444-11502.

45. Sturman, J., et al., *Communication—Design of LiNi0.2Mn0.2Co0.2Fe0.2Ti0.2O2 as a High-Entropy Cathode for Lithium-Ion Batteries Guided by Machine Learning.* Journal of The Electrochemical Society, 2021. **168**(5): p. 050541.
46. Kim, C.-S., et al., *Effects of Capacity Ratios between Anode and Cathode on Electrochemical Properties for Lithium Polymer Batteries.* Electrochimica Acta, 2015. **155**: p. 431-436.
47. Louli, A.J., et al., *Optimizing Cycling Conditions for Anode-Free Lithium Metal Cells.* Journal of The Electrochemical Society, 2021. **168**(2): p. 020515.
48. Xie, Z., et al., *Anode-free rechargeable lithium metal batteries: Progress and prospects.* Energy Storage Materials, 2020. **32**: p. 386-401.
49. Li, N.-W., et al., *A Flexible Solid Electrolyte Interphase Layer for Long-Life Lithium Metal Anodes.* Angewandte Chemie International Edition, 2018. **57**(6): p. 1505-1509.
50. Zou, C., et al., *In Situ Formed Protective Layer: Toward a More Stable Interface between the Lithium Metal Anode and Li6PS5Cl Solid Electrolyte.* ACS Applied Energy Materials, 2022. **5**(7): p. 8428-8436.
51. Liu, J., et al., *In situ regulated solid electrolyte interphase via reactive separators for highly efficient lithium metal batteries.* Energy Storage Materials, 2020. **30**: p. 27-33.
52. Fu, K., et al., *Three-dimensional bilayer garnet solid electrolyte based high energy density lithium metal–sulfur batteries.* Energy & Environmental Science, 2017. **10**(7): p. 1568-1575.
53. Lei, M., et al., *NASICON-based solid state Li-Fe-F conversion batteries enabled by multi-interface-compatible sericin protein buffer layer.* Energy Storage Materials, 2022. **47**: p. 551-560.
54. Tan, D.H.S., et al., *Carbon-free high-loading silicon anodes enabled by sulfide solid electrolytes.* Science, 2021. **373**(6562): p. 1494-1499.
55. Devaux, D., et al., *Effect of Electrode and Electrolyte Thicknesses on All-Solid-State Battery Performance Analyzed With the Sand Equation.* Frontiers in Energy Research, 2020. **7**.
56. Löbberding, H., et al., *From Cell to Battery System in BEVs: Analysis of System Packing Efficiency and Cell Types.* World Electric Vehicle Journal, 2020. **11**(4): p. 77.

Chapter 4: Leveraging Entropy for Enhanced Energy Density in Cathode-Active Materials for Li-ion Batteries

This chapter has been adapted from a research paper submitted to the *Nature communication.*

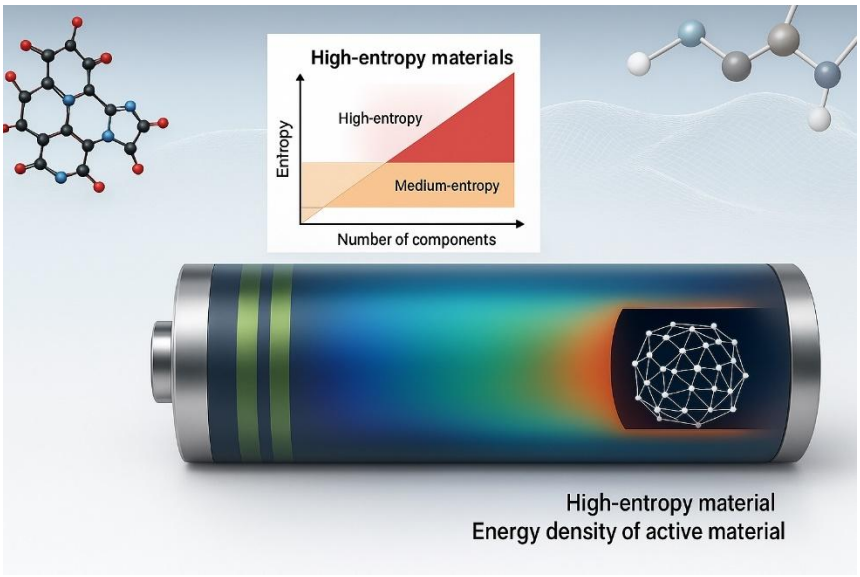
Chapter 3 demonstrated that the achievable energy density of solid-state batteries is far more constrained than often claimed and that maximizing reversible lithium utilization within the cathode active material is the most effective route toward meaningful performance gains. This conclusion shifts the central challenge from cell architecture alone to the fundamental thermodynamic behavior of cathode materials under deep delithiation. In particular, it raises the critical question of why certain cathode compositions tolerate extensive lithium extraction while others undergo irreversible phase transformations and rapid degradation.

Building on this system-level insight, Chapter 4 develops a thermodynamic framework that reframes entropy as a dynamic variable governing cathode stability during electrochemical cycling. Rather than treating entropy as a static material descriptor associated with compositional complexity, this chapter focuses on the magnitude of entropy change during lithiation and delithiation as a rational design constraint. Through analytical modeling of mixing entropy combined with density functional theory calculations, this chapter establishes a quantitative link between entropy change, reversible lithium utilization, and structural stability, thereby introducing an entropy-based design paradigm for high-energy cathode materials.

4.1 Abstract:

Cathode-active materials (CAMs) play a crucial role in enhancing the energy density and reducing the cost of Li-ion battery cells. This improvement can be realized in commercially-relevant layered oxides $LiNi_xMn_yCo_zO_2$, known as NMCs, by maximizing the nickel content at the expense of cobalt. While higher nickel content boosts energy density by increasing both potential and capacity, it can result in lower capacity retention compared to first-generation NMC CAMs with x=y=z=1 or even with z=1 and x=y=0. To address this challenge, the high-entropy concept is being explored as a means to improve the material's structural stability during battery operation, thereby enhancing capacity retention and extending cycle life. This study presents evidence through calculations of the mixing entropy ($\Delta S_{mix} = -nR\sum x \ln x$) effect on CAMs and suggests rational design methods for next-generation CAMs. The mixing entropy is calculated for commercial CAMs and

estimated for potential CAMs to achieve better energy density in layered oxide types such as $LiNi_{0.7}Mn_{0.15}Co_{0.15}O_2$ or $LiNi_{0.7}Mn_{0.25}Al_{0.05}O_2$. The findings underscore the potential of 70% nickel and cobalt-free CAMs, utilizing entropy as a design principle.



4.2 Introduction

The invention and development of the Li-ion battery have been dramatic in the last three decades. Initially used in small handheld electronics, it is now found in all handheld devices, stationary energy storage, and electric vehicles. The popularity of the Li-ion battery can be attributed to its high energy density (150-200 Wh/Kg) at the cell level compared to other battery chemistries. The rapid development of Li-ion batteries is largely driven by the significant pull from the electric vehicle market. Electric vehicles require high-energy-density battery packs (70-100 KWh), and although Li-ion batteries already have the highest energy density at the cell level (200Wh/Kg) among other battery chemistries, there is a need for even higher energy density (>450Wh/Kg) in the market.[1-3]

The cathode active material (CAM) in the Li-ion battery is a major cost factor, accounting for 50% of the total cost. Due to its high cost, extensive research is being conducted to reduce the cost of the cathode or find alternative materials.[4-9] One of the biggest trends in recent years is the use of high nickel content cathodes, which reduce the usage of the more expensive and less abundant cobalt ($24/kg for Co compared to $16/kg for Ni).[10] Another alternative is the use of olivine

cathodes, such as $LiFePO_4$, which utilize more abundant elements and is anticipated to acquire 50% of the market by 2050.[5]

High nickel cathodes belong to the layered oxide family or R3m structure. In this work, studies are focused on the layered oxide cathodes. The initial layered oxide cathode, $LiCoO_2$ (LCO), is still being used but is expensive due to the cost of cobalt. As a result, the battery market has shifted towards reducing cobalt usage and replacing it with manganese, nickel and other elements to stabilize the structure (e.g. Al, Zn, Mg, Ta etc).[6, 11, 12] The second generation of layered oxide cathodes is $LiNi_{1/3}Mn_{1/3}Co_{1/3}O_2$ (NMC111), where the cobalt content is reduced from 100% to 33%. The subsequent generations are geared towards increasing the Ni content. The NMC 111 can be considered as low Ni NMC and others such as $LiNi_{0.5}Mn_{0.3}Co_{0.2}O_2$ (NMC532), $LiNi_{0.6}Mn_{0.2}Co_{0.2}O_2$ (NMC622), can be considered as medium-Nickel NMCs and $LiNi_{0.8}Mn_{0.1}Co_{0.1}O_2$ (NMC811) that can be considered as a high Nickel NMC. These cathodes have reduced cobalt usage by 90% compared to LCO. Additionally, the increase in nickel content in the structure, while reducing cobalt, has led to an increase in the specific capacity of the layered oxide, as shown in Table 4-1. The rise in the capacity, voltage and hence the energy density of the CAM as the nickel content increases is due to Ni-O-Ni binding energy and the redox state of the Ni^{2+}/Ni^{4+}. However, the redox activity of the nickel introduces the risk of cation mixing where Ni cations move to the Li layer.[6, 13, 14]

Table 4-1 Specification of the commercial CAMs[6]

	Practical Capacity (mAh/g)	*Average voltage (V)*	*MW*	*Theoretical Capacity (mAh/g)*	*Yield of Capacity (%)*
LCO	160	3.9	97.87	273.88	58%
NMC111	155	3.75	96.46	277.88	56%
NMC532	165	3.75	96.56	277.61	59%
NMC622	175	3.75	96.93	276.53	63%
NMC811	200	3.75	97.29	275.53	73%

Recently, the high-entropy concept has inspired the development of materials that have garnered significant attention due to their apparent advantages over conventional materials such as metal alloys, ceramics, and many others. Ouyang et al. have summarized the benefits of these high-

entropy battery materials, including the suppression of undesired short-range order, frustration with the energy landscape, decreased volumetric change, and reduced reliance on critical metals[15]

Total mixing entropy has four contributions: configurational, vibrational, magnetic dipole, and electronic randomness. However, configurational entropy is dominant over the other three contributions.[16, 17] Baek et al. have discussed the entropic potential of the cathode and they found that electronic entropy has a minimal effect on the potential. Sakar et al. introduced the mixing entropy for oxide systems using Equation 1,[18] and there are ongoing discussions on how it should be evaluated based on the type and structure of the material. For instance, Oyange et al. claim that configurational entropy should also consider the lattice sites, which is true when the structural stability is considered for R3m layered oxides.[15] However, when the transient state of lithium intercalation is considered it is important to take into account the mix of solids as a single-phase material. For this study to correlate the cathode properties, focusing on layered oxides and discussing the entropy of the solid solution systems, Eq. 4-1 is sufficient. High configurational entropy is defined as five or more elements mixed in equal amounts within a structure or system, resulting in a value greater than 1.6R. This high entropy is sufficient to prevent any strong atomic ordering at high temperatures, thereby resulting in a lower temperature of fusion. [15, 16, 18] Zheng et al. have shown that increasing the configurational entropy in CAMs can also lead to high ionic conductivity due to local disorder and promoted site percolation.[19]

$$\boldsymbol{S_{mix}^{Ideal} = -R\left(\sum_{Cation} xlnx + \sum_{Anion} ylny\right)}$$

Eq. 4-1

To understand the effect of entropy, the fundamental equation, Eq. 4-2, that correlates Gibbs free energy and the electrochemical potential needs to be recalled to find the relationship between entropy and the energy density of the active material.

$$\Delta G = -zFE_{rxn}$$

Eq. 4-2

where z is the number of electrons exchanged during the electrochemical reaction, F is Faraday's constant, and E is the difference in potential between the cathode and anode active materials. The equation is based on two redox half-reactions, and for a Li-ion battery with layered oxide material, the following full reaction is generally considered:

$$LiTMsO_2 + C_6 \rightleftharpoons Li_xTMsO_2 + Li_{1-x}C_6$$

Eq. 4-3

where TMs are transition metals. The reaction can also be separated into two half-reactions as follows:

$$Cathode: LiTMsO_2 \rightleftharpoons Li_xTMsO_2 + Li^+_{1-x} + e^-_{1-x},\ E^o = 3.8{\sim}3.9V\ vs\ Li/Li^+$$

Eq. 4-4

$$Anode: C_6 + Li^+_{1-x} + e^-_{1-x} \rightleftharpoons Li_{1-x}C_6, \qquad E^o = 0.1V\ vs\ Li/Li^+$$

Eq. 4-5

For cathode active materials, during lithium intercalation the phases undergo an ideal mix of solids, causing the potential profile of the mix to change without any major phase transitions, except for NMC811. This can be observed from the potential profile of the cathode active material (CAM), where a smooth slope in potential change is seen as lithium is intercalated, hence charged or discharged. When we look closer at the cathode during lithiation and delithiation, it is a phase change between two structures, Li and $TMsO_2$, which can also be expressed in terms of the Gibbs free energy of the mix as shown:

$$\Delta G_{mix} = \Delta H_{mix} - T\Delta S_{mix}$$

Eq. 4-6

The Gibbs free energy represents the maximum work a battery can perform due to the electrochemical reaction, where ΔH_{mix} is the change in enthalpy (heat of the electrochemical reaction) and ΔS_{mix} is the change in entropy. The changes in Gibbs free energy (ΔG), enthalpy (ΔH), and entropy (ΔS) of the battery's electrochemical reaction can be assessed through electrochemical measurements that observe variations in the open circuit potential as a function of

temperature, using equations 2 and 6. When the temperature varies, the derivative of the potential change corresponds to the change in entropy, as follows:

$$\Delta G_{mix} = \Delta H_{mix} - T\Delta S_{mix} = -zFE$$

Eq. 4-7

$$\frac{dG}{dT} = -\frac{dS}{dT} = -nF\frac{dE}{dT}$$

Eq. 4-8

The Gibbs free energy for a solid mixture is associated only with the half-reaction described in Eq. 4-4, which also relates to the cathode potential in Eq. 4-2. In an ideal mixture, the enthalpy remains constant, leading to a more significant impact of entropy changes on the Gibbs energy and, consequently, on the potential change. [17] The central discussion revolves around whether high entropy contributes to the overall change in Gibb's energy and thus enhances the energy density of a cell. At first glance, it is evident that the high entropy from Eq. 4-6 affects the potential of the half-reaction by reducing the ΔG when enthalpy is assumed constant or experiences minimal change. A larger ΔG in the full reaction is necessary to achieve a higher E, and thus a greater potential. During battery charging and discharging, maintaining a constant or minimal change in ΔG at the cathode will ensure a consistently higher potential for the full cell or reaction. Therefore, minimizing the change in ΔG during the half-reaction is advantageous, and smaller changes in ΔS are also preferable. $LiFePO_4$ (LFP) serves as a prototypical example of a cathode material exhibiting negligible variation in Gibbs free energy during lithiation and delithiation, a consequence of its distinct two-phase reaction between $LiFePO_4$ and $FePO_4$. The absence of a continuous solid-solution region minimizes the configurational entropy change, resulting in a nearly constant Gibbs free energy of mixing (G_{mix}). This thermodynamic stability under cycling conditions contributes to the exceptional capacity retention typically observed for LFP compared with layered oxide cathodes such as $LiNi_xMn_yCo_zO_2$ (NMC).

Extending this thermodynamic understanding to layered oxides suggests that careful control of the entropy of mixing (S_{mix}) is critical for achieving an optimal balance between structural stability and energy density. In these systems, moderate changes in S_{mix} can enhance energy density and maintain reversible Li intercalation, whereas excessive entropy change during cycling may induce

lattice instabilities and promote phase transitions—phenomena particularly evident in high-nickel compositions (>80% Ni). Consequently, fine-tuning both the magnitude and compositional dependence of S_{mix} represents a key design strategy for developing layered oxide cathodes with improved structural robustness and sustained electrochemical performance. Since materials with low or high entropy, NMC811 or NMC111 respectively, can lead to significant changes during lithiation or de-lithiation, there may be an optimal medium-entropy material that stabilizes and enhances high-energy CAM. This analysis suggests that high-entropy CAMs might not necessarily provide the highest energy density overall.

While increasing nickel content in layered oxide cathodes is an effective strategy for enhancing energy density, it is accompanied by pronounced structural instability, phase transitions, and capacity fade under deep delithiation. Recent interest in entropy assisted materials has suggested that configuration disorder may stabilize cathode structures; however, most existing studies treat entropy as a static descriptor evaluated at a fixed composition. In contrast, lithium-ion battery cathodes operate under continuously evolving compositions during charge and discharge. Under these conditions, the absolute magnitude of entropy is insufficient to describe stability. Instead, the change in entropy during lithiation and delithiation emerges as a critical thermodynamic parameter governing reversibility and accessible energy density.

In this chapter, entropy is treated within the framework of mixing entropy (ΔS_{mix}), which governs the Gibbs free energy of lithium intercalation and directly influences the electrochemical potential of the cathode. For layered oxide cathode active materials operating predominantly within a solid solution regime, the composition dependent contribution to the mixing entropy is dominated by configurational disorder, arising primarily from lithium vacancies in the lithium layers and from the distribution of transition-metal species within the octahedral sublattice. Accordingly, the analytical expressions employed in this work explicitly evaluate the configurational component of the mixing entropy, which is used as a mechanostatic descriptor to track entropy change during cycling as a function of lithium content and transition-metal composition. While the total mixing entropy also includes vibrational, electronic, and magnetic contributions, these terms are assumed to exhibit a weaker dependence on state of charge and are therefore not explicitly resolved in the present analysis. Under these assumptions, the configurational contribution provides a physically transparent and composition-sensitive proxy for assessing entropy change during cycling during

lithiation and delithiation, enabling systematic comparison across layered oxide cathodes with varying nickel contents.

Building on this framework, this chapter presents a thermodynamic description in which entropy is treated as a dynamic variable and systematically examines how the configurational component of mixing entropy evolves with lithium content and transition-metal composition in layered oxide cathodes. Using a combination of analytical entropy modeling and density functional theory calculations, this work demonstrates that cathodes with moderate configurational entropy—particularly those containing approximately 70% nickel—exhibit minimal entropy change during delithiation. This reduced entropy variation enables deeper reversible lithium extraction while maintaining structural stability.

Overall, the results establish that the entropy change during cycling, rather than the absolute entropy magnitude, provides a rational thermodynamic design criterion for developing high-energy layered oxide cathode active materials. In this context, "moderate entropy" refers to compositions that exhibit sufficiently low entropy variation during cycling to preserve solid-solution behavior, rather than those characterized by an intermediate absolute entropy value.

4.3 Methods

4.3.1 Mixing entropy.

Mixing entropy provides a first-order thermodynamic descriptor of disorder arising from the distribution of atomic species over crystallographic sites. In layered oxide cathodes of the general form Li_xTMsO_2, mixing entropy is dominated by cation disorder, while the anion sublattice consists exclusively of oxygen and therefore does not contribute to entropy change during cycling. Although total entropy also includes configurational, vibrational, electronic, and magnetic contributions, mixing entropy represents the dominant compositional term relevant to cation mixing and lithium vacancy formation during electrochemical cycling.

In this study, mixing entropy is evaluated to isolate the effect of lithium content and transition-metal composition on entropy change during cycling during lithiation and delithiation. This approach enables direct comparison between cathode materials with different nickel contents while maintaining a consistent thermodynamic basis. Importantly, the focus is placed not on the

absolute value of configurational entropy at a given composition, but on how entropy evolves as lithium is extracted from the structure—an aspect that has been largely overlooked in prior cathode design studies.

$$Li_xNi_zMn_{1-z/2}Co_{1-z/2}O_2$$

where x and z are greater than 0 and less than 1, within the range of the R3m layered oxide. When the cathode is charged, the lithium is taken out from the structure, which results in changes of mixing entropy-based on equation 1 resulting in varying the entropy during the change of the state of charge (SOC). SOC is 0% when x is 1, and x will vary at SOC 100% that depends on the stability of the materials, which will differ based on the nickel content. The exact configurational entropy can be evaluated with the Eq. 4-9:

$$\boldsymbol{S_{mix}[J/mol\,K]} = -\frac{\boldsymbol{R}}{\boldsymbol{1+x}}\left(\boldsymbol{x ln}\frac{\boldsymbol{x}}{\boldsymbol{1+x}} + \boldsymbol{z ln}\frac{\boldsymbol{z}}{\boldsymbol{1+x}} + \boldsymbol{(1-z) ln}\frac{\boldsymbol{1-z}}{\boldsymbol{2(1+x)}}\right)$$

Eq. 4-9

During lithium extraction, the mixing entropy of layered oxide cathodes evolves non-monotonically as a function of lithium content, typically increasing to a maximum at an intermediate state of delithiation before decreasing at higher degrees of lithium extraction. Under thermodynamic equilibrium, this behavior is primarily governed by the lithium occupancy of available lattice sites and is therefore dependent on the state of lithiation rather than the cycle number. Although the intrinsic entropy profile is not directly determined by the lithium extraction rate, deviations may arise under non-equilibrium conditions or as a result of structural degradation during prolonged cycling. Consequently, evaluating entropy solely at the fully lithiated or fully delithiated state does not adequately capture the thermodynamic response of the material throughout the electrochemical cycle. To address this limitation, the entropy change is defined relative to the fully lithiated state and compared with either the maximum entropy attained during

delithiation or the entropy at the experimentally accessible end-of-charge state, whichever exhibits the larger deviation.

This definition ensures that entropy change reflects the maximum thermodynamic perturbation experienced by the cathode during operation. Large entropy changes are indicative of significant rearrangements in local order or phase behavior, which are commonly associated with irreversible structural transformations. Conversely, cathodes that accommodate lithium extraction with minimal entropy change during cycling are expected to exhibit solid-solution-like behavior and enhanced reversibility under deep delithiation.

As mentioned, finding the change in entropy with SOC is a parameter that needs to be studied in this work as studying the entropy of the starting lithiated CAM is not enough to describe what takes place inside the battery that is an overlooked issue in most published papers. During the lithium intercalation, the S_{mix} passes through the maxima and reaches the minimum when all lithium is ejected. As a result, it is necessary to compare the entropy changes between the fully lithiated entropy to maximum S_{mix}, and the state S_{mix} when the lithiation passes the maximum entropy and takes the greater entropy change. As such the following methods are used: The change in S_{mix} is compared with the highest entropy when the nickel content z is constant. The following rules are applied to find the change in S_{conf} along with changes in x or SOC

$$\Delta S_{mix} = |S_{mix}(x) - S_{mix}(1)| \ \ when\ x > x_{max}$$

$$\Delta S_{mix} = \begin{cases} |S_{mix}(x) - S_{mix}(1)| \\ or \\ |S_{mix}(x_{max}) - S_{mix}(1)| \end{cases} \quad when\ x < x_{max}\ greater\ value$$

The equations were calculated using Python, with the Pandas and Matplotlib libraries used to process the data and generate the graphs. The raw code and analysis performed in Python are provided in the Appendix.

4.3.2 Computational method

The Vienna Ab-initio Simulation Package (VASP) was utilized to perform density functional theory (DFT) calculations to study the structure of cathodes at both fully lithiated and 50% lithiated

states. The projector-augmented wave (PAW) method was employed to describe the interaction between valence electrons and ionic cores, as implemented in VASP. Initial structures were optimized until the change in total energy was less than 0.002 eV, with an energy cutoff set to 520 eV. Both lattice parameters and atomic positions were relaxed during the optimization process. Figure 4-1 illustrates the structures of the fully lithiated LNO and the 50% delithiated LNO. These structures were not only relaxed but also modified by substituting nickel with manganese and cobalt in different ratios, given there are 12 nickel sites.

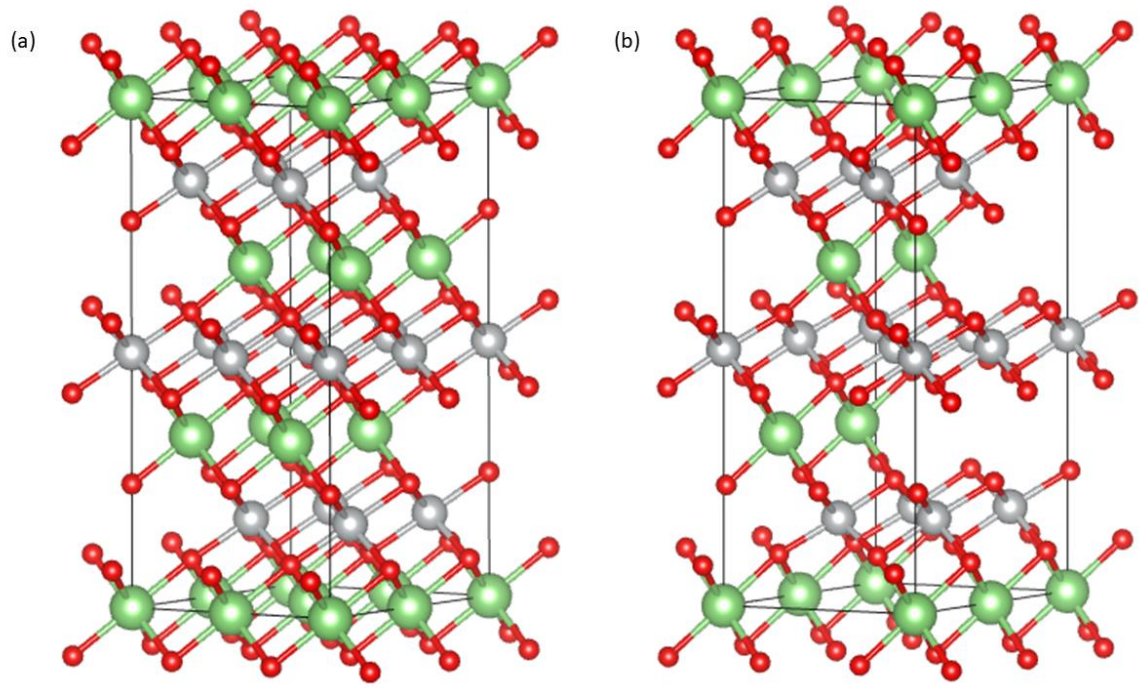


Figure 4-1 Optimized crystal structures of (a) fully lithiated $LiNiO_2$ and (b) 50% delithiated $Li_{0.5}NiO_2$ obtained from density functional theory (DFT) calculations. Lithium, oxygen, and nickel atoms are shown in green, red, and gray, respectively. These structures serve as reference frameworks for evaluating the effect of lithium removal and transition-metal substitution on configurational entropy and energetic stability in layered oxide cathodes.

4.4 Results

The mix entropy consists of two distinct terms in the equation for cations and anions. Cathode materials with layered oxides have only one anion, which is oxygen. As a result, the anion terms become zero. For cations, the remaining elements (Li, Ni, Mn, and Co) should be included in the equation to calculate the entropy mix. The entropy reaches its highest value when all the elements are present in equal amounts. However, this may or may not be based on the ratio of Ni, Mn, and Co, depending on the state of charge.

During charge and discharge, Li^+ shuttles back and forth between the cathode and anode electrodes, causing a change in the mixing entropy of both the cathode and anode. Figure 4-2 illustrates the calculated mixing entropy of the commercial cathode in charged and discharged states, as well as the change in mixing entropy, which is calculated using Eq. 4-1. NMC111 exhibits the highest configuration entropy (11.53 J/mol K at x=0.33) due to the highest equal distribution of cations. As the nickel content increases to 80% in NMC811, the entropy decreases (8.84 J/mol K at x=0.53). It is worth noting that the change in entropy also decreases as the capacity of the cathode increases, where 1.1 and 0.06 J/mol K for NMC111 and NMC811 respectively.

The second law of thermodynamics states that the sum of entropy never decreases, which is difficult to reconcile with the configuration entropy due to the system's boundary. The overall boundary is supposed to include the anode materials. However, it is also possible to suggest that minimizing changes in entropy during the reaction will provide the best equilibrium or reversibility for battery materials.

The mixing entropy of LCO decreases (-0.7 J/mol K) during charging and increases when discharging, which is thermodynamically favorable for creating potential differences in the cell. However, the structural instability prevents further delithiation,[20] limiting the capacity compared to NMCs. Other factors, such as vibrational and electronic entropy, and the study from Baek et al. claimed that configuration entropy is the major contributor to the potential change for homogeneous solid solutions.[17] The findings suggest that high configurational entropy does not provide stability to the structure. However, the change in configuration entropy may offer a better explanation for the stability of materials that undergo reversible changes.

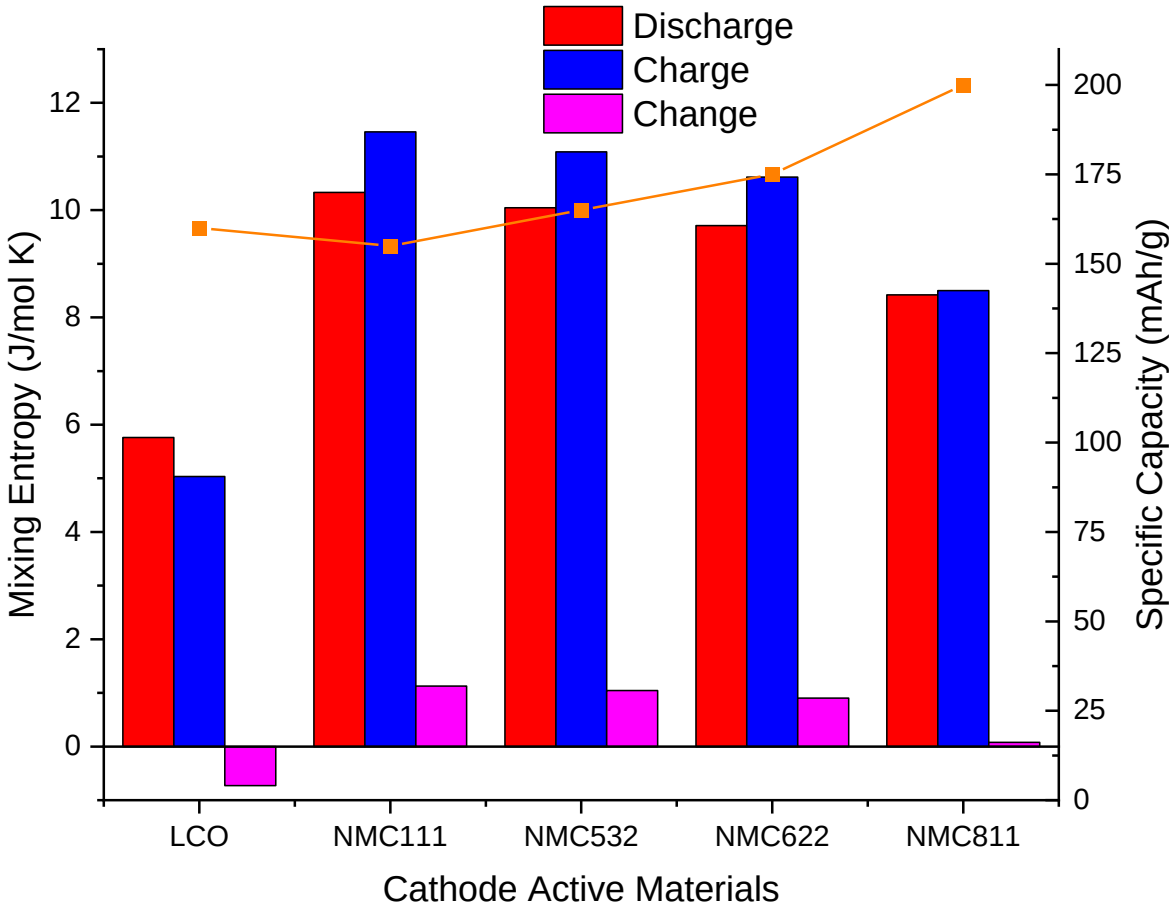


Figure 4-2 mixing entropy of commercial layered oxide cathodes evaluated at the fully lithiated (0% SOC) and fully charged (100% SOC) states, together with their corresponding practical discharge capacities. While low-nickel cathodes exhibit higher absolute mixing entropy, high-nickel cathodes achieve greater lithium utilization with smaller entropy changes, highlighting the decoupling between entropy magnitude and reversible capacity.

While Figure 4-2 illustrates the mixing entropy states during charge and discharge, it is essential to examine how entropy evolves throughout these processes. Figure 4-3 presents the entropy change for various commercial cathode materials as a function of lithium content (x) in LixTMsO2 (TMs = transition metals), where x ranges from 0 to 1. The blue points mark the compositions at which the total configurational entropy reaches its maximum (as summarized in Table 4-2), while the red points correspond to the experimentally observed end of charge.

Among the studied cathodes, only LCO exhibits a decrease in entropy during charging, whereas all others show an entropy increase at the end of charge. Except for LCO, most cathodes approach their maximum entropy point; notably, NMC811 slightly exceeds the calculated maximum entropy

value (8.834 J/mol·K) but still terminates near this point with the smallest overall entropy change among all materials. As nickel content increases, the magnitude of entropy changes decreases, enabling greater lithium extraction with minimal overall entropy change during cycling. Table 4-2 summarizes both the entropy changes up to the maximum and at the end of charge. Remarkably, NMC811 demonstrates the smallest entropy change (0.06 J/mol·K) despite its high capacity of 200 mAh/g, indicating that extensive delithiation can be achieved with minimal entropy fluctuations.

The calculated mixing entropy profiles further reveal a systematic dependence of both entropy magnitude and evolution on nickel content. Low-nickel cathodes such as NMC111 possess high absolute configurational entropy due to their near-equimolar cation distributions but experience large entropy change during cycling during delithiation, reflecting significant thermodynamic perturbation. In contrast, nickel-rich cathodes exhibit lower absolute entropy yet much smaller entropy change during cycling across the accessible lithium composition range.

Overall, NMC811 demonstrates the smallest entropy change among the commercial cathodes examined while achieving the highest specific capacity. This finding suggests that high reversible delithiation can occur with minimal entropy change during cycling when the cathode composition is properly optimized. The results highlight that entropy change during cycling—rather than absolute entropy magnitude—governs the stability–energy trade-off in layered oxide cathodes.

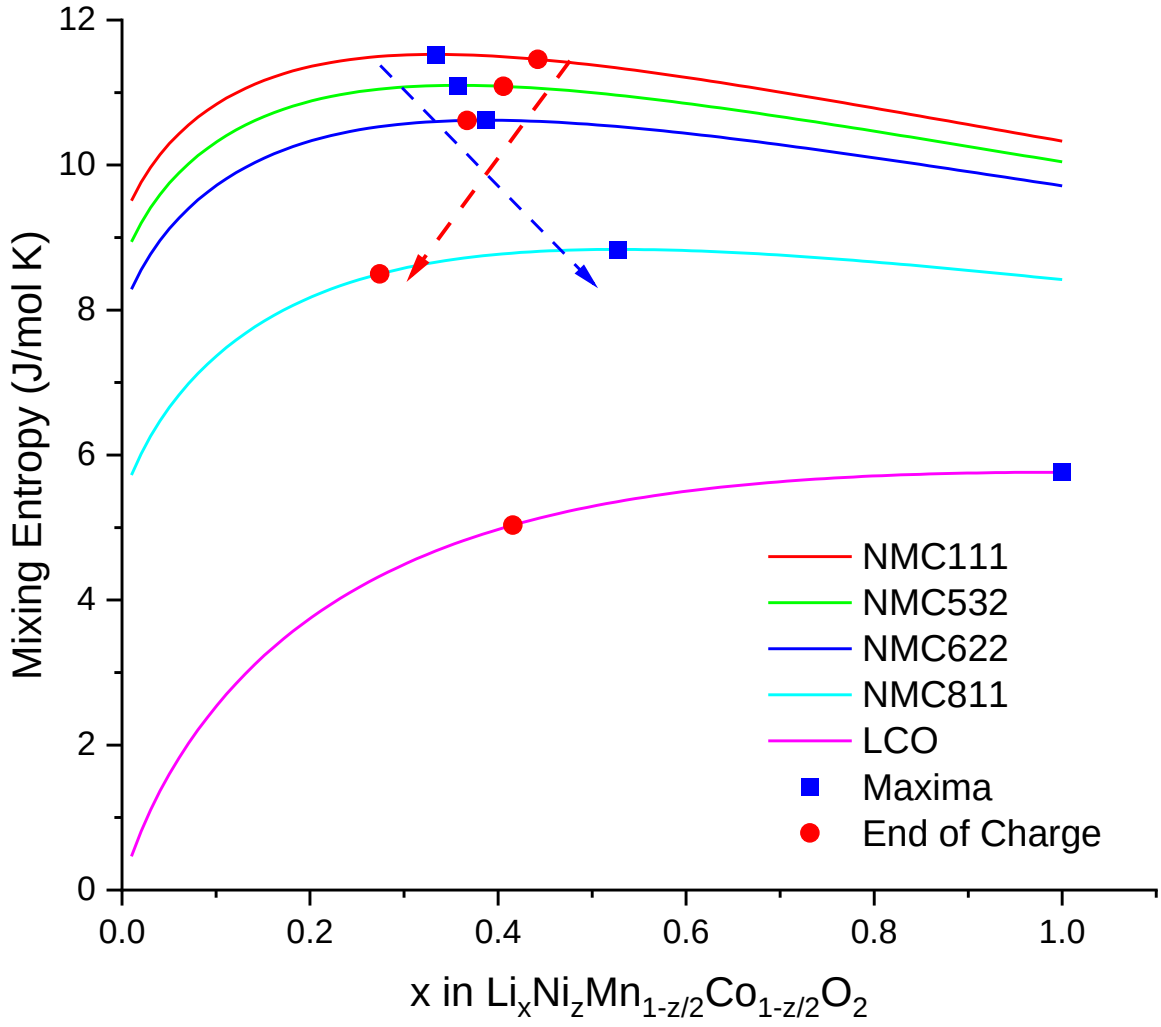


Figure 4-3 Evolution of mixing entropy as a function of lithium content (x) for commercial cathode materials Li_xTMsO_2. Blue arrows indicate the lithium composition at which maximum configurational entropy occurs, while red arrows denote the experimentally accessible end-of-charge state. The shift of entropy maxima toward higher lithium content with increasing nickel concentration demonstrates how compositional tuning governs entropy change during cycling during delithiation.

Table 4-2 Mixing entropy values (Unit: J/mol K, x in Li_x in CAMs in parenthesis)

	LCO	111	532	622	811
MAXIMA	5.763 (1.00)	11.53 (0.33)	11.10 (0.36)	10.62 (0.37)	8.834 (0.53)
0% SOC	5.763 (1.00)	10.33 (1.00)	10.04 (1.00)	9.713 (1.00)	8.419 (1.00)
100% SOC	5.049 (0.42)	11.46 (0.44)	11.08 (0.41)	10.62 (0.37)	8.485 (0.27)

To identify the optimal compositional ratio within the NMC family, a plot was constructed to illustrate the variation in mixing entropy as a function of nickel content, while maintaining constant

manganese and cobalt proportions in the formulation $Li_xNi_zMn_{(1-z)/2}Co_{(1-z)/2}O_2$, Figure 4-4. The mixing entropy reaches a maximum value of 11.53 J mol^{-1} K^{-1} when both the nickel and lithium fractions are 0.33. This maximum arises from the nearly equivalent distribution of manganese and cobalt within the transition-metal layer, which promotes a highly disordered cation mix. In contrast, $LiCoO_2$ (LCO) exhibits somewhat different behavior: the fully lithiated phase possesses the highest mixing entropy, which gradually decreases upon delithiation. It is also noteworthy that variations in lithium content exert a more pronounced influence on the overall entropy change than adjustments in transition-metal composition.

For a clearer visualization, Figure 4-5 illustrates the entropy change with different nickel contents overlaid on a single graph. As expected, the mixing entropy is highest when the nickel content is 33%. However, it is challenging to observe the total change in entropy throughout the range of lithium variation.

It is evident that lower nickel contents, up to 33%, exhibit the highest entropy when the lithium content is at 33%. As the nickel content increases, the maximum entropies of the CAMs also shift towards higher lithium contents. Eventually, when the nickel content reaches 100%, the maximum entropy occurs when the lithium content is 1, exactly in the case of LNO.

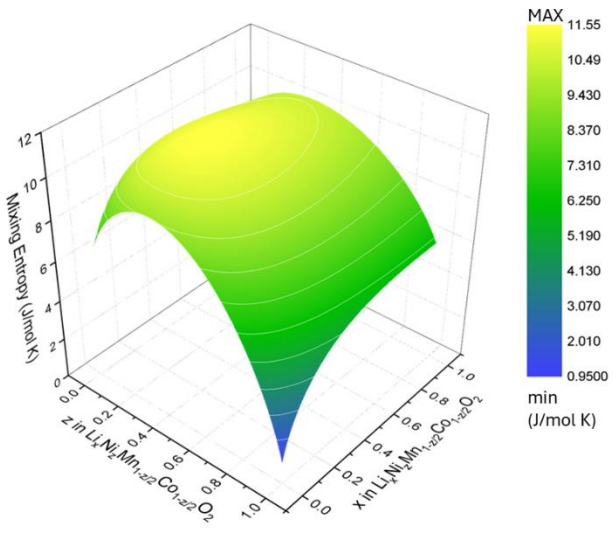


Figure 4-4 Calculated mixing entropy profiles for layered oxide cathodes with varying nickel content, illustrating the shift in entropy maxima as a function of lithium composition. As nickel concentration increases, the maximum entropy shifts toward higher lithium fractions, indicating a reduced entropy change during cycling during deep delithiation for nickel-rich compositions.

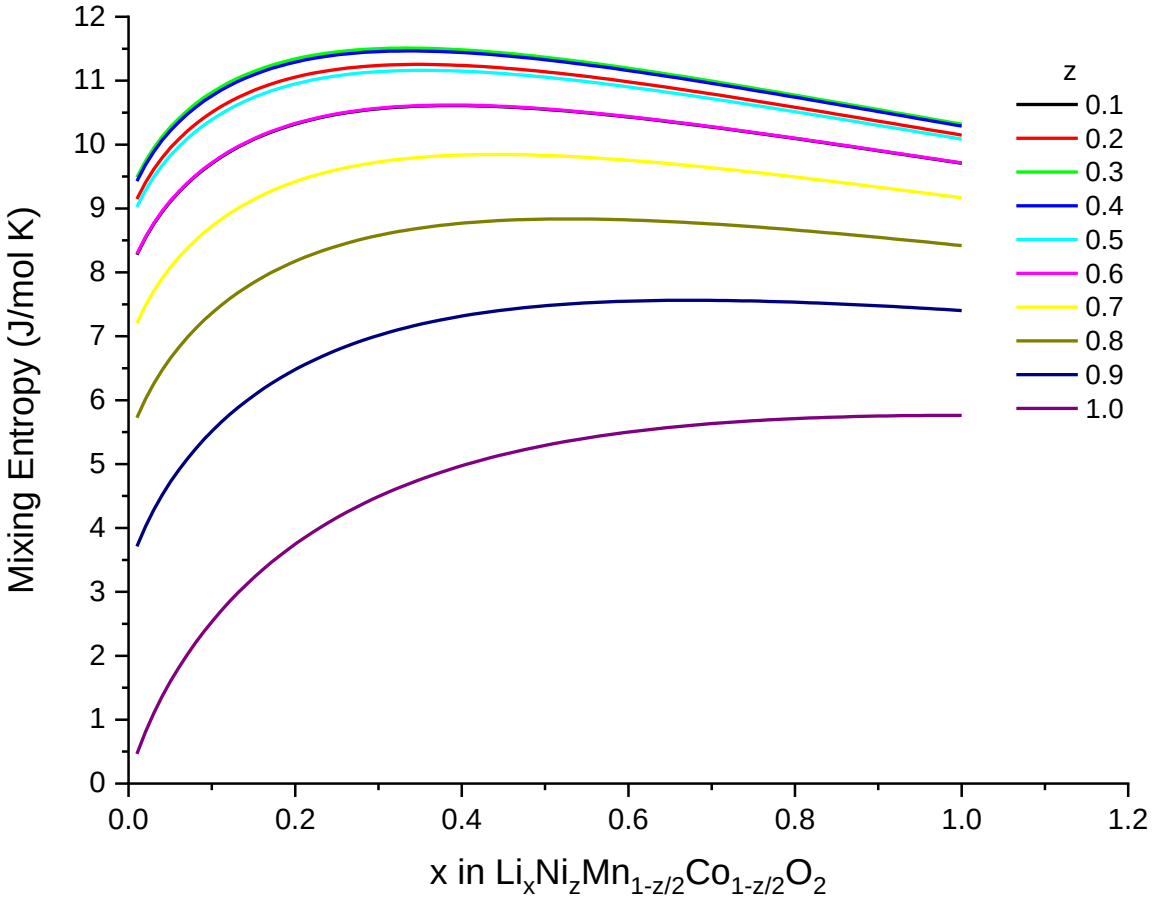


Figure 4-5 Comparison of mixing entropy change during cycling across cathodes with different nickel contents plotted on a common scale. Although cathodes with approximately 33% nickel exhibit the highest absolute entropy, the total entropy change during cycling during lithiation and delithiation decreases systematically with increasing nickel content, emphasizing the importance of entropy change rather than entropy magnitude.

It is reasonable to assume that lithiation and delithiation should occur with minimal changes in mixing entropy to maintain the structural reversibility of the material that is observed from the commercial CAM and illustrated in Figure 4-3 and Table 4-2. However, from the perspective of the cathode, it is challenging to avoid any change in mixing entropy as the lithium content varies within the structure. Therefore, it is crucial to determine the maximum allowable change in mixing entropy before a phase change occurs, which typically requires extensive molecular simulations.

Figure 4-6 illustrates the maximum entropy change from 0% state of charge (SOC) to the end of charge. As the degree of delithiation decreases, SOC increases, meaning that achieving a maximum delithiation state of 0.1 corresponds to the highest SOC. Although maximum delithiation leads to the highest SOC, it also significantly influences entropy change. For example,

at a delithiation state of 0.1, a nickel content of 0.9 produces a larger entropy change than a nickel content of 0.8, corresponding to NMC811. Another notable observation is that when the maximum delithiation reaches 0.9—where only 10% of lithium remains intercalated—the entropy change across different nickel contents becomes minimal. This trend aligns with experimental findings from other studies, which demonstrate that cycling batteries within narrower SOC windows can extend battery life [21].

Examining the entropy change during lithiation for various nickel contents (Figure 4-6b) reveals significant distinctions. The NMC composition with 90% nickel exhibits a greater entropy change than the 80% nickel composition when the lithiation state is below 0.3. NMCs containing less than 60% nickel show entropy changes exceeding 0.8 J/mol·K and cannot be delithiated beyond 63%. In contrast, NMC with 70% nickel can be delithiated up to 90% before the entropy change begins to rise sharply. Previous studies have shown that 70% nickel NMC can achieve a specific capacity of 200 mAh/g, comparable to that of NMC811 with 80% nickel, suggesting that a small entropy change is acceptable [14, 22, 23]. Furthermore, evidence indicates that maintaining the entropy change below 0.8 J/mol·K helps stabilize the cathode structure, though the long-term stability of these materials remains to be validated.

Systematic variation of nickel content identifies a compositional regime near 65–70% nickel where mixing entropy change during delithiation is minimized while retaining high lithium utilization. Below this range, entropy change during cycling increases rapidly with delithiation, limiting reversible capacity. Above this range, although entropy change remains low, the onset of phase transitions and oxygen lattice instability introduces additional enthalpic penalties that reduce reversibility.

Collectively, these results highlight approximately 70% nickel as a critical compositional window in which entropy change is sufficiently small to preserve solid-solution-like behavior, while nickel redox activity remains high enough to achieve energy densities comparable to high-nickel cathodes. This finding offers a thermodynamic explanation for the experimentally observed balance between energy density and structural stability in mid-nickel layered oxides.

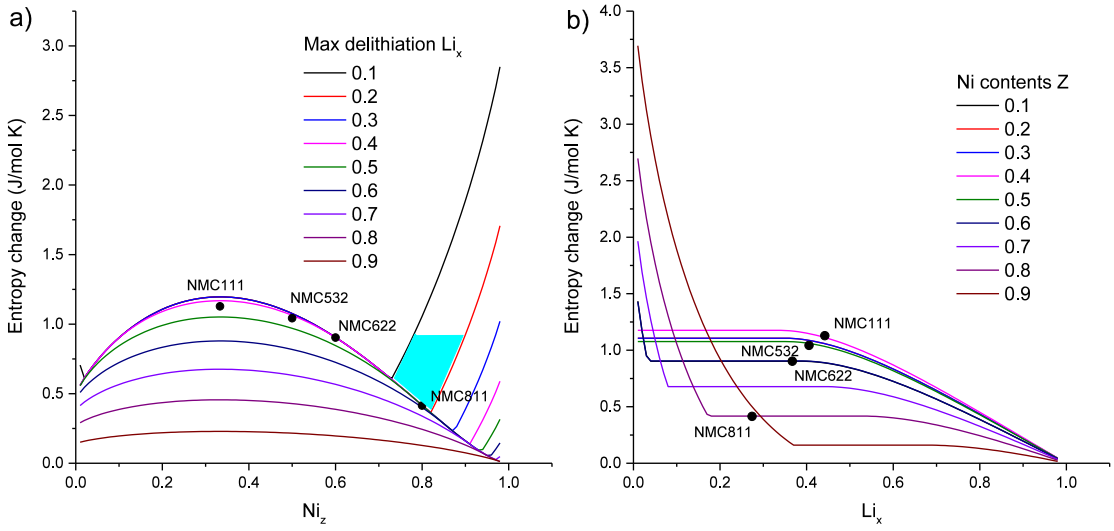


Figure 4-6 (a) Maximum mixing entropy change from the fully lithiated state to the end-of-charge state as a function of nickel content under different delithiation limits. (b) Entropy changes as a function of lithiation depth for fixed nickel compositions. Cathodes containing approximately 70% nickel exhibit minimized entropy change during cycling while enabling deep delithiation, identifying a thermodynamically favorable compositional window for high reversible energy density.

Figure 4-7 illustrates the energy evaluations of the cathodes obtained from VASP calculations. The varying nickel content impacts the total final energy and the formation energy changes before and after lithiation. To ensure a fair comparison, all structures were evaluated in both fully lithiated and 50% lithiated states, corresponding to different states of charge (SOC) for each structure. This consistent lithiation state allows for a controlled comparison of structural stability. The results indicate that the structure with 67% nickel, which is close to the 70% nickel structure, exhibits the least or even negative change in energy, -0.03 ev/atom and 0.378 eV/atom for final energy and formation energy per atom respectively. These findings are consistent with the configurational entropy results discussed earlier. The structural stability during lithiation is not maximized at the

highest entropy, but rather at a low to moderate configurational entropy, which results in the lowest de-lithiation and highest stability, thereby achieving higher energy density.

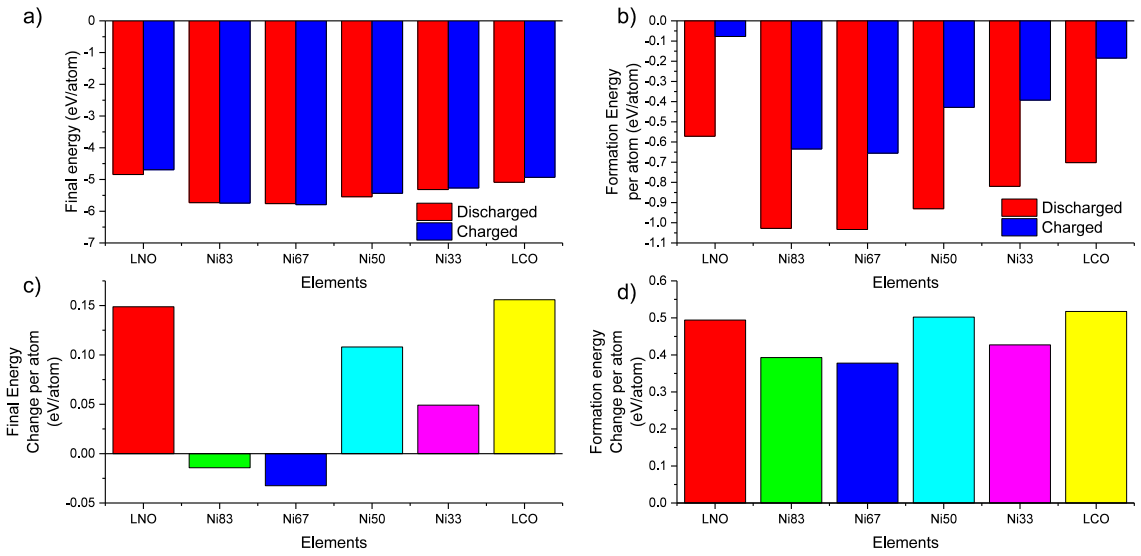


Figure 4-7 DFT-calculated energetic changes associated with lithiation and delithiation of layered oxide cathodes with varying nickel content. Shown are the total energy and formation energy differences between fully lithiated and 50% delithiated states. The composition near 67–70% nickel exhibits the smallest energetic penalty upon lithium removal, corroborating entropy-based predictions of enhanced thermodynamic stability and reversible lithium utilization.

4.5 Discussion

The high entropy material may offer structural stability, but as shown by Otto et al., it does not provide phase stability at maximum delithiation.[24] This finding aligns well with results obtained from commercial materials. For instance, NMC111, which has the highest configurational entropy (11 J/mol K), does not offer phase stability and has the smallest delithiation, 56%, among other NMCs, which is also lower than LCO (5.7 J/mol K) at 58%. Furthermore, as the nickel content increases, reducing the configurational entropy, the reversible capacity increases, hence increasing delithiation up to 73% for NMC811 (8.4 J/mol K). Unlike other CAMs, NMC811 does not intercalate lithium by solid solution; instead, it starts showing phase changes that can be observed when LNO is cycled, displaying distinctive peaks of H1, M, H2, and H3 during cycling.[13, 14, 25, 26] Studies find that Mn and Co in the TM layers stabilize the phase reversibility and prevent any cation mixing of Ni in the Li layer. These results indicate that from other studies that up to

70% nickel NMCs cycle as if the CAMs are solid solutions.[11, 14] Noh et al. has synthesized five different NMCs with different nickel contents and have clearly shown the potential profile where, the lower or equal to 70% nickel NMC is clearly showing the solid-solution behavior. Their study has also shown the capacity retention lowered as the nickel contents increased which might be due to the redox of nickel based on Liu et al. study from NMC111 where they have shown clear evidence of actual redox metal was nickel while the manganese and cobalt stayed at constant oxidation state. Which also suggest, why the change of the phases was more visual in the potential profile for higher nickel NMC compared to below 70% NMCs. These two studies suggest the evidence of the high nickel can provide the high energy density but also capacity retention is lowered due to the repeatable phase change resulting on volume change that ends up in loss of capacity. This suggests that with the study of entropy change that the optimum nickel contents for NMCs are close to range of 70% to balance the energy density and capacity retention. Also, the change in entropy during lithium intercalation gets smaller as the nickel content increases. Based on the collected information and the limit of the entropy change during intercalation, the entropy change must be below 0.8 J/mol K. This observation and results also raise other arguments on high-entropy materials are necessary for high energy density cathode, but also the local regional entropy structure could be more important to stabilize the structure to improve the energy density of the cathode.

The lithiation and delithiation processes for cathodes do not conclusively show that entropy can provide stability. However, the effect of entropy change on stable lithiation is observed. Mixing entropy is a tiny portion compared to the contribution of the enthalpy, and the type of elements used affects the material characteristics more than entropy. Due to the nature of the cathode, where chemical elements change during battery operation, stability is important, but so is reversibility. Entropy can provide a good indication of the material's stability. Furthermore, the results suggest that doping methods might be more feasible for active materials like cathodes.

One can argue that LCO and LNO have the same configurational entropy but different energy densities. However, these two CAMs have different vibrational and electronic entropy. The density of states shows that LCO is non-conductive, while LNO is conductive due to the partially filled orbitals of nickel. As a result, the electronic potential of LCO is minimal, but configurational entropy affects its potential profile. For LNO, the partially filled orbitals of nickel exhibit magnetic

effects in the density of states. Additionally, the lithiation processes differ: LCO shows a solid solution type, while LNO shows minor phase changes. Furthermore, as aligned with Baek et al.'s discussion, the magnetism of nickel also causes shifts and changes in the phase of LNO or high-nickel CAMs. Consequently, LNO shows a capacity close to 200 mAh/g but with low durability, whereas LCO has shown promising durability with a capacity of 160 mAh/g, as also claimed by Sun et al.[6]

The battery market has shifted to high-nickel cathodes due to political and environmental issues related to cobalt mining, as well as the higher energy density of high-nickel cathodes. This shift has driven extensive research on cathodes containing higher than 80% nickel. However, challenges remain, such as low-capacity retention and stability issues in ambient conditions due to increased surface reactivity. Some practical solutions provided by manufacturers include using narrow state-of-charge (SOC) windows for charging and discharging to extend capacity retention.

These findings indicate that the optimal design of layered oxide cathodes does not occur at the extremes of low- or high-entropy compositions, but rather within a moderate-entropy regime that minimizes thermodynamic disruption during cycling. Notably, minimizing entropy change does not necessitate equimolar multicomponent systems; instead, it can be achieved through careful tuning of transition-metal ratios to balance redox activity and structural stability.

From a materials design perspective, entropy change serves as a quantitative thermodynamic metric that complements conventional structural and electrochemical descriptors. By constraining entropy change during cycling below a critical threshold, it becomes possible to identify cathode compositions capable of deep delithiation without triggering irreversible phase transformations. This framework provides a rational pathway for the development of next-generation layered oxide cathodes that simultaneously maximize practical energy density and cycling stability.

At the material level, achieving high capacity and retention with cobalt-free cathodes would offer significant advantages. The most promising solution may not lie in high-nickel compositions but rather in cobalt-free alternatives with optimized nickel content. Our results suggest that controlling phase transitions enables high capacity and retention in cathodes containing approximately 70% nickel, which exhibit solid-solution-like behavior while minimizing enthalpy variation. As shown in Figure 6b, the 70% nickel cathode maintains a nearly constant enthalpy change until lithium

content drops below 0.1, whereas the 80% nickel cathode exhibits a more pronounced change. This observation highlights the potential of 70% nickel compositions to combine the structural stability of mid- to low-nickel cathodes with the high capacity typical of high-nickel materials, while preserving solid-solution characteristics.

Consequently, cathodes with around 70% nickel content can achieve high delithiation with minimal or sub-critical entropy changes, ensuring both high energy density and excellent capacity retention. Previous studies support this conclusion, showing that 70% nickel cathodes can deliver 200 mAh/g of capacity with strong retention performance [14, 23]. However, the potential of this composition has been overlooked due to market trends favoring high-nickel systems.

The lithiation and delithiation processes for cathodes do not conclusively demonstrate that entropy alone can provide stability. However, the effect of entropy change on stable lithiation is observed. Mixing entropy is a minor component compared to the contribution of enthalpy, and the type of elements used affects the material characteristics more significantly than entropy. Due to the nature of the cathode, chemical elements change during battery operation, both stability and reversibility are important. Entropy can provide a good indication of the material's stability through its changes; a substantial change in entropy can result in instability and phase changes in the structure. Furthermore, entropy can be manipulated to minimize its change and provide stable lithiation by doping with more than two, or even three to five, elements, which is more feasible for creating stable and high-energy-dense active materials.

A study by Noh et al. clearly shows that cathode active materials (CAMs) with 70% nickel exhibit solid-solution behavior, while those with 80% nickel show clear phase changes in the potential profiles.[14] Given the key issues associated with cobalt use in cathodes, it might be better to avoid using cobalt and maintain nickel content at 70% to achieve high capacity and retention. The primary challenge would be to control the mix of entropy to prevent phase changes, as seen in 80% nickel CAMs. This approach would also lead to minimal entropy change and the highest delithiation from the CAM.

This could be achieved by testing multi-doping elements into the transition metal layers. As Zhao et al. have shown for Na-ion batteries, different elements have specific purposes and roles in layered oxides. A similar effect could be observed in nickel-manganese-cobalt (NMC) cathodes.

Applying knowledge of the roles of various elements and the resulting changes in mixing entropy could lead to the design of high-density CAMs.

4.6 Conclusion

High entropy materials are a captivating field of study that has garnered significant interest from researchers. However, some studies related to battery materials advise proceeding with caution and recommend careful application of the theory. Mixing entropy is undeniably a valuable tool for designing and developing materials, and research has been conducted across various applications. In our study, we concluded that achieving high energy density in layered oxide cathodes necessitates minimal mixing entropy. It is important to highlight that the change in mixing entropy during lithiation, rather than the mixing entropy itself, is more critical for designing cathode active materials (CAMs).

Our findings suggest that a nickel content of approximately 70% in the structure can deliver high energy density, supported by mixing entropy with less than 0.8 J/mol K of entropy change. Currently, only two elements from Mn, Co, and Al are typically used, but exploring additional elements to minimize entropy change could enhance energy density and capacity retention. This approach would also optimize the benefits of utilizing high-nickel cathodes.

4.7 References

1. Li, W., E.M. Erickson, and A. Manthiram, *High-nickel layered oxide cathodes for lithium-based automotive batteries.* Nature Energy, 2020. **5**(1): p. 26-34.
2. *U.S. DRIVE Electrochemical energy storage technical team roadmap*. 2017, US Council for Automotive Research.
3. Muralidharan, N., et al., *Next-Generation Cobalt-Free Cathodes – A Prospective Solution to the Battery Industry's Cobalt Problem.* Advanced Energy Materials, 2022. **12**(9): p. 2103050.
4. Houache, M.S.E., et al., *On the Current and Future Outlook of Battery Chemistries for Electric Vehicles—Mini Review.* Batteries, 2022. **8**(7): p. 70.
5. Xu, C., et al., *Future material demand for automotive lithium-based batteries.* Communications Materials, 2020. **1**(1): p. 99.
6. Sun, H.H., et al., *Beyond Doping and Coating: Prospective Strategies for Stable High-Capacity Layered Ni-Rich Cathodes.* ACS Energy Letters, 2020. **5**(4): p. 1136-1146.
7. Xi, Z., et al., *Modification strategies of high-energy Li-rich Mn-based cathodes for Li-ion batteries: A Review.* Molecules, 2024. **29**(5): p. 1064.
8. Kaushik, S., et al., *Recent advancements in cathode materials for high-performance Li-ion batteries: Progress and prospects.* Journal of Energy Storage, 2024. **97**: p. 112818.

9. Nasajpour-Esfahani, N., et al., *Comprehensive review of lithium-ion battery materials and development challenges.* Renewable and Sustainable Energy Reviews, 2024. **203**: p. 114783.
10. *Cobalt*.
11. Choi, J.U., et al., *Recent Progress and Perspective of Advanced High-Energy Co-Less Ni-Rich Cathodes for Li-Ion Batteries: Yesterday, Today, and Tomorrow.* Advanced Energy Materials, 2020. **10**(42): p. 2002027.
12. Kim, H., et al., *Controlling the Microstructure of Cobalt-Free, High-Nickel Cathode Materials with Dopant Solubility for Lithium-Ion Batteries.* ACS Applied Materials & Interfaces, 2023. **15**(22): p. 26585-26592.
13. Jung, R., et al., *Oxygen Release and Its Effect on the Cycling Stability of LiNixMnyCozO2 (NMC) Cathode Materials for Li-Ion Batteries.* J. Electrochem. Soc., 2017. **164**: p. A1361.
14. Noh, H.-J., et al., *Comparison of the structural and electrochemical properties of layered Li[NixCoyMnz]O2 (x = 1/3, 0.5, 0.6, 0.7, 0.8 and 0.85) cathode material for lithium-ion batteries.* Journal of Power Sources, 2013. **233**: p. 121-130.
15. Ouyang, B. and Y. Zeng, *The rise of high-entropy battery materials.* Nature Communications, 2024. **15**(1): p. 973.
16. Murty, B.S., et al., *2 - High-entropy alloys: basic concepts*, in *High-Entropy Alloys (Second Edition)*, B.S. Murty, et al., Editors. 2019, Elsevier. p. 13-30.
17. Baek, S.W., et al., *Thermodynamic Analysis and Interpretative Guide to Entropic Potential Measurements of Lithium-Ion Battery Electrodes.* The Journal of Physical Chemistry C, 2022. **126**(14): p. 6096-6110.
18. Sarkar, A., et al., *High-Entropy Oxides: Fundamental Aspects and Electrochemical Properties.* Advanced Materials, 2019. **31**(26): p. 1806236.
19. Zeng, Y., et al., *High-entropy mechanism to boost ionic conductivity.* Science, 2022. **378**(6626): p. 1320-1324.
20. Sun, X., et al., *New phases and phase transitions observed in over-charged states of LiCoO2-based cathode materials.* Journal of Power Sources, 2001. **97-98**: p. 274-276.
21. Gauthier, R., et al., *How do Depth of Discharge, C-rate and Calendar Age Affect Capacity Retention, Impedance Growth, the Electrodes, and the Electrolyte in Li-Ion Cells?* Journal of The Electrochemical Society, 2022. **169**(2): p. 020518.
22. You, Y., et al., *Modified High-Nickel Cathodes with Stable Surface Chemistry Against Ambient Air for Lithium-Ion Batteries.* Angewandte Chemie International Edition, 2018. **57**(22): p. 6480-6485.
23. Sim, R., L. Su, and A. Manthiram, *A High Energy-Density, Cobalt-Free, Low-Nickel LiNi0.7Mn0.25Al0.05O2 Cathode with a High-Voltage Electrolyte for Lithium-Metal Batteries.* Advanced Energy Materials, 2023. **13**(21): p. 2300096.
24. Otto, F., et al., *Relative effects of enthalpy and entropy on the phase stability of equiatomic high-entropy alloys.* Acta Materialia, 2013. **61**(7): p. 2628-2638.
25. Egorov, K., et al., *Mitigating First-Cycle Capacity Losses in NMC811 via Lithicone Layers Grown by Molecular Layer Deposition.* ACS Appl Mater Interfaces, 2023. **15**(16): p. 20075-20080.
26. Peres, J.P., F. Weill, and C. Delmas, *Lithium/vacancy ordering in the monoclinic LixNiO2 ($0.50 \leq x \leq 0.75$) solid solution.* Solid State Ionics, 1999. **116**(1): p. 19-27.

Chapter 5: Measuring mixed entropy to assess the effect of the configurational entropy on layered oxide cathode active materials in Li-ion batteries

This chapter has been adapted from a research paper submitted to the *Journal of Power Sources.*

Chapter 4 introduced an entropy-based thermodynamic framework that identifies entropy change during cycling as a key determinant of cathode stability and reversible energy density. While analytical modeling and first principles calculations provide strong theoretical support for this concept, experimental validation is essential to confirm that entropy change manifests in measurable electrochemical behavior under realistic operating conditions. Direct experimental probing is required to determine whether cathodes predicted to exhibit minimized entropy change indeed shows enhanced thermodynamic stability during cycling.

In this context, Chapter 5 presents an experimental investigation of entropy change in commercial layered oxide cathodes using temperature-dependent open circuit potential measurements. By systematically comparing cathodes with varying nickel content but identical crystal structure, this chapter experimentally evaluates entropy evolution as a function of state of charge. The results provide critical validation of the entropy change framework developed in Chapter 4 and establish entropy measurements as a practical diagnostic tool for assessing cathode stability and energy density tradeoffs.

5.1 Abstract

This study examines the influence of mixing entropy on the electrochemical performance and structural stability of layered oxide cathodes in lithium-ion batteries. The effect was evaluated experimentally by determining the dependence of open-circuit voltage on temperature, expressed as the potential thermal coefficient (dE/dT), for four commercial Li-ion cathode materials with varying compositions but identical R3m layered structures: $LiCoO_2$ (LCO), $LiNi_{0.33}Mn_{0.33}Co_{0.33}O_2$ (NMC111), $LiNi_{0.5}Mn_{0.3}Co_{0.2}O_2$ (NMC532), and $LiNi_{0.8}Mn_{0.1}Co_{0.1}O_2$ (NMC811). The measured entropy values ranged from 5 to 15 $J \cdot K^{-1}$ for NMC-type materials and from 50 to 80 $J \cdot K^{-1}$ for LCO. Our findings underscore the subtle role of entropy in stabilizing the transition-metal layer, its minimal impact on capacity, and the trade-offs associated with high nickel content.

5.2 Introduction

Cathodes are the primary lithium reservoirs in lithium-ion batteries and represent the main limiting factor for energy density. They are also the most expensive component, driving extensive research into improving both performance and cost-efficiency. $LiCoO_2$ (LCO), the first-generation cathode material, offers a specific capacity of approximately 150 mAh/g and an average operating potential of 3.9 V.[1, 2] Despite its high energy density, the increasing cost and ethical concerns surrounding cobalt mining have led to the development of alternative materials such as olivine-type $LiFePO_4$ (LFP) and spinel-type $LiMn_{1.5}Ni_{0.5}O_2$ (LMNO). However, LFP suffers from lower energy density, and LMNO's high operating voltage lacked compatible electrolytes at the time, limiting their commercial viability.[3-7]

To address these limitations, layered oxide cathodes such as $LiNi_{0.33}Mn_{0.33}Co_{0.33}O_2$ (NMC111) were introduced, reducing cobalt content by 67% and lowering production costs. Subsequent generations, $LiNi_{0.5}Mn_{0.3}Co_{0.2}O_2$ (NMC532), $LiNi_{0.6}Mn_{02}Co_{0.2}O_2$ (NMC622), and $LiNi_{0.8}Mn_{0.1}Co_{0.1}O_2$ (NMC811), increased nickel content, boosting energy density up to 190 mAh/g. However, this came at the expense of reduced capacity retention due to phase transitions during lithiation and delithiation.[3, 8, 9]

The concept of high entropy, originally developed in alloy research, has gained traction in materials science for its potential to stabilize structures. In battery applications, high-entropy oxides have shown promise, particularly in anodes, offering capacities exceeding 500 mAh/g.[10, 11] However, their higher average voltage (~1.0 V) compared to graphite (0.1 V) limits their overall energy output.

In cathodes, disordered rock salt (DRX) structures have demonstrated capacities over 300 mAh/g and energy densities around 950 Wh/kg, though their long-term stability remains under investigation.[12] Similar to DRX, high entropy theory was also adapted to lithium rich layered oxide (LLO) by Kim et al.[13] LLO cathode consists of monoclinic (C2/*m*) and rhombohedra (R-2m) structure. LLO provides the energy from anionic redox from monoclinic structure and from the transition metal from rhomnohedra structure, that results in greater discharge capacity and higher working potential (>4.0V). As the kinetic of the lithiation is slightly different for LLO due to the redox of the oxygen in monoclinic structure, the stability of the structures is important for reversibility of the lithiation. Similarly a study from Sturman et al. in layered cathodes with

equimolar mixtures of five transition metals have shown improved structural stability and broader potential windows (1.5 V to 4.2 V), albeit without significant performance gains.[14]

This study focuses on measuring mixing entropy in commercial layered cathodes, LCO, NMC111, NMC532, and NMC811, to assess its impact on mixing entropy and overall performance. These materials share the same R3m crystal structure but differ in transition metal composition, providing an ideal basis for comparison.

During charging and discharging, cathode structures undergo delithiation and lithiation, respectively. At certain states of delithiation, changes in configurational entropy are expected. Zheng et al. expressed configurational entropy using the following equation:[15]

$$S_{mix}^{Ideal} = -R\left(\sum_{Cation} xlnx + \sum_{Anion} ylny\right)$$

Eq. 5-1

This equation suggests that delithiation contributes to mixing entropy. While lithium removal alters occupancy in the lithium layers, the transition metal layers—typically composed of Ni, Mn, and Co—retain their fixed positions in the R3m structure. Thus, unless delithiation induces significant cation mixing or phase transitions, the mixing entropy of the transition metal layers remains largely unchanged. Lithium vacancies may contribute to entropy, but their impact is minimal due to weak interactions among lithium sites.

Total mixing entropy comprises four components: configurational, vibrational, magnetic dipole, and electronic randomness. However, configurational entropy is typically the dominant contributor. [16, 17] Therefore, changes in mixing entropy are primarily attributed to configurational effects.

Mixing entropy can be experimentally measured by observing potential changes with temperature, derived from the Gibbs free energy equation for electrochemical cells:

$$\Delta G = -zFE_{rxn}$$

Eq. 5-2

Where z is the number of electrons exchanged, F is Faraday's constant, and E_{rxn} is the potential difference between cathode and anode materials. Gibbs free energy for mixed materials is also expressed as:

$$\Delta G_{mix} = \Delta H_{mix} - T\Delta S_{mix}$$

Eq. 5-3

Combining these equations yields:

$$\frac{dG}{dT} = -dS = -nF\frac{dE}{dT}$$

Eq. 5-4

This relationship indicates that temperature-dependent changes in electrode potential can be used to evaluate mixing entropy. To isolate the cathode's contribution, experiments were performed using half-cells with lithium metal as the counter electrode. Although lithium exhibits a temperature-dependent potential shift (~1.03 $mV \cdot K^{-1}$)[18], its influence is negligible in this context. Details of the procedure for measuring potential changes with temperature variations are provided in the Experimental section. In brief, the measurements were conducted using a water bath and a galvanostat while maintaining the cells at specific states of charge (SOC). Different SOC levels correspond to varying lithium concentrations in the cathode active material (CAM), which in turn affect the degree of mixing entropy.

In this work, we present the first direct measurements of mixing entropy in commercial layered cathodes under controlled conditions. These measurements provide insights into the role of configurational entropy in determining energy density and structural stability across different states of charge.

Building on the entropy evolution framework developed in Chapter 4, this chapter experimentally probes the thermodynamic response of layered oxide cathodes during delithiation. By directly measuring temperature dependent equilibrium potentials, the present work tests whether cathodes predicted to exhibit minimal entropy change—particularly high nickel and moderate entropy compositions—indeed display reduced thermodynamic perturbation during cycling. These measurements provide critical experimental validation of entropy change as a governing design constraint for cathode stability and practical energy density.

5.3 Experimental

Single-side coated electrodes of LCO, NMC811, NMC532, and NMC111m were purchased from NEI Corporation and used directly to assemble 2325-type coin cells, supplied by the National Research Council of Canada. Detailed specifications of the electrodes are available on the NEI Corporation website,[19] which is shown in Table 5-1.

Table 5-1 Specification of the cathode active materials from NEI Corporation

Cathode active materials	Particle Size	1st Charge capacity @0.1C
$LiCoO_2$	12 µm	≥ 170 mAh/g
$LiNi_{0.33}Mn_{0.33}Co_{0.33}O_2$	11 µm	≥ 170 mAh/g
$LiNi_{0.5}Mn_{0.3}Co_{0.2}O_2$	11 µm	≥ 185 mAh/g
$LiNi_{0.8}Mn_{0.1}Co_{0.1}O_2$	8 µm	≥ 210 mAh/g

Disk electrodes (Ø = 12.5 mm) were punched out and dried overnight at 80 °C under vacuum. Lithium metal disks (Ø = 16.5 mm) served as both counter and reference electrodes. Each cell contained 75 µL of electrolyte solution consisting of 1 M $LiPF_6$ in ethylene carbonate–ethyl methyl carbonate (EC:EMC, 3:7 v/v), applied over a double layer of microporous polypropylene separators (Celgard 2500, thickness = 30 µm, Ø = 21 mm).

Cell assembly was performed in an argon-filled dry glove box at room temperature. Assembled cells were rested at open circuit potential (OCP) overnight before testing. Capacity measurements were conducted using galvanostatic cycling on a multichannel Arbin battery cycler (BT2000). Cells were cycled at C/24 for the first two cycles within a voltage window of 2.5–4.5 V, followed by five additional cycles at C/10 under the same voltage range prior to entropy measurements. These cycles are formation cycle that stabilize the active materials to minimize any irreversible capacity due to solid electrolyte interphases or cathode electrolyte interphases.

To evaluate mixing entropy and temperature-dependent potential changes, cells were connected to copper wires at both the anode and cathode, then sealed in two plastic zipper bags per cell. The sealed cells were immersed in a temperature-controlled water bath ranging from 5 °C to 45 °C in 10 °C increments. At each temperature, the cells could rest for at least 30 minutes or until the potential stabilized. All potential measurements were performed using a Solartron SI 1287. For

each state of charge (SOC), a 15-minute window of the open-circuit potential (OCP) was recorded to calculate the average potential. The standard deviation within this window was used to estimate measurement error, while the instrument resolution was 1 μV.

Before temperature cycling, cells were fully discharged to 2.5 V and rested for 30 minutes. The cells were then charged to 3.7 V, followed by temperature cycling, and then this was repeated at 3.8, 3.9, 4.0, 4.1, and 4.2 V for each cell independently. For LCO, the 0% SOC potential was already above 3.8 V, so temperature cycling began at that voltage and continued up to 4.2 V in 0.1 V increments.

SEM and XRD measurements were also performed and are provided in the Appendix for reference.

5.4 Results

5.4.1 Electrochemical Performance

Figure 5-1 presents the potential profiles and differential capacity (dQ/dV) curves of commercial cathode materials, all the four cathode active materials (CAMs). As widely recognized, NMC111 (150 mAh/g) exhibits the lowest capacity among the NMCs, while NMC811 offers the highest, 190 mAh/g. The capacity of NMC111 is comparable to that of LCO; however, its average operating voltage is slightly lower due to the presence of nickel and manganese.

As the nickel content increases from NMC111 to NMC811, the specific capacity improves, while the average voltage remains relatively consistent. This behavior is attributed to the redox activity of nickel, which undergoes oxidation and reduction between Ni^{2+} and Ni^{4+} at lower voltages. Meanwhile, manganese and cobalt primarily contribute to structural stability rather than capacity.

The dQ/dV curve of NMC811 reveals three distinct peaks, in contrast to the single peak observed in LCO and lower-nickel NMCs. This multi-peak feature arises from cobalt's role in stabilizing the octahedral structure and mitigating phase transitions from the O3-type layered structure.

Although NMC811 delivers higher capacity, LCO and lower-nickel NMCs are known for superior capacity retention. This is largely due to the stronger cobalt–oxygen bonds and reduced cation mixing, which enhance structural integrity and long-term cycling stability.

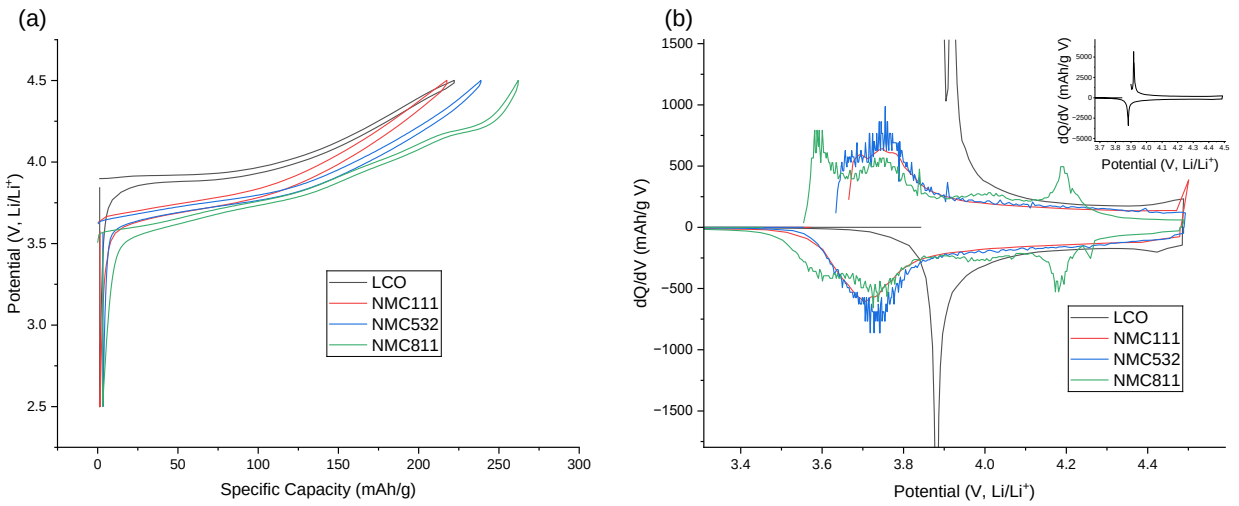


Figure 5-1 (a) Galvanostatic charge–discharge voltage profiles and (b) corresponding differential capacity (dQ/dV) curves of commercial layered oxide cathodes (LCO, NMC111, NMC532, and NMC811) measured in Li half-cells. Increasing nickel content leads to higher specific capacity, while the emergence of multiple dQ/dV peaks in NMC811 indicates phase transitions associated with deep delithiation. Lower nickel cathodes exhibit smoother voltage profiles consistent with solid-solution behavior and enhanced structural reversibility.

5.4.2 Entropy measurements

Figure 5-2 illustrates the potential measurements of commercial cells at various voltages and temperatures. Figure 5-2a show the results for LCO, where the potential measurements begin at 3.9 V. This starting point reflects the higher redox potential of the Co^{3+}/Co^{4+} couple compared to the Ni^{3+}/Ni^{4+} redox pair in NMCs. This trend is also evident in Figure 5-1, where the average voltages of NMC cathode active materials (CAMs) are lower than that of LCO.

When cells were charged and measured across different temperatures, NMCs exhibited potentials close to the target voltage, with only slight deviations. In contrast, LCO showed significantly larger potential differences—up to 0.3 V—due to its higher polarization resistance and lower conductivity relative to NMCs.

Among the materials tested, NMC811 demonstrated the smallest potential variation across temperatures, with a change of only 0.002 V. In comparison, NMC532, NMC111, and LCO showed changes of 0.004 V, 0.01 V, and 0.03 V, respectively. This trend indicates that as the nickel content in the cathode decreases, the temperature-induced potential variation increases.

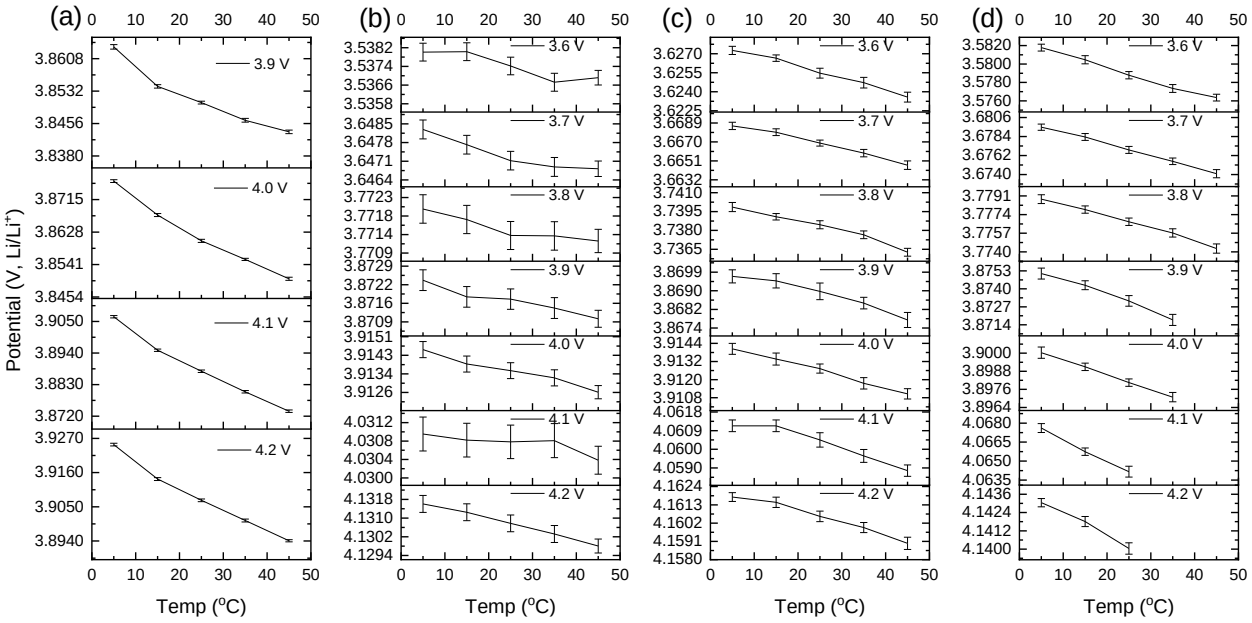


Figure 5-2 Open-circuit potential (OCP) measurements as a function of temperature and state of charge for (a) LCO, (b) NMC811, (c) NMC532, and (d) NMC111 measured in half-cells against lithium metal. The temperature-dependent shift in equilibrium potential (dE/dT) provides direct experimental access to entropy changes associated with lithium insertion and extraction. Nickel-rich cathodes exhibit smaller temperature-induced potential variations, indicating reduced entropy change during cycling during cycling.

From the potential measurements, mixing entropy was evaluated using Eq. 5-4, while Gibbs free energy was calculated using Eq. 5-2. Subsequently, Eq. 5-3 was applied to derive the enthalpy. The results are summarized in Figure 5-3. LCO exhibited significantly higher entropy across the entire potential range compared to the other cathode active materials (CAMs), with values ranging from 50 $kJ \cdot mol^{-1}$ to 78 $kJ \cdot mol^{-1}$, which is consistent with previously reported ranges. In contrast, NMC811 showed the lowest entropy throughout the potential range. A general trend was observed for NMC-type materials, where entropy increased with higher nickel content, aligning with the expected behavior of mixing entropy—except for LCO, which deviates from this trend.

The Gibbs free energy decreased from −340 kJ to −399 kJ as the potential increased from 3.6 V to 4.2 V for the NMCs. In comparison, the ΔG values for LCO remained relatively constant across the same potential range. A similar trend was observed for enthalpy (ΔH), which remained stable due to the relatively small entropy values and the consistency of potential.[17]

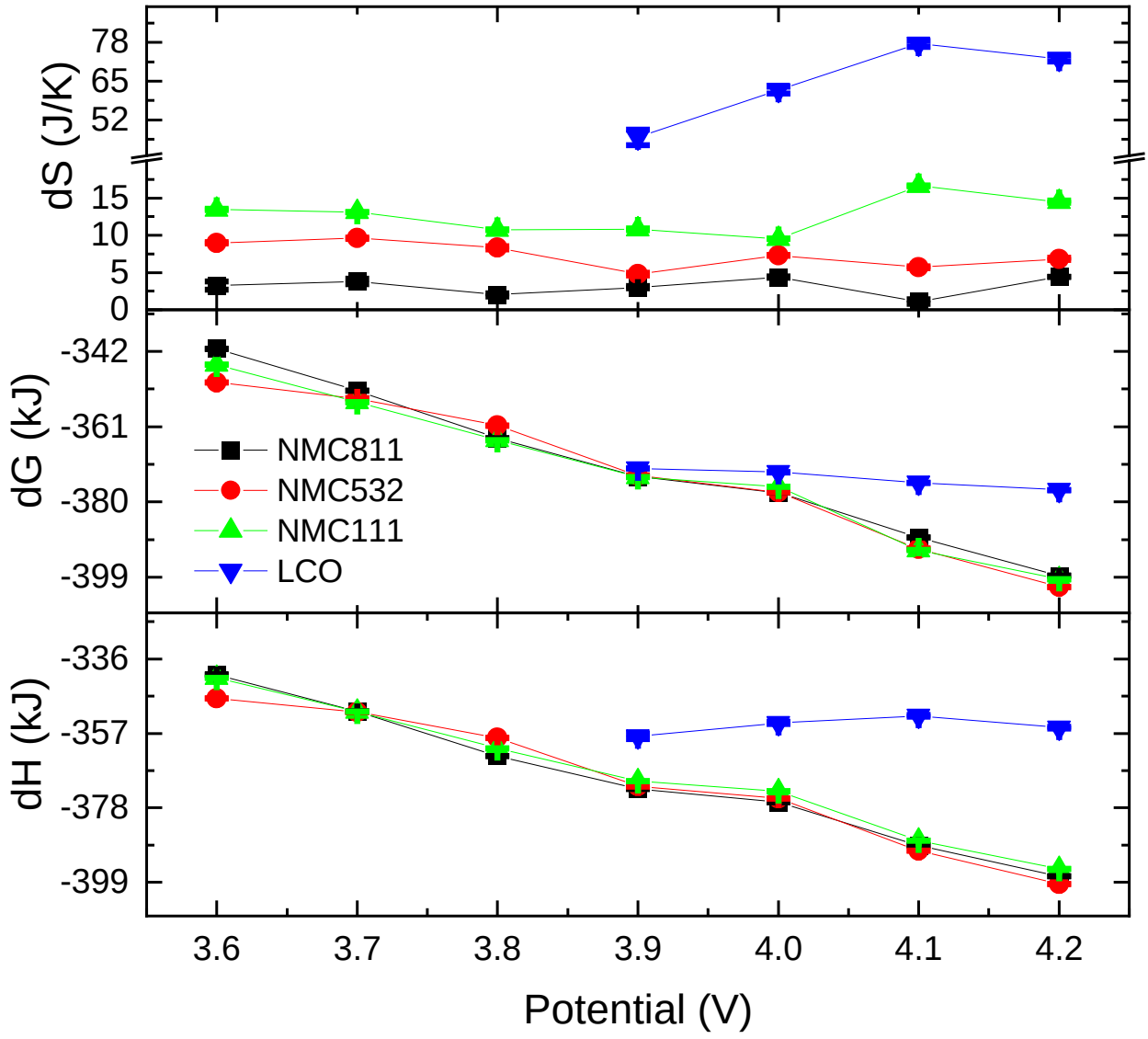


Figure 5-3 Thermodynamic quantities derived from temperature-dependent OCP measurements for commercial layered oxide cathodes: (a) entropy change (ΔS), (b) Gibbs free energy change (ΔG), and (c) enthalpy change (ΔH) as a function of cell potential. LCO exhibits substantially larger entropy values compared to NMC-type cathodes, reflecting significant electronic and vibrational contributions, while NMC811 shows minimal entropy change during cycling across the operating voltage range. The relatively constant ΔH and smooth ΔG evolution for NMC cathodes indicate that entropy change, rather than enthalpy, governs thermodynamic stability during delithiation.

5.5 Discussion

Although high mixing entropy is theorized to stabilize the transition-metal (TM) layer by promoting a random distribution of multiple cations and reducing the likelihood of structural collapse, it does not necessarily correspond to increased delithiation capacity. For instance,

NMC111—with its more balanced and compositionally diverse TM layer, and therefore higher mixing entropy—exhibits a lower delithiation capacity than NMC811. In contrast, the simpler, nickel-rich composition of NMC811 yields lower entropy yet enables deeper lithium extraction. This comparison suggests that while elevated mixing entropy can enhance structural resilience and mitigate irreversible phase transitions, it does not directly translate to higher capacity. Because potentiometric measurements capture the total entropy contribution—including configurational, vibrational, and electronic components—the experimentally measured values reflect all these effects; nevertheless, the composition-dependent trends observed remain consistent with configurational entropy predictions.

The superior capacity of NMC811 is primarily attributed to nickel's high redox activity, which enables multiple oxidation states ($Ni^{2+} \rightarrow Ni^{3+} \rightarrow Ni^{4+}$) and allows for greater electron transfer per formula unit. In contrast, manganese remains largely electrochemically inactive in the layered structure, and cobalt contributes modestly due to its narrower redox window.[20-24] Consequently, increasing nickel content—as seen in the progression from NMC111 to NMC811—leads to higher energy density but also introduces challenges such as structural instability and reduced cycle life. These issues necessitate mitigation strategies such as doping, surface coatings, and particle morphology control.

Despite nickel's dominant role in capacity, cobalt plays a critical role in maintaining structural integrity during delithiation. It stabilizes the TM layer by suppressing cation mixing, particularly the migration of Ni^{2+} into lithium layers. This stabilization is facilitated by cobalt's strong bonding with oxygen and its relatively stable oxidation states (Co^{3+}/Co^{4+}), which help preserve the layered O3-type structure and delay phase transitions such as O3 → H1-3 →O1/O2. These transitions are evident in sharp peaks in dQ/dV profiles of high-nickel cathodes like NMC811.[20-25] In contrast, low-nickel NMCs with higher cobalt content exhibit broader, more diffuse dQ/dV peaks, indicative of a solid-solution delithiation mechanism. Thus, while cobalt's direct contribution to capacity is limited, its structural role is essential for mitigating degradation and enhancing cycle life.

Our findings confirm that higher mixing entropy does not equate to higher energy density. Moreover, the stability observed in lower-nickel cathodes appears to stem from the structural roles of manganese and cobalt. The measured mixing entropy remains relatively constant across

different potentials, despite changes in lithium concentration, suggesting that mixing entropy does not vary significantly during cycling. These results imply that high-entropy designs in layered oxide cathodes may offer limited benefits in terms of capacity enhancement.

Nonetheless, there remains potential to refine high-entropy strategies for cathode design. Given the stabilizing effects of manganese and cobalt—such as preventing phase transitions and mitigating structural degradation—future research should explore optimized combinations of transition metals that balance high capacity, improved cycle life, and reduced reliance on cobalt. A deeper understanding of the specific roles and redox behaviors of individual transition metals will be essential for developing next-generation cathodes that meet the demands of high energy density and long-term durability.

5.6 Conclusion

This study presents the first comparative analysis of experimentally measured mixing entropy in commercial layered oxide cathodes. While LCO exhibits the highest mixing entropy, its mixing entropy is lowest. In contrast, NMC cathodes demonstrate that mixing entropy is influenced by configurational entropy, which remains largely unchanged during delithiation and across different potentials.

These findings suggest that high mixing entropy does not directly enhance energy density. However, this insight opens opportunities for optimizing NMC cathodes to improve both capacity retention and energy density. The high-entropy design approach remains valuable in cathode engineering, particularly for mitigating phase transitions—such as the O3-type to H1-3-type—while enabling higher nickel content through the strategic incorporation of other transition metals.

Our measurements further confirm that delithiation does not significantly affect mixing entropy, reinforcing the conclusion that mixing entropy remains stable during charge-discharge cycles. While NMC811 and other high-nickel cathodes exhibit superior capacity, this is primarily due to nickel's redox activity rather than enhanced structural stability. However, by applying mixing entropy principles, it may be possible to improve the stability of high-nickel cathodes.

Future cathode designs should leverage entropy-based strategies to balance energy density and durability. This includes exploring alternative transition metals that can replicate cobalt's

stabilizing effects, thereby reducing reliance on cobalt while maintaining structural integrity and electrochemical performance.

5.7 References

1. Lyu, Y., et al., *An Overview on the Advances of LiCoO2 Cathodes for Lithium-Ion Batteries.* Advanced Energy Materials, 2021. **11**(2): p. 2000982.
2. Zhang, S.-D., et al., *Advancing to 4.6 V Review and Prospect in Developing High-Energy-Density LiCoO2 Cathode for Lithium-Ion Batteries.* Small Methods, 2022. **6**(5): p. 2200148.
3. Houache, M.S., et al., *On the current and future outlook of battery chemistries for electric vehicles—mini review.* Batteries, 2022. **8**(7): p. 70.
4. Fergus, J.W., *Recent developments in cathode materials for lithium ion batteries.* Journal of Power Sources, 2010. **195**(4): p. 939-954.
5. Whittingham, M.S., *Lithium Batteries and Cathode Materials.* Chemical Reviews, 2004. **104**(10): p. 4271-4302.
6. Abe, Y., et al., *Cathode active materials using rare metals recovered from waste lithium-ion batteries: A review.* Heliyon, 2024. **10**(7).
7. Schipper, F., et al., *Study of Cathode Materials for Lithium-Ion Batteries: Recent Progress and New Challenges.* Inorganics, 2017. **5**(2): p. 32.
8. Sun, H.H., et al., *Beyond Doping and Coating: Prospective Strategies for Stable High-Capacity Layered Ni-Rich Cathodes.* ACS Energy Letters, 2020. **5**(4): p. 1136-1146.
9. Sun, Y., C. Chang, and J. Zheng, *Doping Effects on Ternary Cathode Materials for Lithium-Ion Batteries: A Review.* ChemPhysChem, 2024. **25**(17): p. e202300966.
10. Shin, D., et al., *Rational engineering of high-entropy oxides for Li-ion battery anodes with finely tuned combustion syntheses.* NPG Asia Materials, 2023. **15**(1): p. 54.
11. Xiao, B., et al., *High-entropy oxides as advanced anode materials for long-life lithium-ion Batteries.* Nano Energy, 2022. **95**: p. 106962.
12. Lun, Z., et al., *Cation-disordered rocksalt-type high-entropy cathodes for Li-ion batteries.* Nature materials, 2021. **20**(2): p. 214-221.
13. Kim, J., et al., *High-entropy Li-rich layered oxide cathode for Li-ion batteries.* Journal of Power Sources, 2025. **628**: p. 235915.
14. Sturman, J., et al., *Communication—Design of LiNi0. 2Mn0. 2Co0. 2Fe0. 2Ti0. 2O2 as a high-entropy cathode for lithium-ion batteries guided by machine learning.* Journal of The Electrochemical Society, 2021. **168**(5): p. 050541.
15. Zeng, Y., et al., *High-entropy mechanism to boost ionic conductivity.* Science, 2022. **378**(6626): p. 1320-1324.
16. Murty, B.S., et al., *2 - High-entropy alloys: basic concepts*, in *High-Entropy Alloys (Second Edition)*, B.S. Murty, et al., Editors. 2019, Elsevier. p. 13-30.
17. Baek, S.W., et al., *Thermodynamic Analysis and Interpretative Guide to Entropic Potential Measurements of Lithium-Ion Battery Electrodes.* The Journal of Physical Chemistry C, 2022. **126**(14): p. 6096-6110.
18. Swiderska-Mocek, A., E. Rudnicka, and A. Lewandowski, *Temperature coefficients of Li-ion battery single electrode potentials and related entropy changes – revisited.* Physical Chemistry Chemical Physics, 2019. **21**(4): p. 2115-2120.
19. *Cathode and Anode Powders for Li-ion Batteries, NEI Corporation*. [cited 2025 December 26th]; Available from: https://www.neicorporation.com/products/batteries/cathode-anode-powders/lithium-ion/.

20. Cui, Z., Q. Xie, and A. Manthiram, *Zinc-Doped High-Nickel, Low-Cobalt Layered Oxide Cathodes for High-Energy-Density Lithium-Ion Batteries.* ACS Applied Materials & Interfaces, 2021. **13**(13): p. 15324-15332.
21. Lee, S., S. Kmiec, and A. Manthiram, *Effects of Coprecipitation Conditions on the Electrochemical Properties of Cobalt-Free LiNi0.9Mn0.1-xAlxO2 Cathodes.* Small, 2024. **20**(50): p. 2406947.
22. Li, W., S. Lee, and A. Manthiram, *High-Nickel NMA: A Cobalt-Free Alternative to NMC and NCA Cathodes for Lithium-Ion Batteries.* Advanced Materials, 2020. **32**(33): p. 2002718.
23. Yi, M., et al., *Roles of Mn and Co in the Air Synthesizability of Layered Oxide Cathodes for Lithium-Based Batteries.* Chemistry of Materials, 2023. **35**(21): p. 9352-9361.
24. Yi, M., W. Li, and A. Manthiram, *Delineating the Roles of Mn, Al, and Co by Comparing Three Layered Oxide Cathodes with the Same Nickel Content of 70% for Lithium-Ion Batteries.* Chemistry of Materials, 2022. **34**(2): p. 629-642.
25. Garayt, M.D.L., et al., *Single Crystal Li1+x[Ni0.6Mn0.4]1−xO2 Made by All-Dry Synthesis.* Journal of The Electrochemical Society, 2023. **170**(6): p. 060529.

Chapter 6: Conclusion and Future work

6.1 Overall Conclusions

The growing demand for higher energy density and improved safety in electrochemical energy storage systems necessitates the development of next generation battery technologies beyond conventional lithium-ion batteries. Among the proposed solutions, solid-state battery (SSB) technology has emerged as a promising pathway due to its inherent safety advantages and its potential to enable high-capacity lithium metal anodes. While the replacement of flammable liquid electrolytes with solid electrolytes represents the defining technological distinction of solid-state batteries, this thesis demonstrates that cathode active materials remain the primary bottleneck governing achievable energy density, cost, and long-term stability**.**

Chapter 3 established a system level perspective on solid-state batteries by critically evaluating realistic energy density limits under practical constraints. Through quantitative modeling, it was shown that the often-cited doubling of energy density in solid-state batteries is overly optimistic under current technological conditions. Instead, achievable near-term improvements are strongly constrained by solid electrolyte thickness, cathode formulation, active material volume fraction, and anode excess. Importantly, this analysis revealed that maximizing reversible lithium utilization in the cathode active material is the most impactful lever for improving practical energy density, thereby motivating a deeper examination of cathode thermodynamics and stability under deep delithiation.

Building on this motivation, Chapter 4 introduced an entropy based thermodynamic framework for cathode design, in which entropy is treated as a dynamic variable that evolves during lithiation and delithiation rather than as a static material descriptor. By formulating entropy within the framework of mixing entropy and evaluating its configurational contribution analytically, this chapter demonstrated that the magnitude of entropy changes during cycling**,** rather than the absolute entropy value, governs the reversibility and stability of layered oxide cathodes. Systematic analysis across the NMC compositional space revealed that cathodes with moderate configurational entropy—particularly those containing approximately 65–70% nickel—exhibit minimized entropy change during cycling during delithiation, enabling deep reversible lithium extraction while maintaining solid-solution like behavior. Density functional theory calculations further supported these findings by showing that compositions near this nickel content incur the

smallest energetic penalty upon lithium removal, providing independent thermodynamic validation of the entropy-based design principle.

Chapter 5 provided experimental validation of the proposed framework through direct measurements of mixing entropy using temperature-dependent open-circuit potential techniques. For the first time, the mixing entropy of multiple commercial layered oxide cathodes was systematically compared under controlled electrochemical conditions. While the experimentally measured entropy reflects the combined contributions of configurational, electronic, and vibrational terms, the observed trends across compositions were consistent with the predictions of Chapter 4. In particular, nickel rich cathodes exhibited smaller temperature-induced potential variations, indicating reduced entropy change during cycling during cycling. These results confirm that entropy change during cycling during delithiation is a meaningful thermodynamic indicator of cathode stability, even when configurational contributions cannot be isolated experimentally.

Taken together, the results of this thesis establish a new thermodynamic design paradigm for cathode active materials, in which minimizing entropy change during electrochemical cycling, rather than maximizing entropy or compositional complexity, appears as a rational strategy for achieving high reversible energy density. This framework provides a quantitative explanation for the experimentally seen balance between energy density and stability in mid-nickel layered oxides and offers clear guidance for the development of next-generation cathode materials tailored for solid-state battery applications.

6.2 Implications for Cathode and Solid-state Battery Design

The findings of this work have several important implications for the design of cathode materials and solid-state battery architectures. First, they demonstrate that increasing nickel content beyond a critical threshold does not necessarily maximize practical energy density, particularly under the mechanical and electrochemical constraints imposed by solid electrolytes. Instead, compositions that minimize entropy change during cycling during delithiation can achieve comparable capacity while offering superior thermodynamic stability.

Second, this work suggests that high entropy cathode design strategies should be applied with caution in electrochemically active materials. While high configurational entropy can stabilize

static structures, excessive entropy change during cycling during cycling may promote phase transitions, oxygen lattice instability, and irreversible degradation. In contrast, moderate-entropy compositions engineered to suppress entropy fluctuations provide a more effective pathway toward durable, high-energy cathodes.

Finally, the entropy-based framework developed here is particularly relevant to solid-state batteries, where rigid interfaces and narrow electrochemical stability windows amplify the consequences of cathode instability. By linking entropy change during cycling directly to reversible lithium utilization, this thesis provides a thermodynamic foundation for reconciling cathode material selection with realistic solid-state battery design constraints.

6.3 Future Work

While this thesis establishes entropy change as a governing design constraint for layered oxide cathodes, several important directions remain for future research.

First, the entropy framework developed here should be extended to cobalt-free and multi doped cathode compositions, including Ni–Mn–Al and more complex transition-metal systems. Systematic exploration of how individual dopants influence entropy change during cycling could enable the design of cathodes that retain the stabilizing role of cobalt while eliminating its economic and ethical drawbacks.

Second, the application of entropy-based design principles should be expanded beyond layered oxides to other cathode families, including lithium rich layered oxides, disordered rock-salt cathodes, and sodium-ion battery materials. These systems exhibit fundamentally different lithiation mechanisms and entropy landscapes, offering an opportunity to test the generality of entropy change as a unifying stability metric.

Finally, integrating entropy optimized cathode materials into full solid-state battery cells represent a critical next step toward practical implementation. Coupling entropy-stable cathodes with thin solid electrolytes and lithium-metal or anode-free configurations will enable direct evaluation of how thermodynamic stability at the material level translates to improvements in cell-level performance, cycle life, and safety.

6.4 Concluding Remarks

This thesis demonstrates that entropy, when treated as a dynamic thermodynamic variable, provides a powerful and previously underutilized lens for understanding and designing cathode active materials. By shifting the focus from static material descriptors to entropy change during cycling during cycling, this work bridges fundamental thermodynamics and practical battery engineering. The entropy-based design framework established here offers a clear pathway toward cathode materials that balance high energy density, structural stability, and long-term durability, thereby contributing to the realization of safe, high performance solid-state battery technologies.

Chapter 7: Appendix

7.1 Appendix form chapter 4

7.1.1 Jupyter notebook coding for analysis

```
import numpy as np
from mpl_toolkits import mplot3d
import matplotlib.pyplot as plt
from matplotlib import cm
# plt.style.use('seaborn-poster')
%matplotlib notebook
#%matplotlib qt
# fig = plt.figure(figsize = (8,8))
fig = plt.figure(figsize=(8, 8))
ax = plt.axes(projection='3d')
ax.grid()
R=8.314
y = np.arange(0, 1, 0.01)
x = np.arange(0, 1, 0.01)
X, Y = np.meshgrid(x, y)
Z = -R*(X * np.log(X / (X + 1)) + Y * np.log(Y / (X + 1)) + (1 - Y) * np.log((1 - Y) / (2 * (X + 1)))) / (X + 1)

# Add heat map
surf = ax.plot_surface(Y, X, Z, cmap='viridis', vmin=0, vmax=12)

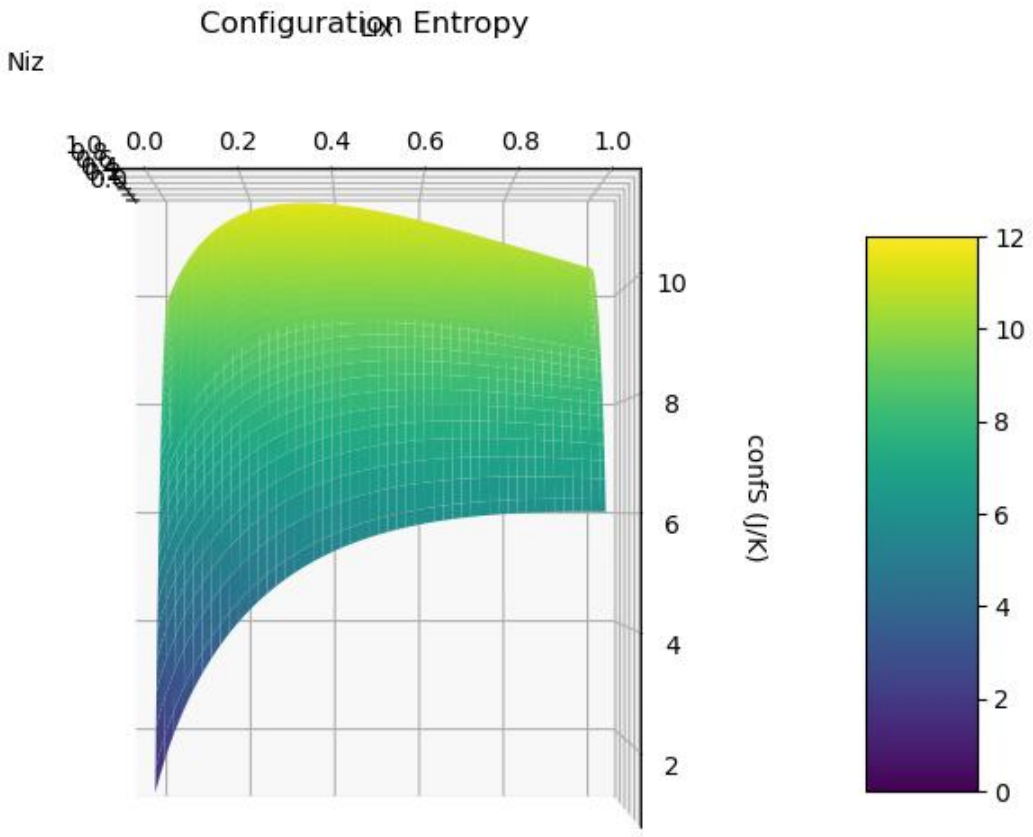
# Add color bar
fig.colorbar(surf, ax=ax, shrink=0.5, aspect=5)

#ax.plot_surface(Y, X, Z)

ax.set_title('Configuration Entropy')

# Set axes label
ax.set_xlabel('Niz', labelpad=20)
ax.set_ylabel('Lix', labelpad=20)
ax.set_zlabel('confS (J/K)', labelpad=20)

plt.show()
```




```
 if __name__ == '__main__':
 if sys.path[0] == '':
z_values = [0.1, 0.2, 0.3, 0.4, 0.5, 0.6, 0.7, 0.8, 0.9, 0.99]
x = np.arange(0.1, 1, 0.01)
R = 8.314

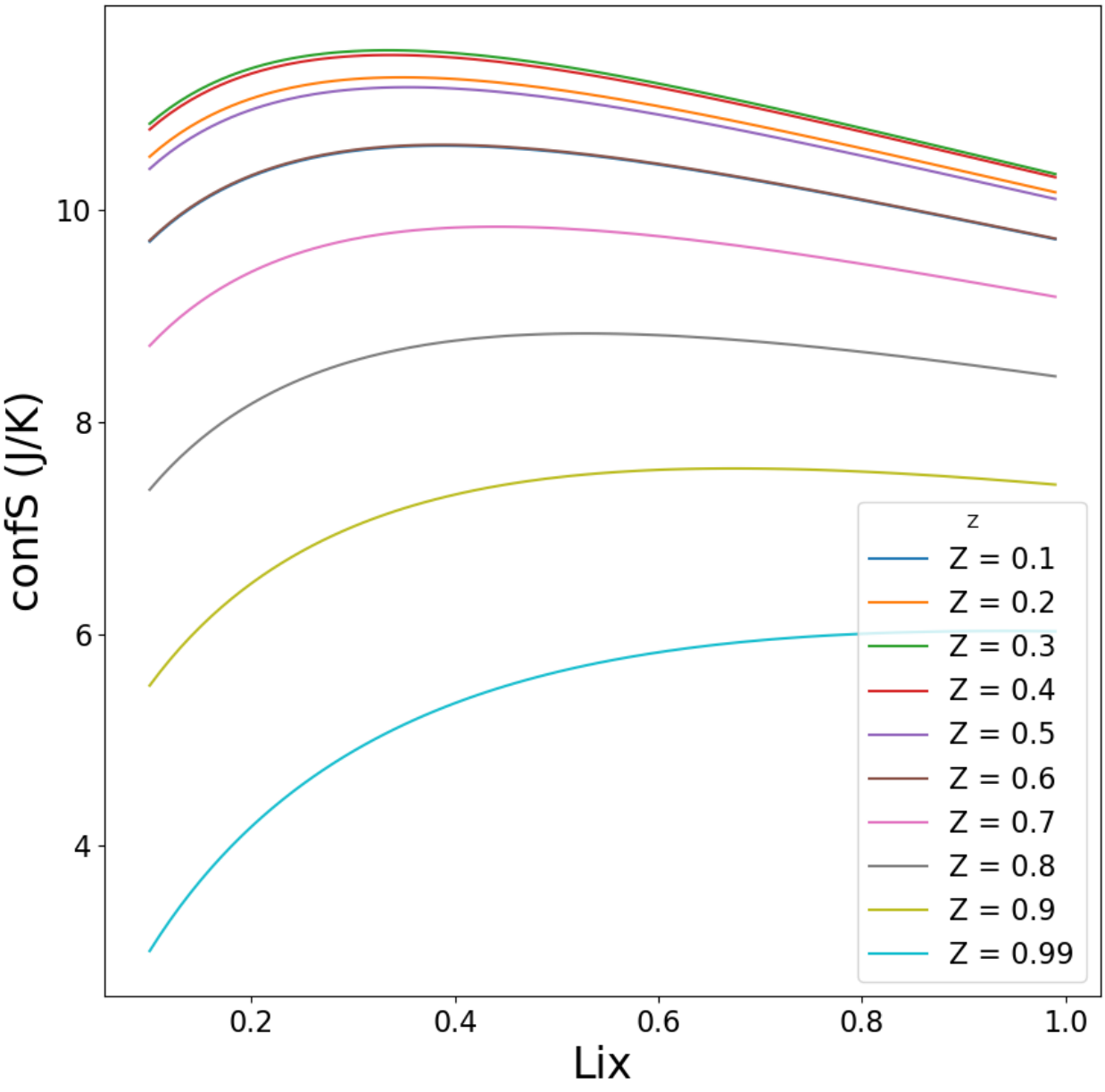
fig, ax = plt.subplots(figsize=(10, 10))

for z in z_values:
   y = -R*(x*np.log(x/(x+1)) + z*np.log(z/(x+1)) + (1-z)*np.log((1-z)/(2*(x+1))))/(x+1)
```

```
    ax.plot(x, y, label=f'Z = {z}')

ax.set_xlabel('Lix', fontsize=24)  # Increase the font size of x-axis label
ax.set_ylabel('confS (J/K)', fontsize=24)  # Increase the font size of y-axis label
ax.legend(title='Z', fontsize=16)  # Increase the font size of the legend
ax.tick_params(axis='both', labelsize=16)  # Increase the font size of the axis tick labels

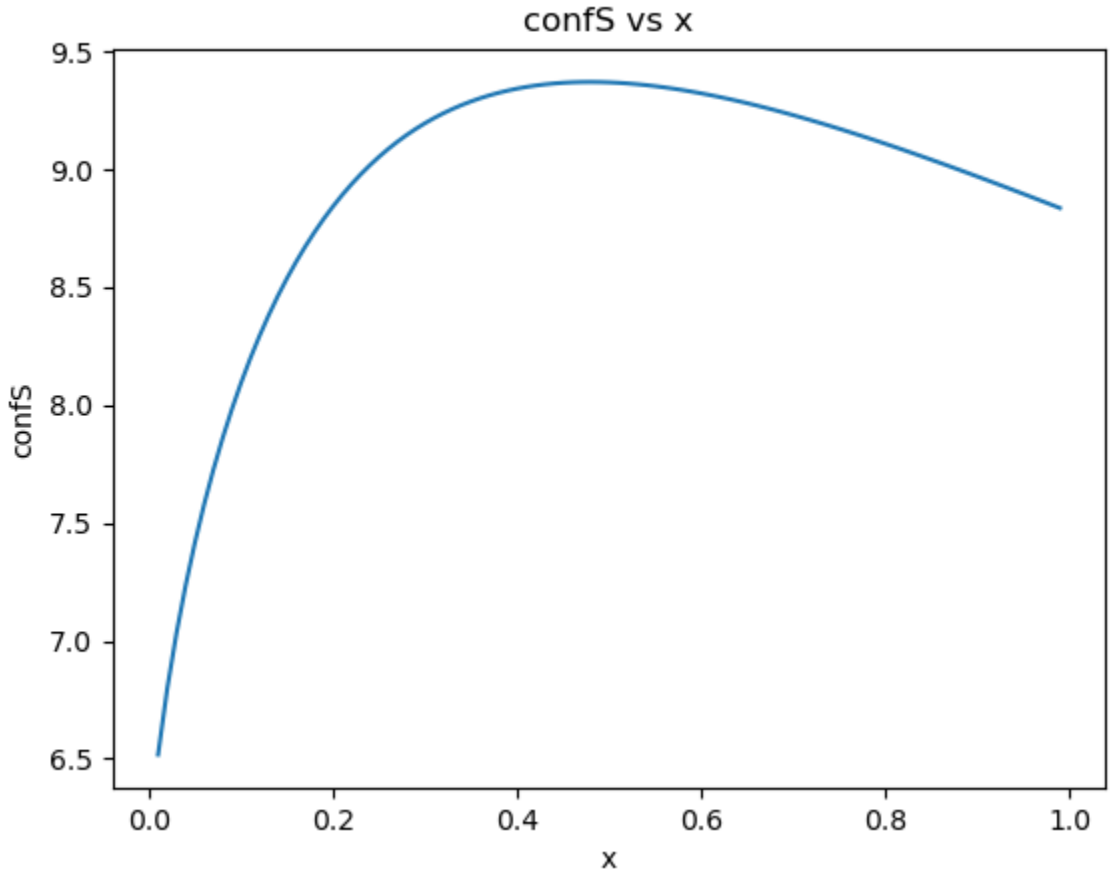
plt.show()
```




```
x = np.arange(0.01, 1, 0.01)
z = 0.75
```

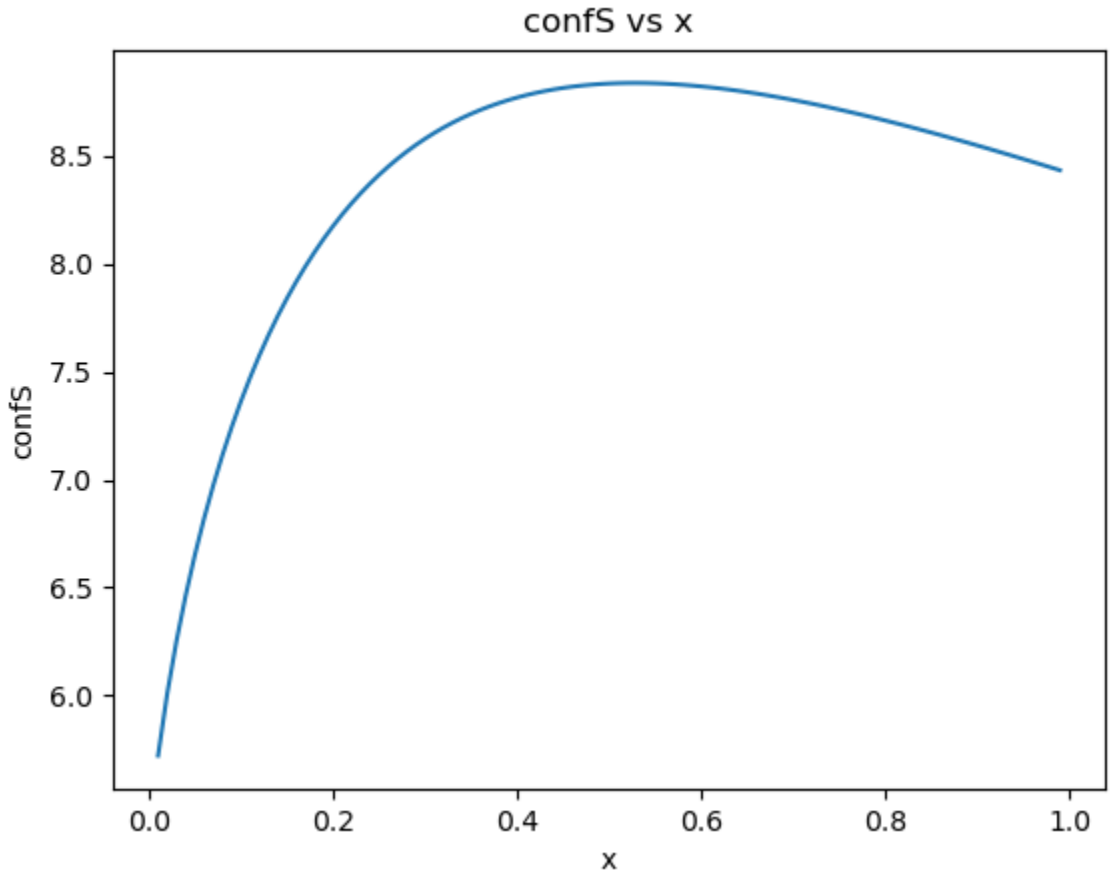
```
y = x*np.log(x/(x+1))/(x+1) + z*np.log(z/(x+1))/(x+1) + (1-z)*np.log((1-z)/(2*(x+1)))/(x+1)
y = -R*y
fig, ax = plt.subplots()
ax.plot(x,y)
ax.set(xlabel='x', ylabel='confS',
       title='confS vs x')


plt.show()
```



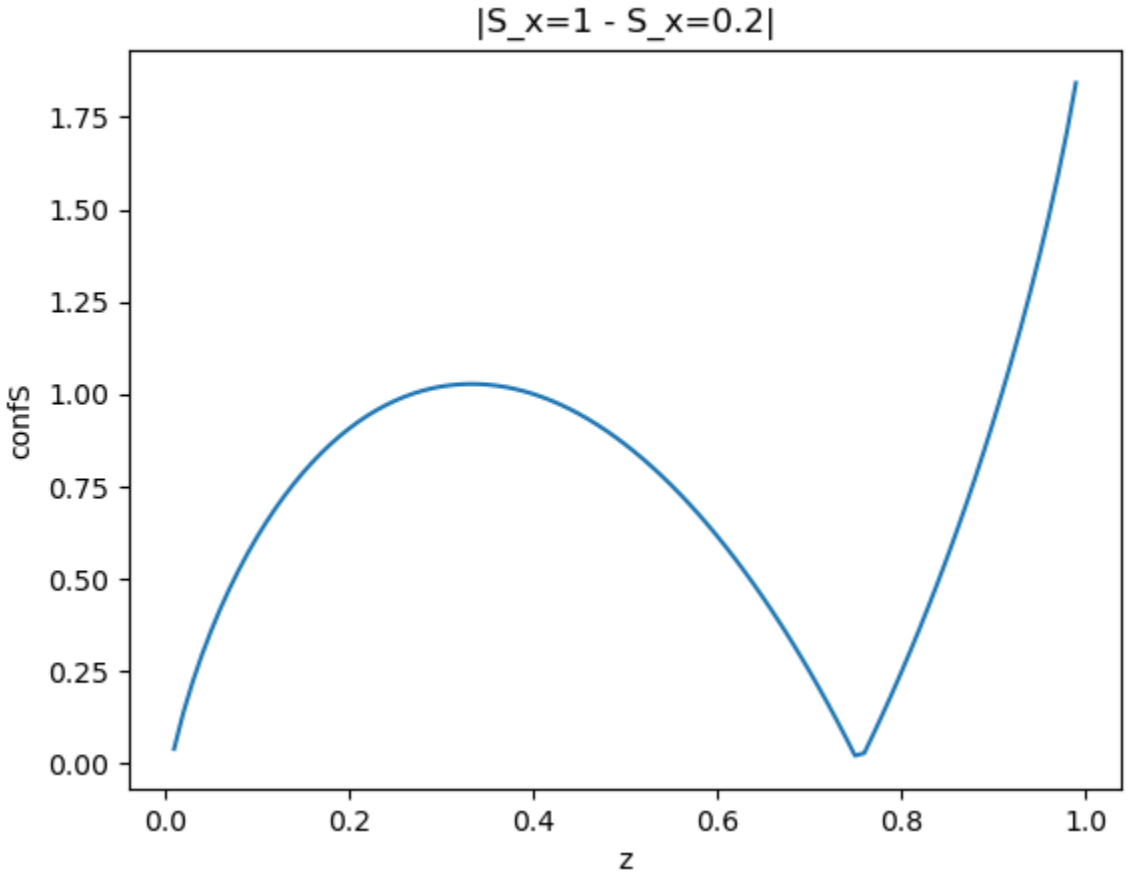

```
x = np.arange(0.01, 1, 0.01)
z = 0.8
y = x*np.log(x/(x+1))/(x+1) + z*np.log(z/(x+1))/(x+1) + (1-z)*np.log((1-z)/(2*(x+1)))/(x+1)
y=-R*y
fig, ax = plt.subplots()
ax.plot(x,y)
ax.set(xlabel='x', ylabel='confS',
       title='confS vs x')


plt.show()
```




```
z = np.arange(0.01, 1, 0.01)
# x = 1
y = np.absolute((np.log(1/2) + z*np.log(z/2) + (1-z)*np.log((1-z)/4))/2 - (0.2*np.log(1/6) + z*np.log(z/1.2) + (1-
z)*np.log((1-z)/2.4))/1.2)
y=R*y
fig, ax = plt.subplots()
ax.plot(z,y)
ax.set(xlabel='z', ylabel='confS',
       title='|S_x=1 - S_x=0.2|')


plt.show()
```

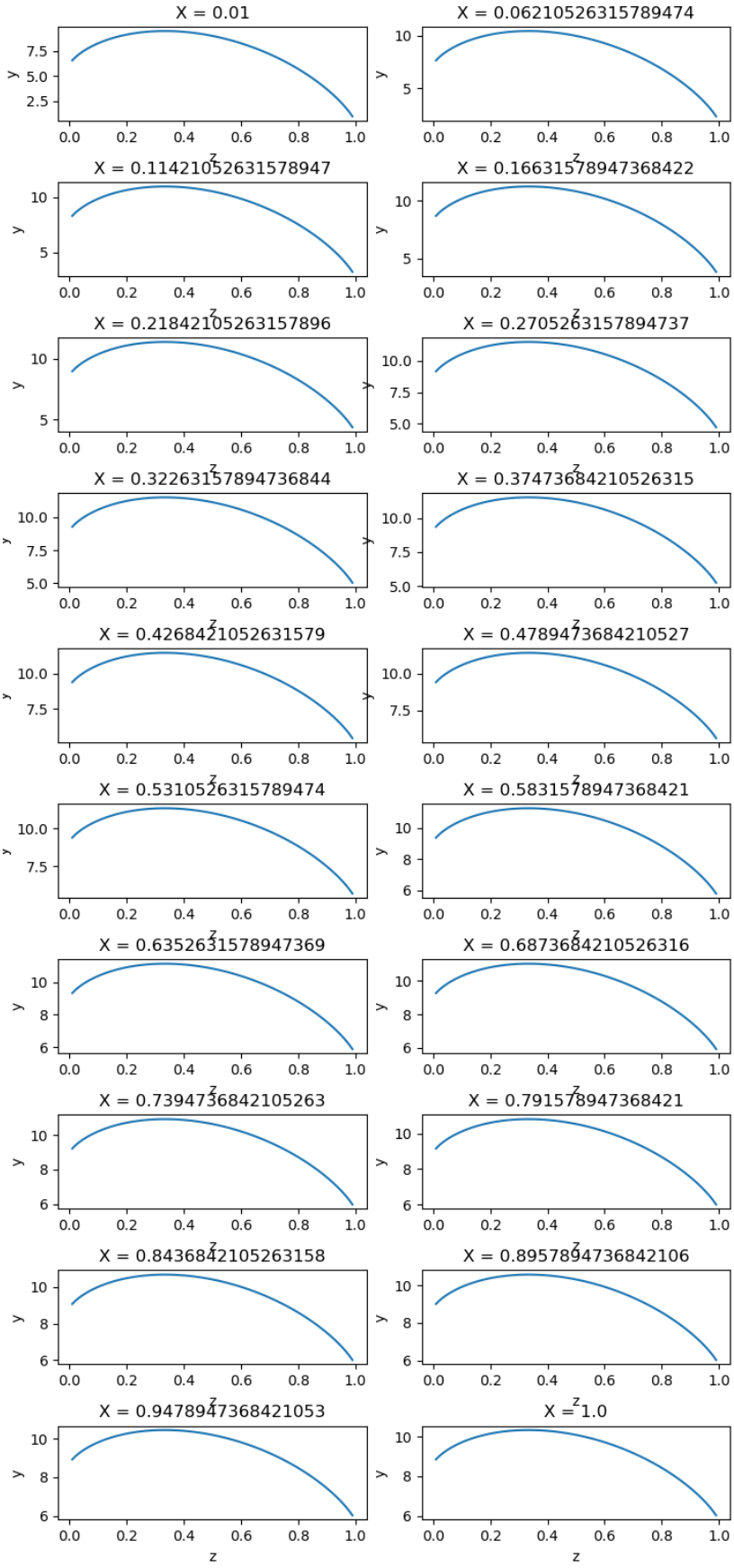



```
x_values = np.linspace(0.01, 1.0, 20)
z = np.arange(0.01, 1, 0.01)

fig, axs = plt.subplots(10, 2, figsize=(10, 20))

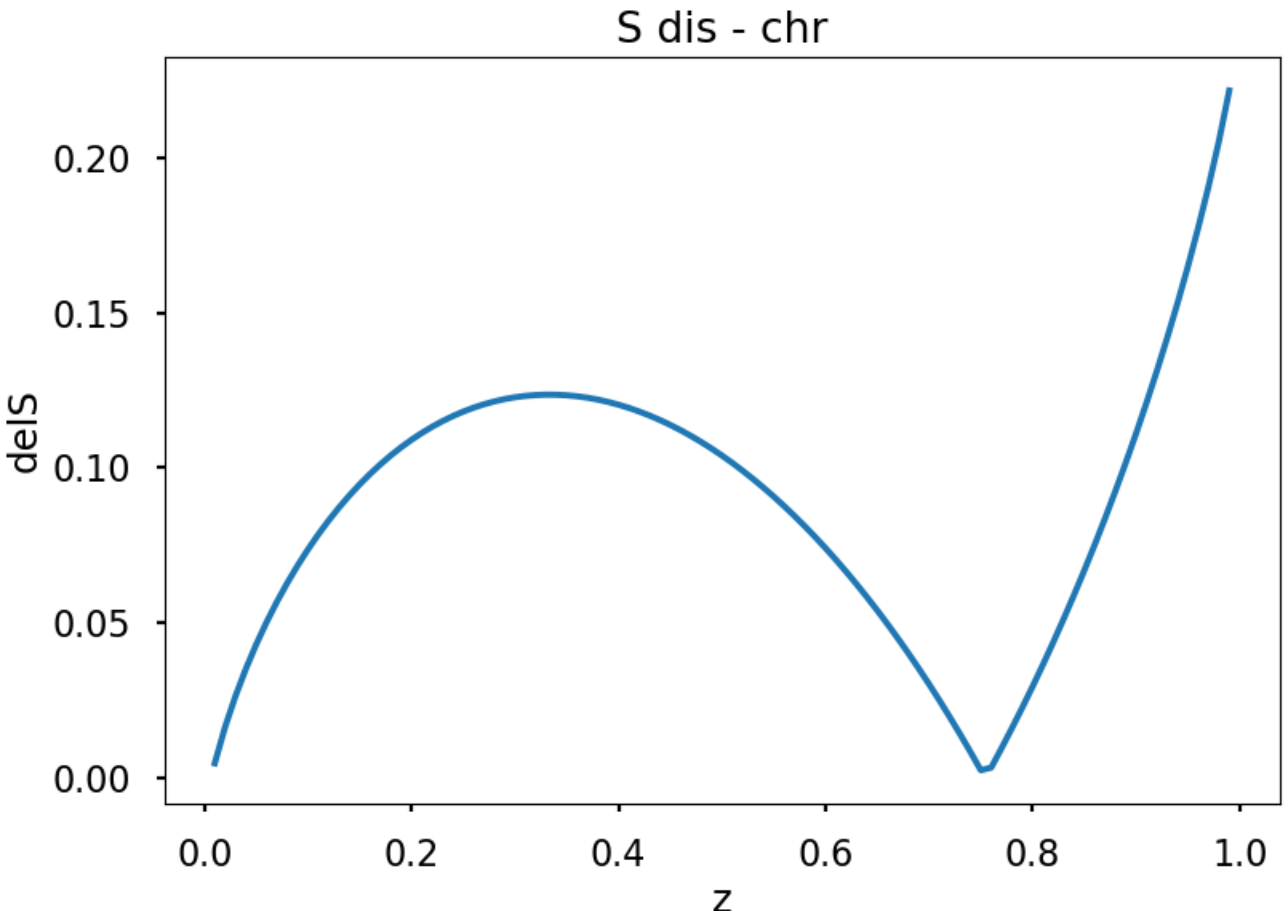
for i, x in enumerate(x_values):
    y = -8.314*(x*np.log(x/(x+1)) + z*np.log(z/(x+1)) + (1-z)*np.log((1-z)/(2*(x+1))))/(x+1)
    row = i // 2
    col = i % 2
    axs[row, col].plot(z, y)
    axs[row, col].set_title(f'X = {x}')
    axs[row, col].set_xlabel('z')
    axs[row, col].set_ylabel('y')

plt.tight_layout()
plt.show()
```


X = 0.01
X = 0.06210526315789474
X = 0.11421052631578947
X = 0.16631578947368422
X = 0.21842105263157896
X = 0.2705263157894737
X = 0.32263157894736844
X = 0.37473684210526315
X = 0.4268421052631579
X = 0.4789473684210527
X = 0.5310526315789474
X = 0.5831578947368421
X = 0.6352631578947369
X = 0.6873684210526316
X = 0.7394736842105263
X = 0.7915789473684211
X = 0.8436842105263158
X = 0.8957894736842106
X = 0.9478947368421053
X = 1.0
y
z

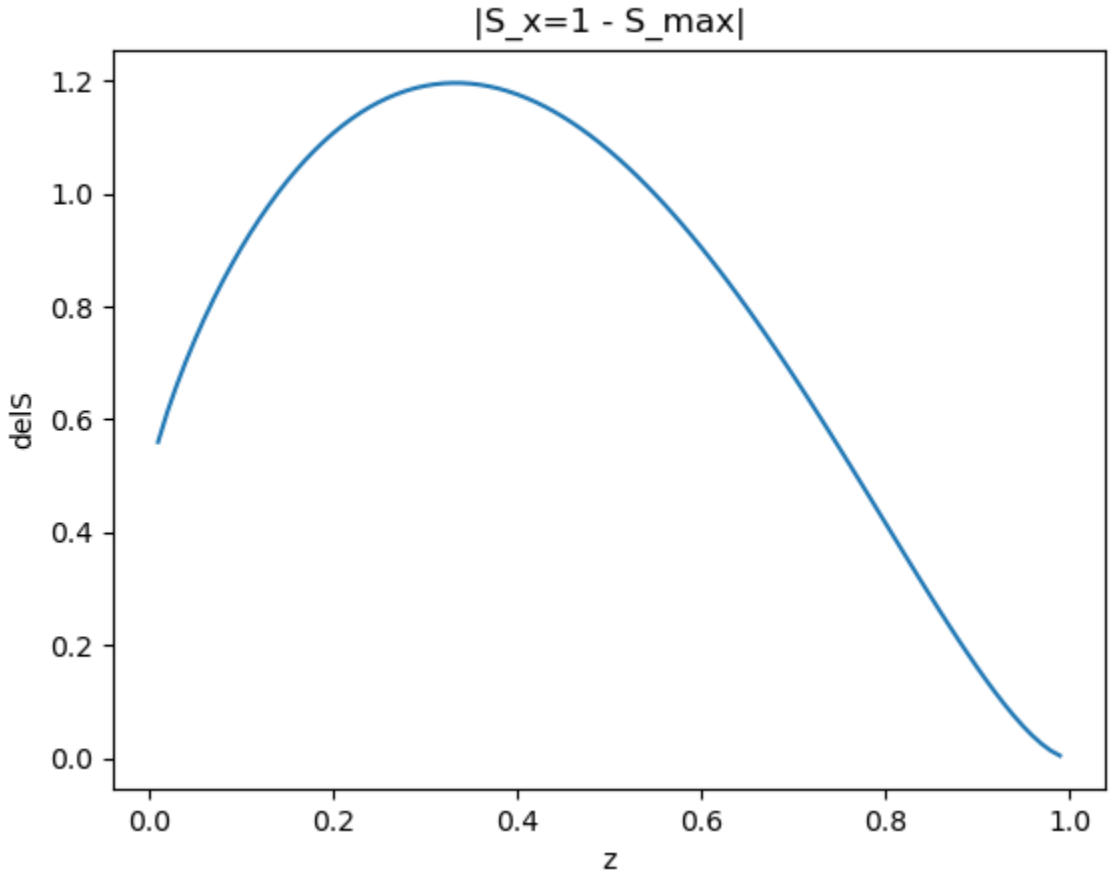
```
z = np.arange(0.01, 1, 0.01)
# x = 1
y = np.absolute((np.log(1/2) + z*np.log(z/2) + (1-z)*np.log((1-z)/4))/2 - (0.2*np.log(1/6) + z*np.log(z/1.2) + (1-
z)*np.log((1-z)/2.4))/1.2)
fig, ax = plt.subplots()
ax.plot(z,y)
ax.set(xlabel='z', ylabel='delS',
    title='S dis - chr')


plt.show()
```



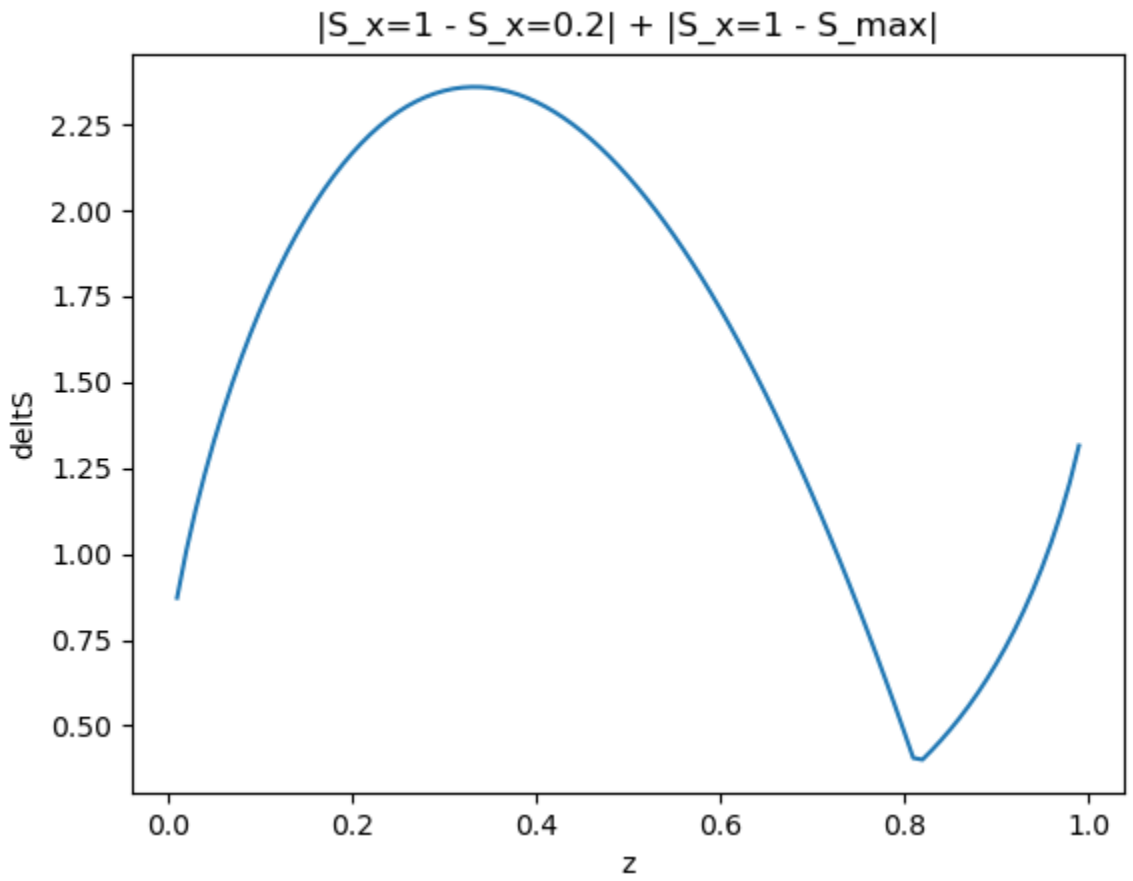

```
z = np.arange(0.01, 1, 0.01)
x = np.exp(z*np.log(z)+(1-z)*np.log((1-z)/2))
y = np.absolute((np.log(1/2) + z*np.log(z/2) + (1-z)*np.log((1-z)/4))/2 - (x*np.log(x/(x+1)) + z*np.log(z/(x+1)) + (1-
z)*np.log((1-z)/(2*(x+1))))/(x+1))
y = R*y
fig, ax = plt.subplots()
ax.plot(z,y)
ax.set(xlabel='z', ylabel='delS',
    title='|S_x=1 - S_max|')


plt.show()
```



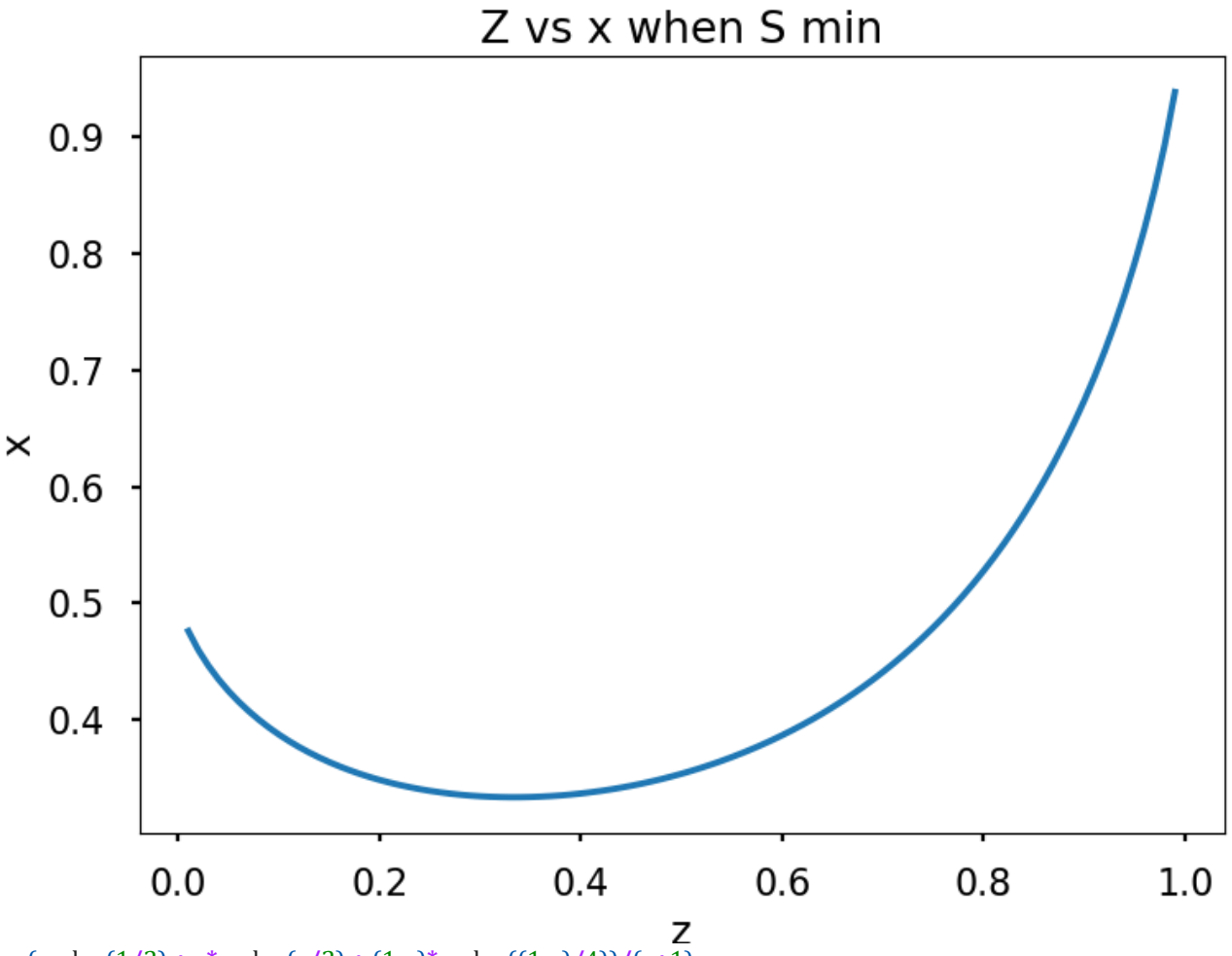

```
z = np.arange(0.01, 1, 0.01)
x = np.exp(z*np.log(z)+(1-z)*np.log((1-z)/2))
y1 = np.absolute((np.log(1/2) + z*np.log(z/2) + (1-z)*np.log((1-z)/4))/2 - (0.27*np.log(0.27/1.27) + z*np.log(z/1.27) + (1-
z)*np.log((1-z)/2.54))/1.27)
y2 = np.absolute((np.log(1/2) + z*np.log(z/2) + (1-z)*np.log((1-z)/4))/2 - (x*np.log(x/(x+1)) + z*np.log(z/(x+1)) + (1-
z)*np.log((1-z)/(2*(x+1))))/(x+1))
y = y1+y2
y = R*y
fig, ax = plt.subplots()
ax.plot(z,y)
ax.set(xlabel='z', ylabel='deltS',
       title='|S_x=1 - S_x=0.2| + |S_x=1 - S_max|')


plt.show()
```




```
z = np.arange(0.01, 1, 0.01)
x = np.exp(z*np.log(z)+(1-z)*np.log((1-z)/2))
# y = np.absolute((np.log(1/2) + z*np.log(z/2) + (1-z)*np.log((1-z)/4))/2 - (x*np.log(x/(x+1)) + z*np.log(z/(x+1)) + (1-z)*np.log((1-z)/(2*(x+1))))/(x+1))
fig, ax = plt.subplots()
ax.plot(z,x)
ax.set(xlabel='z', ylabel='x',
       title='Z vs x when S min')


plt.show()
```




```
S_1 = (np.log(1/2) + z*np.log(z/2) + (1-z)*np.log((1-z)/4))/(x+1)
# S_x = (x*np.log(x/(x+1)) + z*np.log(z/(x+1)) + (1-z)*np.log((1-z)/(2*(x+1))))/(x+1)
S_a = (a*np.log(a/(a+1)) + z*np.log(z/(a+1)) + (1-z)*np.log((1-z)/(2*(a+1))))/(a+1)

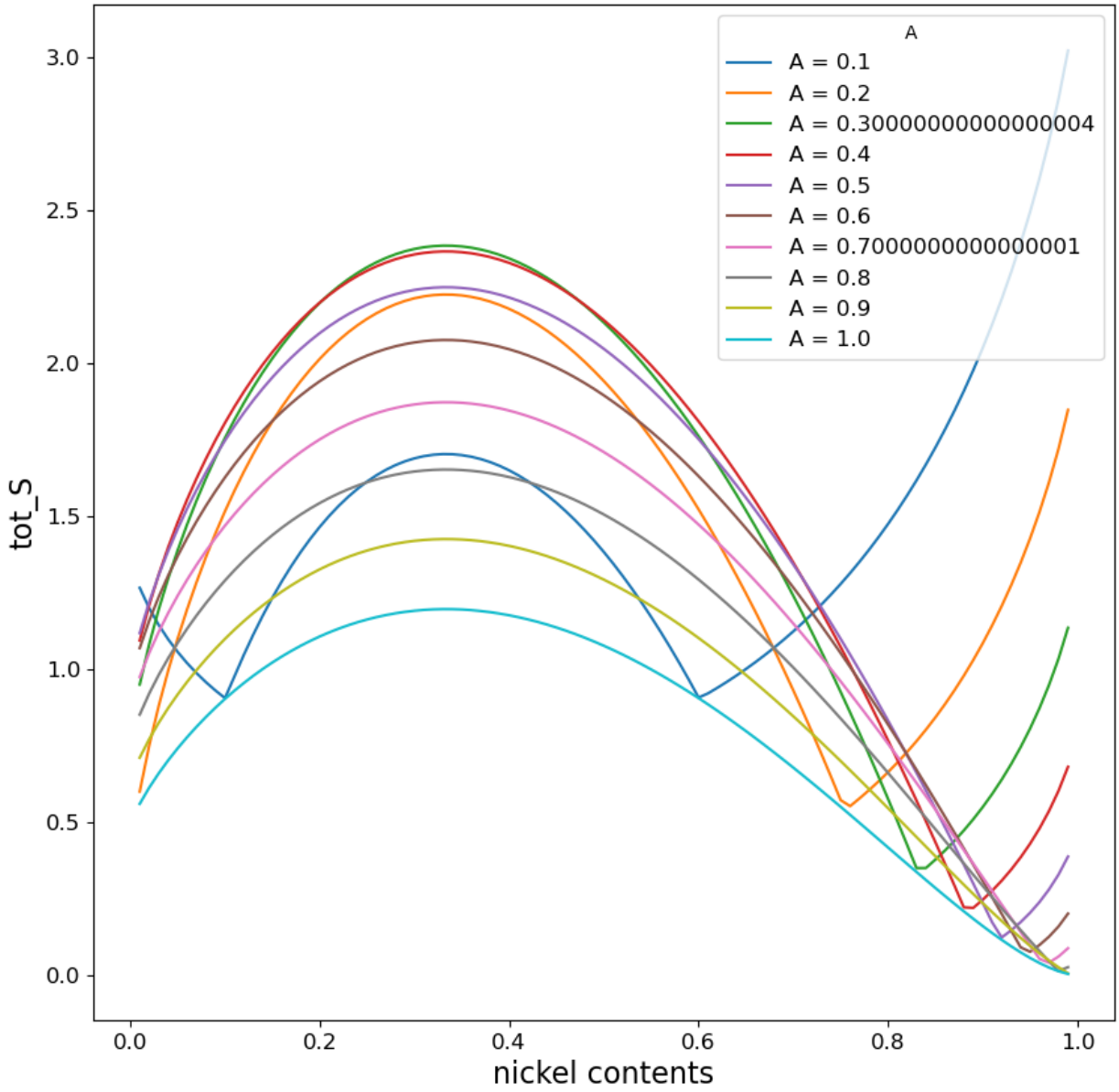
z = np.arange(0, 1, 0.1)
x = np.exp(z*np.log(z)+(1-z)*np.log((1-z)/2))
y1 = np.absolute((np.log(1/2) + z*np.log(z/2) + (1-z)*np.log((1-z)/4))/2 - (0.2*np.log(1/6) + z*np.log(z/1.2) + (1-
z)*np.log((1-z)/2.4))/1.2)
y2 = np.absolute((np.log(1/2) + z*np.log(z/2) + (1-z)*np.log((1-z)/4))/2 - (x*np.log(x/(x+1)) + z*np.log(z/(x+1)) + (1-
z)*np.log((1-z)/(2*(x+1))))/(x+1))
y = y1+y2


a_values = np.linspace(0.1, 1.0, 10)
z = np.arange(0.01, 1, 0.01)
x_min = np.exp(z*np.log(z) + (1-z)*np.log((1-z)/2))
S_1 = (np.log(1/2) + z*np.log(z/2) + (1-z)*np.log((1-z)/4))/2
S_min = (x_min*np.log(x_min/(x_min+1)) + z*np.log(z/(x_min+1)) + (1-z)*np.log((1-z)/(2*(x_min+1))))/(x_min+1)
y2 = np.absolute(S_1 - S_min)
y2 = 8.314 * y2

fig, ax = plt.subplots(figsize=(10, 10))
```

```
for a in a_values:
    S_a = (a*np.log(a/(a+1)) + z*np.log(z/(a+1)) + (1-z)*np.log((1-z)/(2*(a+1))))/(a+1)
    y1 = np.absolute(S_1 - S_a)
    y1 = 8.314 * y1
    y = y1 + y2
    ax.plot(z, y, label=f'A = {a}')

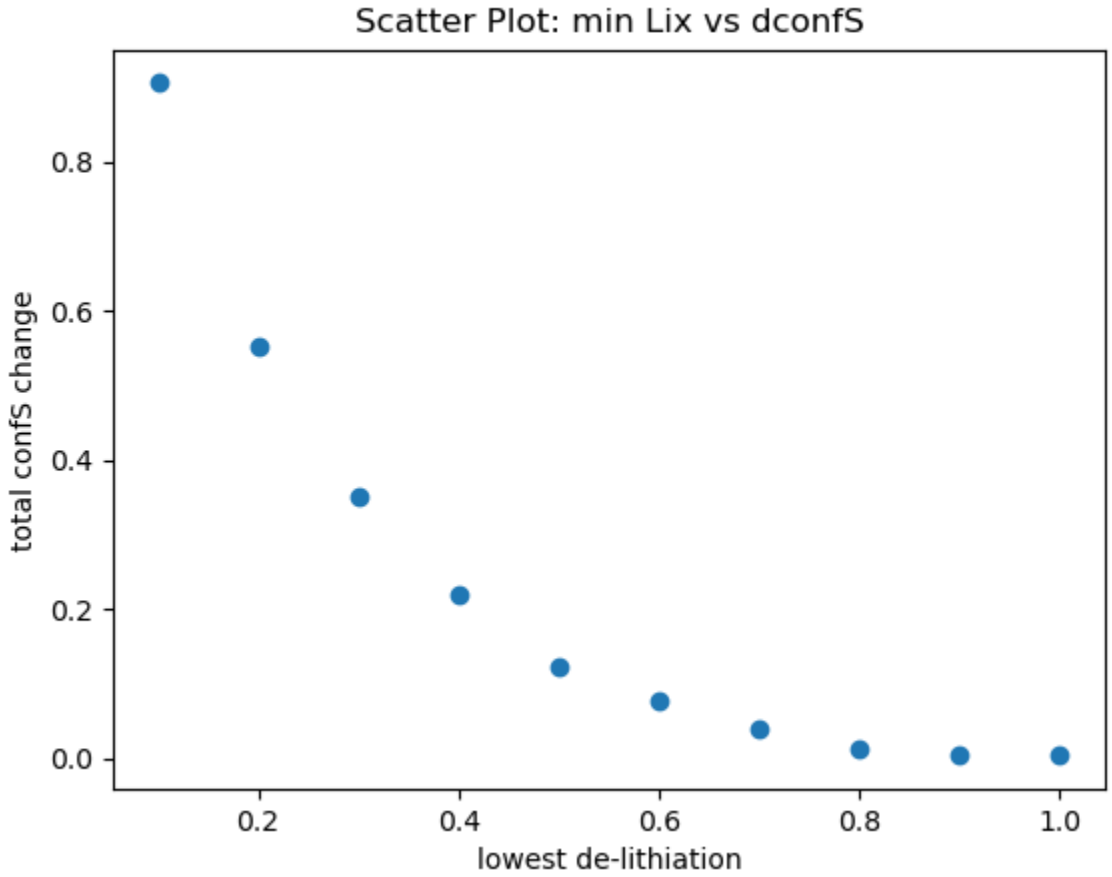
ax.set_xlabel('nickel contents', fontsize=16)
ax.set_ylabel('tot_S', fontsize=16)
ax.legend(title='A', fontsize=12)
ax.tick_params(axis='both', labelsize=12)
```




```
x = a_values
y = min_values

fig = plt.subplots()
plt.scatter(x, y)
plt.xlabel('lowest de-lithiation')
plt.ylabel('total confS change')
plt.title('Scatter Plot: min Lix vs dconfS')

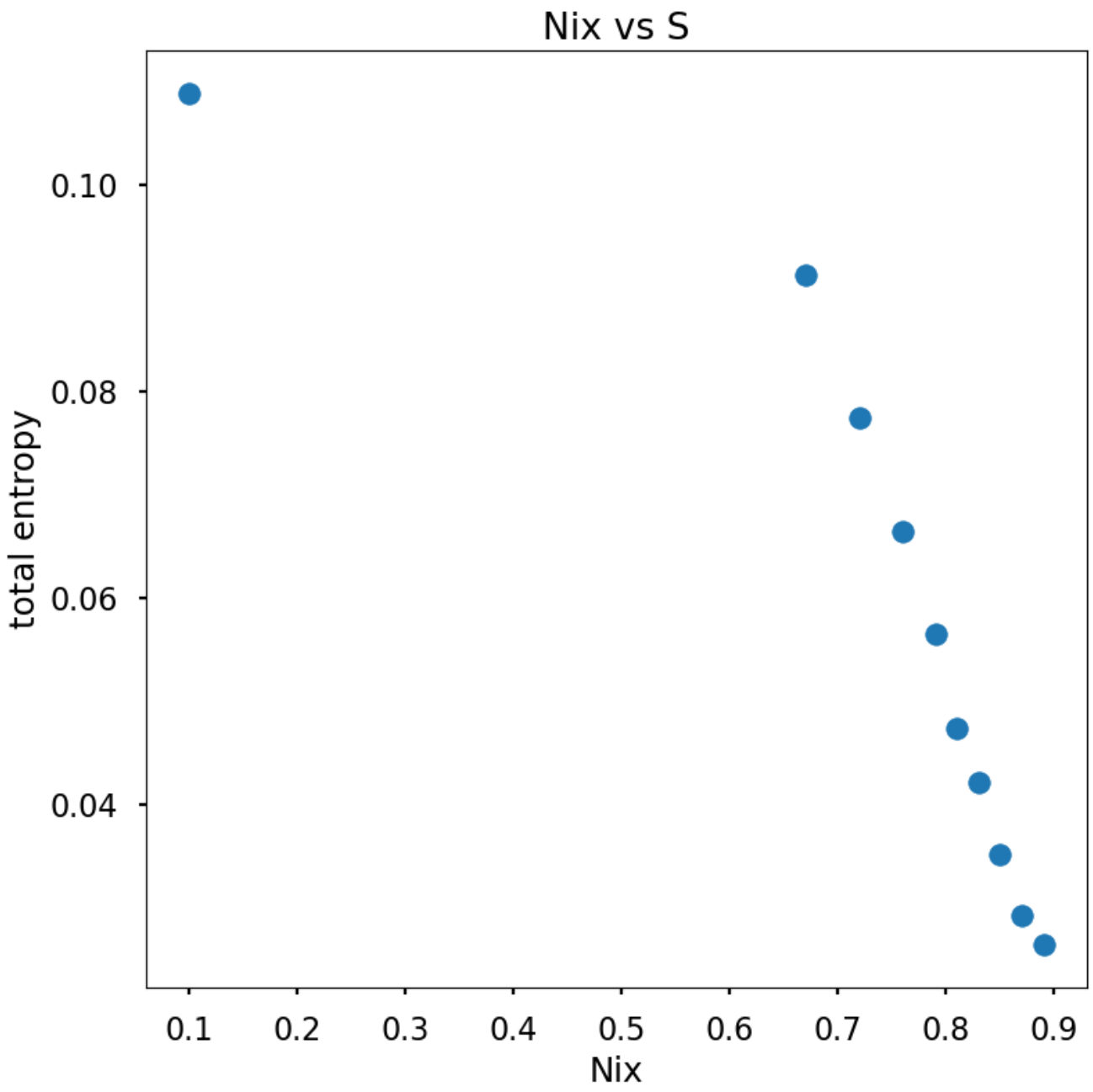
plt.show()
```




```
x = min_x_values
y = min_values

fig = plt.subplots()
plt.scatter(x, y)
plt.xlabel('Nix')
plt.ylabel('total entropy')
plt.title('Nix vs S')

plt.show()
```



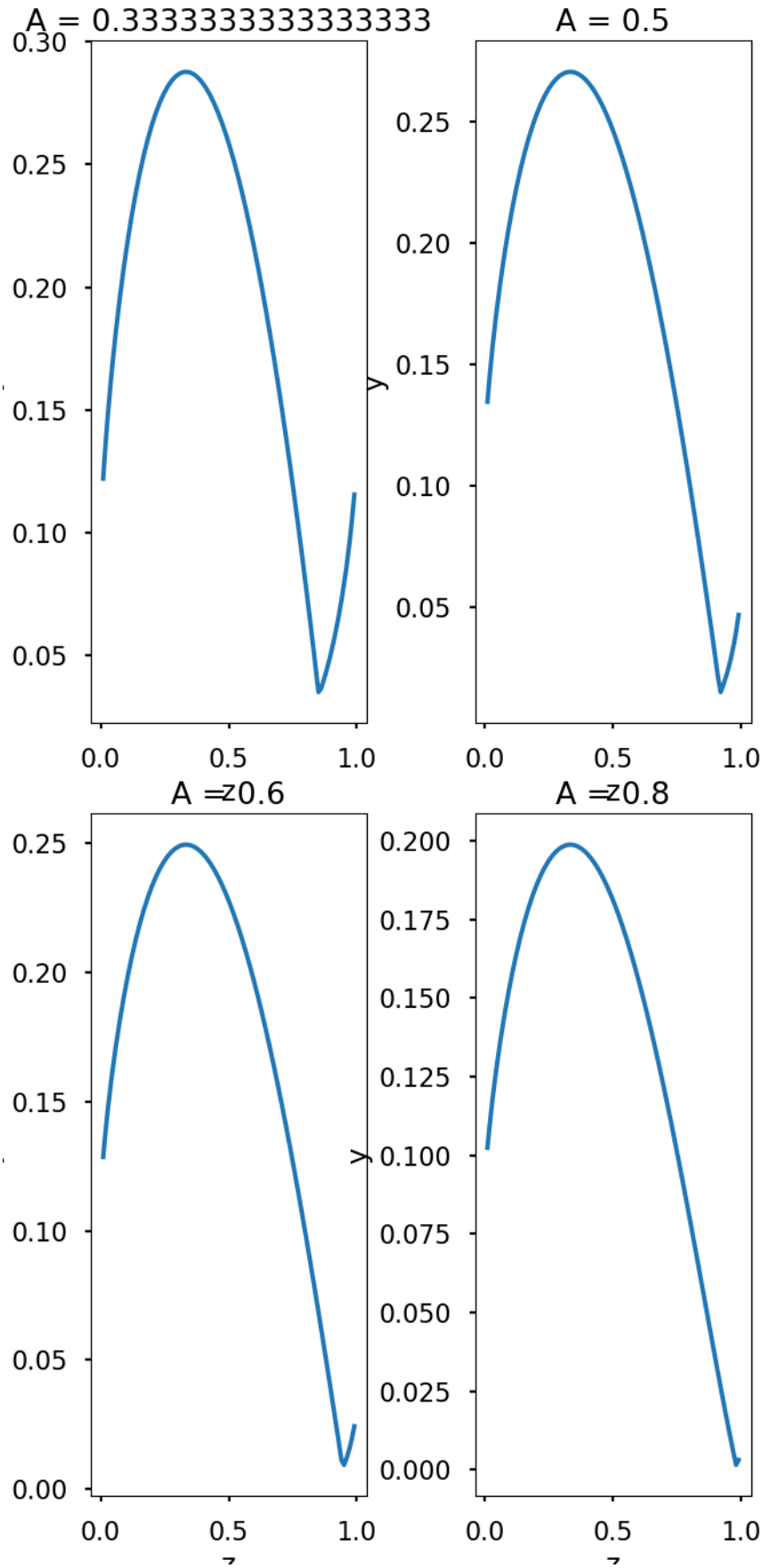

```
a_values = [1/3, 0.5, 0.6, 0.8]

z = np.arange(0.01, 1, 0.01)
x_min = np.exp(z*np.log(z)+(1-z)*np.log((1-z)/2))
S_1 = (np.log(1/2) + z*np.log(z/2) + (1-z)*np.log((1-z)/4))/2
S_min = (x_min*np.log(x_min/(x_min+1)) + z*np.log(z/(x_min+1)) + (1-z)*np.log((1-z)/(2*(x_min+1))))/(x_min+1)
y2 = np.absolute(S_1 - S_min)

fig, axs = plt.subplots(2, 2, figsize=(10, 20))
```

```
for i, a in enumerate(a_values):
    S_a = (a*np.log(a/(a+1)) + z*np.log(z/(a+1)) + (1-z)*np.log((1-z)/(2*(a+1))))/(a+1)
    y1 = np.absolute(S_1 - S_a)
    y = y1 + y2
    row = i // 2
    col = i % 2
    axs[row, col].plot(z, y)
    axs[row, col].set_title(f'A = {a}')
    axs[row, col].set_xlabel('z')
    axs[row, col].set_ylabel('y')

plt.tight_layout()
plt.show()
```


A = 0.3333333333333333
A = 0.5
A =z0.6
A =z0.8
y
z
0.0
0.5
1.0
0.30
0.25
0.20
0.15
0.10
0.05
0.00
0.200
0.175
0.150
0.125
0.100
0.075
0.050
0.025
0.000

```
a_values = np.linspace(0.1, 0.3, 10)
z = np.arange(0.01, 1, 0.01)
x_min = np.exp(z * np.log(z) + (1 - z) * np.log((1 - z) / 2))
S_1 = (np.log(1 / 2) + z * np.log(z / 2) + (1 - z) * np.log((1 - z) / 4)) / 2
S_min = (x_min * np.log(x_min / (x_min + 1)) + z * np.log(z / (x_min + 1)) + (1 - z) * np.log((1 - z) / (2 * (x_min + 1)))) / (x_min
+ 1)
y2 = np.absolute(S_1 - S_min)

min_values = []

for i, a in enumerate(a_values):
    S_a = (a * np.log(a / (a + 1)) + z * np.log(z / (a + 1)) + (1 - z) * np.log((1 - z) / (2 * (a + 1)))) / (a + 1)
    y1 = np.absolute(S_1 - S_a)
    y = y1 + y2
    min_value = np.min(y)
    min_values.append(min_value)

plt.plot(a_values, min_values)
plt.title('Minimum Values')
plt.xlabel('A values')
plt.ylabel('Minimum Tot_S')
plt.show()
import numpy as np
from scipy.optimize import differential_evolution

# Define the equation
def equation(x):
    z = 0.8
    y = x*np.log(x/(x+1))/(x+1) + z*np.log(z/(x+1))/(x+1) + (1-z)*np.log((1-z)/(2*(x+1)))/(x+1)
    y = -8.314 * y
    return y

# Find the maximum and minimum points
result_max = differential_evolution(lambda x: -equation(x), bounds=[(0, 1)])
result_min = differential_evolution(equation, bounds=[(0, 1)])

# Print the results
print("Maximum point: ({}, {})".format(result_max.x[0], -result_max.fun))
print("Minimum point: ({}, {})".format(result_min.x[0], result_min.fun))
Maximum point: (0.5278031537284288, [8.83664068])
Minimum point: (4.403721287787876e-05, 5.31671529300319)
C:\Users\Yimc\Anaconda3\lib\site-packages\ipykernel_launcher.py:7: RuntimeWarning: divide by zero encountered in log
  import sys
C:\Users\Yimc\Anaconda3\lib\site-packages\ipykernel_launcher.py:7: RuntimeWarning: invalid value encountered in
multiply
  import sys
z = 0.8
x=1
y1 = x*np.log(x/(x+1))/(x+1) + z*np.log(z/(x+1))/(x+1) + (1-z)*np.log((1-z)/(2*(x+1)))/(x+1)
y1=-R*y1
S=8.83664068-y1
S
0.4173595802588306
import numpy as np

# Define the equation
```

```
def equation(x):
    z = 0.8
    y = x*np.log(x/(x+1))/(x+1) + z*np.log(z/(x+1))/(x+1) + (1-z)*np.log((1-z)/(2*(x+1)))/(x+1)
    y = -8.314 * y
    return y

# Set the threshold
threshold = 0.4173595802588306

# Initialize variables
max_diff_x = 0
max_diff_y = 0

# Iterate through different values of x
for x in np.linspace(0, 1, num=1000):
    y = equation(x)
    diff_y = abs(y - equation(1))
    if diff_y < threshold:
        diff_x = abs(x - 1)
        if diff_x > max_diff_x:
            max_diff_x = diff_x
            max_diff_y = diff_y

# Print the maximum differences
print("Maximum difference of x: {}".format(max_diff_x))
print("Difference of y when x is 1 and y is max: {}".format(max_diff_y))
```

```
Maximum difference of x: 0.8268268268268268
Difference of y when x is 1 and y is max: 0.41085147878119166
C:\Users\Yimc\Anaconda3\lib\site-packages\ipykernel_launcher.py:6: RuntimeWarning: divide by zero encountered in log

C:\Users\Yimc\Anaconda3\lib\site-packages\ipykernel_launcher.py:6: RuntimeWarning: invalid value encountered in
double_scalars
```

```
import numpy as np
from scipy.optimize import minimize

# Define the equation
def equation(x, z):
    y = x*np.log(x/(x+1))/(x+1) + z*np.log(z/(x+1))/(x+1) + (1-z)*np.log((1-z)/(2*(x+1)))/(x+1)
    y = -8.314 * y
    return y

# Set the threshold
threshold = 0.4173595802588306

# Define the objective function
def objective(xz):
    x, z = xz
    return -abs(equation(x, z) - equation(1, 1))

# Define the constraint function
def constraint(xz):
    x, z = xz
    return threshold - abs(equation(1, 1) - equation(x, z))

# Set the initial guess
```

```
x0 = [0.5, 0.8]

# Set the bounds for x and z
bounds = [(0, 1), (0.7, 0.9)]

# Define the optimization problem
problem = {'type': 'ineq', 'fun': constraint}

# Solve the optimization problem
result = minimize(objective, x0, bounds=bounds, constraints=problem)

# Extract the optimal values
optimal_x, optimal_z = result.x

# Calculate the maximum differences
max_diff_x = abs(optimal_x - 1)
max_diff_y = abs(equation(optimal_x, optimal_z) - equation(1, 1))

# Print the results
print("Optimal x: {}".format(optimal_x))
print("Optimal z: {}".format(optimal_z))
print("Maximum difference of x: {}".format(max_diff_x))
print("Difference of y when x is 1 and y is max: {}".format(max_diff_y))
Optimal x: 0.5
Optimal z: 0.8
Maximum difference of x: 0.5
Difference of y when x is 1 and y is max: nan
C:\Users\Yimc\Anaconda3\lib\site-packages\ipykernel_launcher.py:6: RuntimeWarning: divide by zero encountered in log

C:\Users\Yimc\Anaconda3\lib\site-packages\ipykernel_launcher.py:6: RuntimeWarning: invalid value encountered in
double_scalars

a_values = np.linspace(0.1,1.0,10)

z = np.arange(0.7, 1, 0.01)
x_max = np.exp(z*np.log(z)+(1-z)*np.log((1-z)/2))
S_1 = (np.log(1/2) + z*np.log(z/2) + (1-z)*np.log((1-z)/4))/2
S_max = (x_max*np.log(x_max/(x_max+1)) + z*np.log(z/(x_max+1)) + (1-z)*np.log((1-z)/(2*(x_max+1))))/(x_max+1)
y2 = np.absolute(S_1 - S_min)
y2=R*y2

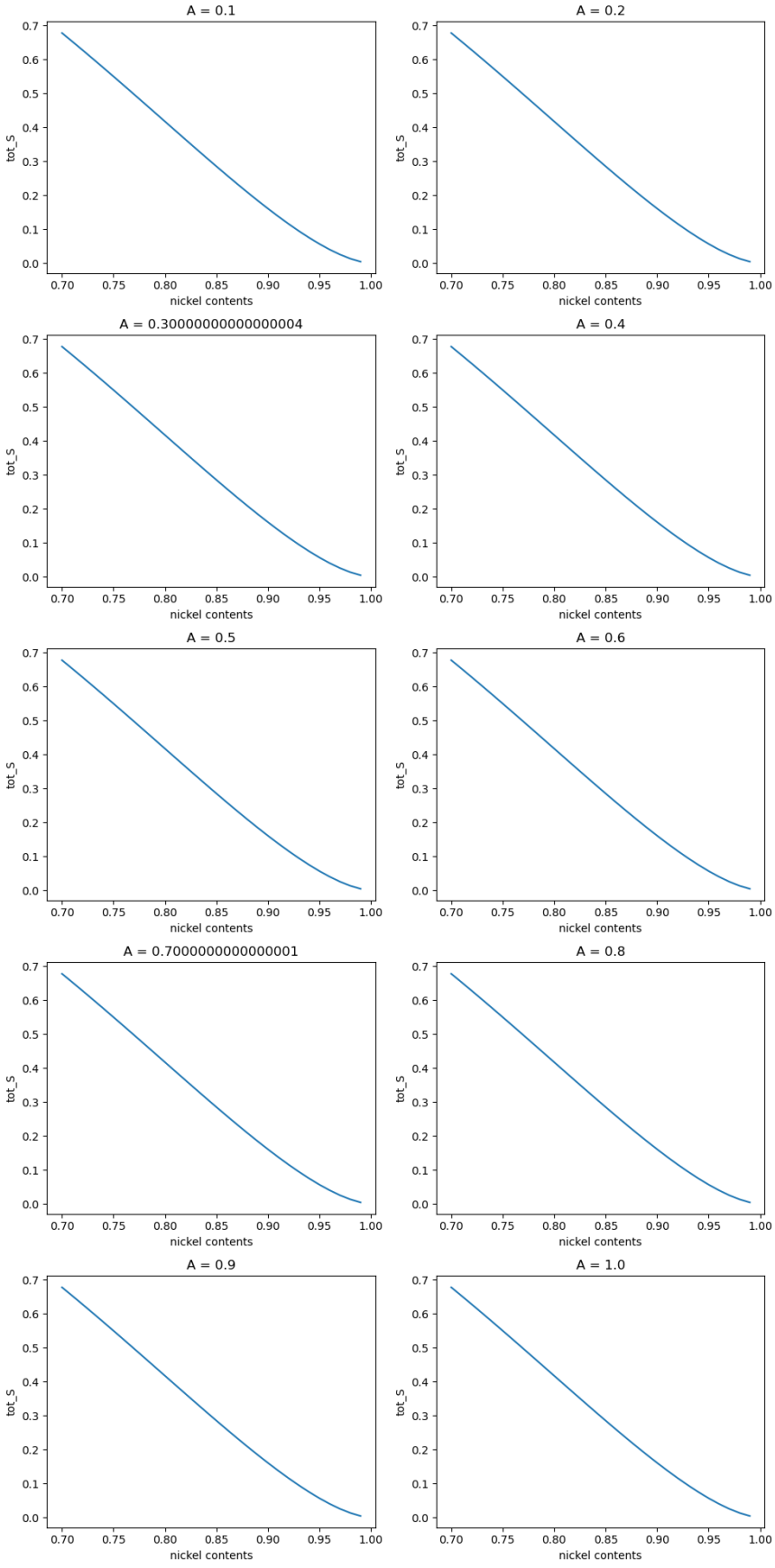
fig, axs = plt.subplots(5, 2, figsize=(10, 20))

min_values = []
min_indices = []

for i, a in enumerate(a_values):
    #S_a = (a*np.log(a/(a+1)) + z*np.log(z/(a+1)) + (1-z)*np.log((1-z)/(2*(a+1))))/(a+1)
    #y1 = np.absolute(S_1 - S_a)
    #y1=R*y1
    y = y2 # + y1
    row = i // 2
    col = i % 2
    axs[row, col].plot(z, y)
    axs[row, col].set_title(f'A = {a}')
    axs[row, col].set_xlabel('nickel contents')
```

```
    axs[row, col].set_ylabel('tot_S')
    min_value = np.min(y)
    min_index = np.argmin(y)
    min_values.append(min_value)
    min_indices.append(min_index)

min_x_values = z[min_indices]
plt.tight_layout()
plt.show()
C:\Users\Yimc\Anaconda3\lib\site-packages\ipykernel_launcher.py:4: RuntimeWarning: invalid value encountered in log
  after removing the cwd from sys.path.
C:\Users\Yimc\Anaconda3\lib\site-packages\ipykernel_launcher.py:5: RuntimeWarning: invalid value encountered in log
  """
```


A = 0.1
A = 0.2
A = 0.30000000000000004
A = 0.4
A = 0.5
A = 0.6
A = 0.7000000000000001
A = 0.8
A = 0.9
A = 1.0
tot_S
nickel contents
0.0
0.1
0.2
0.3
0.4
0.5
0.6
0.7
0.70
0.75
0.80
0.85
0.90
0.95
1.00

```
import numpy as np
from scipy.optimize import fsolve

def equation(x, z):
    R = 1.0  # Set the value of R
    return -R*(x*np.log(x/(x+1)) + z*np.log(z/(x+1)) + (1-z)*np.log((1-z)/(2*(x+1))))/(x+1)

def find_intercept(z):
    # Define the equation to find the intercept
    def intercept_equation(x):
        return equation(x, z)

    # Use scipy's fsolve function to find the intercept
    intercept = fsolve(intercept_equation, 0.5)

    return intercept[0]

# Set the range of z values
z_values = np.linspace(0.7, 1, 10)

# Find the intercept for each z value
intercepts = []
for z in z_values:
    intercept = find_intercept(z)
    intercepts.append(intercept)
    print(f"For z={z}, the intercept is x={intercept}")

# Print the corresponding values of x for each z value
for z, x in zip(z_values, intercepts):
    print(f"For z={z}, the intercept is x={x}")
```

```
For z=0.7, the intercept is x=2.6002120040829792e+85
For z=0.7333333333333333, the intercept is x=3.884518116046214e+85
For z=0.7666666666666666, the intercept is x=5.108258442469903e+85
For z=0.7999999999999999, the intercept is x=0.5
For z=0.8333333333333333, the intercept is x=0.5
For z=0.8666666666666667, the intercept is x=0.5
For z=0.9, the intercept is x=0.5
For z=0.9333333333333333, the intercept is x=0.5
For z=0.9666666666666667, the intercept is x=0.5
For z=1.0, the intercept is x=0.5
For z=0.7, the intercept is x=2.6002120040829792e+85
For z=0.7333333333333333, the intercept is x=3.884518116046214e+85
For z=0.7666666666666666, the intercept is x=5.108258442469903e+85
For z=0.7999999999999999, the intercept is x=0.5
For z=0.8333333333333333, the intercept is x=0.5
For z=0.8666666666666667, the intercept is x=0.5
For z=0.9, the intercept is x=0.5
For z=0.9333333333333333, the intercept is x=0.5
For z=0.9666666666666667, the intercept is x=0.5
For z=1.0, the intercept is x=0.5
C:\Users\Yimc\Anaconda3\lib\site-packages\ipykernel_launcher.py:6: RuntimeWarning: invalid value encountered in log

C:\Users\Yimc\Anaconda3\lib\site-packages\ipykernel_launcher.py:6: RuntimeWarning: divide by zero encountered in log

C:\Users\Yimc\Anaconda3\lib\site-packages\ipykernel_launcher.py:6: RuntimeWarning: invalid value encountered in
multiply
```

```
import numpy as np
import matplotlib.pyplot as plt
from scipy.optimize import fsolve

%matplotlib notebook

R = 8.314

def equation1(x, z):
    return -R*(np.log(1/(1+1)) + z*np.log(z/(1+1)) + (1-z)*np.log((1-z)/(2*(1+1))))/(1+1)

def equation2(x, z):
    return -R*(x*np.log(x/(x+1)) + z*np.log(z/(x+1)) + (1-z)*np.log((1-z)/(2*(x+1))))/(x+1)

def find_intercept(z):
    def intercept_equation(vars):
        x, y = vars
        eq1 = equation1(x, z)
        eq2 = equation2(x, z)
        return [eq1 - eq2, y - eq1]

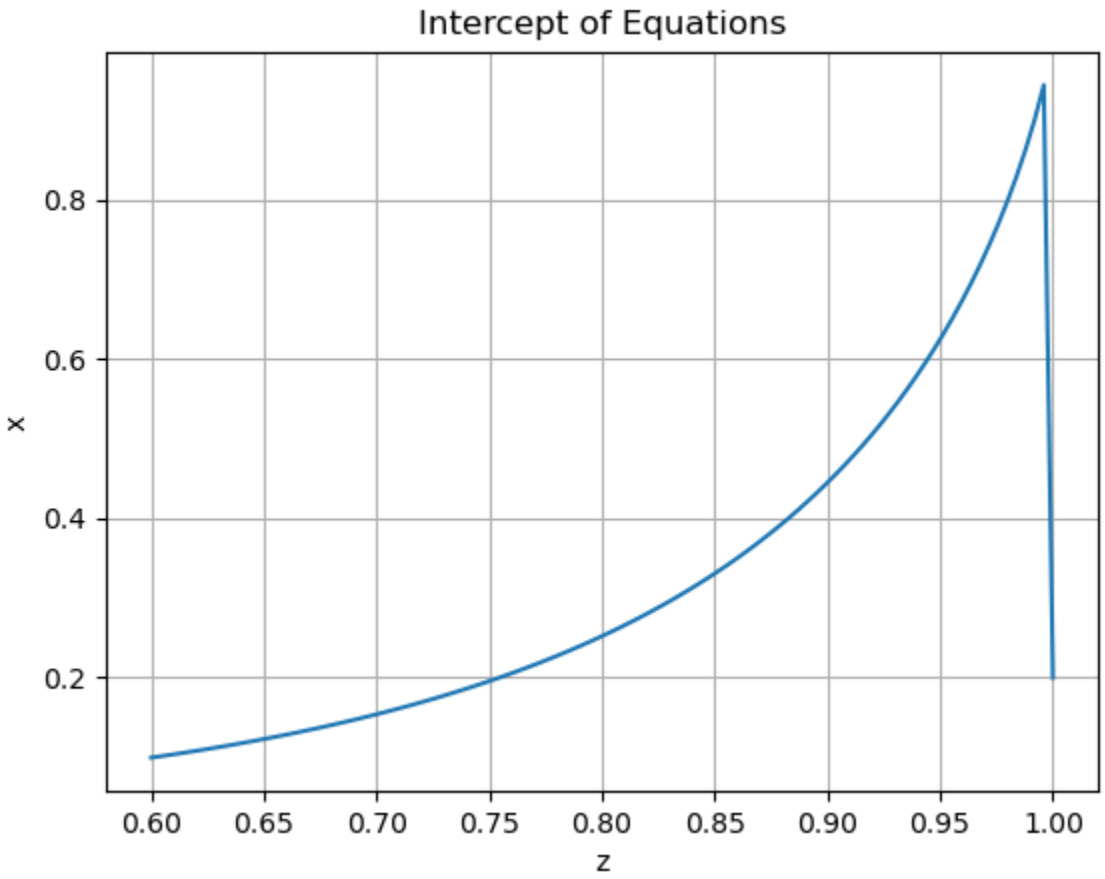
    initial_guess = [0.2, equation1(0.5, z)]
    intercept = fsolve(intercept_equation, initial_guess)
    return intercept[0]

z_values = np.linspace(0.6, 1, 100)

intercepts = [find_intercept(z) for z in z_values]

plt.plot(z_values, intercepts)
plt.xlabel('z')
plt.ylabel('x')
plt.title('Intercept of Equations')
plt.grid(True)
plt.show()
```

```
C:\Users\Yimc\Anaconda3\lib\site-packages\ipykernel_launcher.py:10: RuntimeWarning: divide by zero encountered in log
  # Remove the CWD from sys.path while we load stuff.
C:\Users\Yimc\Anaconda3\lib\site-packages\ipykernel_launcher.py:10: RuntimeWarning: invalid value encountered in
double_scalars
  # Remove the CWD from sys.path while we load stuff.
C:\Users\Yimc\Anaconda3\lib\site-packages\ipykernel_launcher.py:13: RuntimeWarning: divide by zero encountered in log
  del sys.path[0]
C:\Users\Yimc\Anaconda3\lib\site-packages\ipykernel_launcher.py:13: RuntimeWarning: invalid value encountered in
double_scalars
  del sys.path[0]
C:\Users\Yimc\AppData\Roaming\Python\Python37\site-packages\scipy\optimize\minpack.py:162: RuntimeWarning: The
iteration is not making good progress, as measured by the
  improvement from the last ten iterations.
  warnings.warn(msg, RuntimeWarning)
```



7.1.2 Jupyter code to create VASP input files

```
from pymatgen.io.vasp.sets import MPRelaxSet
from pymatgen.core import Lattice, Structure
from pymatgen.symmetry.analyzer import SpacegroupAnalyzer
from pymatgen.transformations.standard_transformations import
OrderDisorderedStructureTransformation
location = "NMCs/"

# file_name = "POSCAR"
# user_incar_settings = {"NCORE": 4, "NPAR":4, "KPAR": 4}
# vasp_input_set = MPRelaxSet(structure, user_incar_settings=user_incar_settings)
# structure = Structure.from_file(location + file_name)
# vasp_input_set.write_input("./" + location)

sub_locations = ["LNO221","dLNO221","LCO221","dLCO221"]
```

```
sub_locations =
["NiMnCo","dLNiMnCo","Ni50MnCo","dLNi50MnCo","Ni67MnCo","dLNi67MnCo","Ni85MnCo","dLNi85MnCo"]

for sub_location in sub_locations:
    structure = Structure.from_file(location + sub_location + "/" + file_name)
    user_incar_settings = {"ISMEAR": -1, "NCORE": 4, "NPAR":4, "KPAR": 4}
    vasp_input_set = MPRelaxSet(structure, user_incar_settings=user_incar_settings)
    vasp_input_set.write_input("./" + location + sub_location + "/")
    vasp_input_set.write_input("./")
```

7.1.3 Jupyter code to dope

```
from pymatgen.io.vasp import Poscar
from pymatgen.io.cif import CifWriter
from pymatgen.core import Lattice, Structure
from pymatgen.io.vasp.sets import MPRelaxSet
location = "Ni85/Ni85CoMn/"
file_name = "POSCAR"
structure = Structure.from_file(location + file_name)
species = ["Al", "Mg", "Fe", "Zn", "Ti"]
for specie in species:
    new_structure = structure.copy().replace_species({"Mn":specie})
    location = "Ni85/Ni85Co" + specie + "/"
    user_incar_settings = {"ISMEAR": -1, "NCORE": 4, "NPAR":4, "KPAR": 4}
    vasp_input_set = MPRelaxSet(new_structure, user_incar_settings=user_incar_settings)
    vasp_input_set.write_input("./" + location)
```

7.1.4 Examples of VASP input files

7.1.4.1 POSCAR FILE

Li12 Co12 O24

1.0

5.7146615982000002 0.0000000000000000 0.0000000000000000

-2.8573307991000001 4.9490421181000004 0.0000000000000000

0.0000000000000000 0.0000000000000000 14.0615682601999996

Li Co O

12 12 24

direct

0.0000000000000000 0.0000000000000000 0.0000000000000000 Li

0.0000000000000000 0.5000000000000000 0.0000000000000000 Li

0.5000000000000000 0.0000000000000000 0.0000000000000000 Li

0.5000000000000000 0.5000000000000000 0.0000000000000000 Li

0.3333333130000000 0.1666666720000000 0.3333333130000000 Li

0.3333333130000000 0.6666666870000000 0.3333333130000000 Li

0.8333333130000000 0.1666666720000000 0.3333333130000000 Li

0.8333333130000000 0.6666666870000000 0.3333333130000000 Li

0.1666666720000000 0.3333333130000000 0.6666666870000000 Li

0.1666666720000000 0.8333333130000000 0.6666666870000000 Li

0.6666666870000000 0.3333333130000000 0.6666666870000000 Li

0.6666666870000000 0.8333333130000000 0.6666666870000000 Li

0.4999999700000000 0.4999999700000000 0.5000000000000000 Co

0.1666666720000000 0.3333333130000000 0.1666666270000000 Co

0.1666666720000000 0.8333333130000000 0.1666666270000000 Co

0.6666666870000000 0.3333333130000000 0.1666666270000000 Co

0.6666666870000000 0.8333333130000000 0.1666666270000000 Co

0.4999999700000000 0.0000000000000000 0.5000000000000000 Co

0.0000000000000000 0.4999999700000000 0.5000000000000000 Co

0.0000000000000000 0.0000000000000000 0.5000000000000000 Co

0.3333333130000000 0.1666666720000000 0.8333332540000000 Co

0.3333333130000000 0.6666666870000000 0.8333332540000000 Co

0.8333333130000000 0.1666666720000000 0.8333332540000000 Co

0.8333333130000000 0.6666666870000000 0.8333332540000000 Co

0.3333333130000000 0.1666666720000000 0.0923492910000000 O

0.3333333130000000 0.6666666870000000 0.0923492910000000 O

0.8333333130000000 0.1666666720000000 0.0923492910000000 O

0.8333333130000000 0.6666666870000000 0.0923492910000000 O

0.0000000000000000 0.0000000000000000 0.2409839030000000 O

0.0000000000000000 0.5000000000000000 0.2409839030000000 O

0.5000000000000000 0.0000000000000000 0.2409839030000000 O

0.5000000000000000 0.5000000000000000 0.2409839030000000 O

0.1666666720000000 0.3333333130000000 0.4256826040000000 O

0.1666666720000000 0.8333333130000000 0.4256826040000000 O

0.6666666870000000 0.3333333130000000 0.4256826040000000 O

0.6666666870000000 0.8333333130000000 0.4256826040000000 O

0.3333333130000000 0.1666666720000000 0.5743173360000000 O

0.3333333130000000 0.6666666870000000 0.5743173360000000 O

0.8333333130000000 0.1666666720000000 0.5743173360000000 O

0.8333333130000000 0.6666666870000000 0.5743173360000000 O

0.0000000000000000 0.0000000000000000 0.7590159180000000 O

0.0000000000000000 0.5000000000000000 0.7590159180000000 O

0.5000000000000000 0.0000000000000000 0.7590159180000000 O

0.5000000000000000 0.5000000000000000 0.7590159180000000 O

0.1666666720000000 0.3333333130000000 0.9076505900000000 O

0.1666666720000000 0.8333333130000000 0.9076505900000000 O

0.6666666870000000 0.3333333130000000 0.9076505900000000 O

0.6666666870000000 0.8333333130000000 0.9076505900000000 O

7.1.4.2 Example of INCAR file

ALGO = Fast

EDIFF = 0.0024000000000000002

ENCUT = 520.0

IBRION = 2

ISIF = 3

ISMEAR = -1

ISPIN = 2

KPAR = 4

LASPH = True

LDAU = True

LDAUJ = 0 0 0

LDAUL = 0 2 0

LDAUPRINT = 1

LDAUTYPE = 2

LDAUU = 0 3.32 0

LMAXMIX = 4

LORBIT = 11

LREAL = Auto

LWAVE = False

MAGMOM = 48*0.6

NCORE = 4

NELM = 100

NPAR = 4

NSW = 99

PREC = Accurate

SIGMA = 0.05

7.1.4.3 Example of KPOINT file

pymatgen with grid density = 1916 / number of atoms

0

Gamma

4 4 1

7.2 Appendix for chapter 5

7.2.1 SEM images of the commercial electrodes

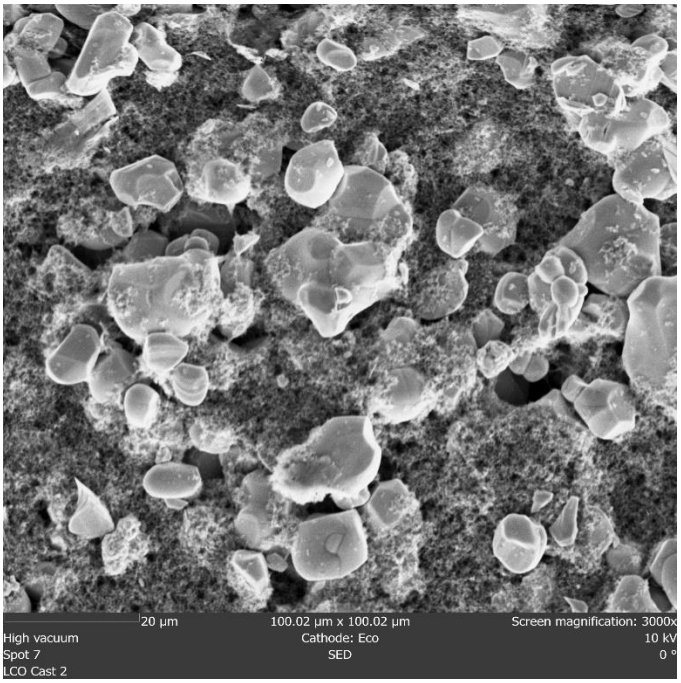


Figure 7-1LiCoO2 electrodes

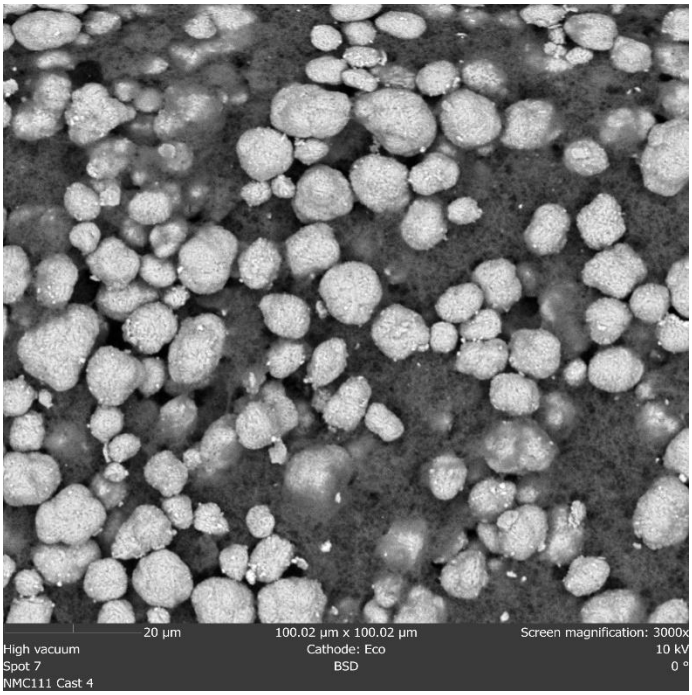


Figure 7-2 NMC111

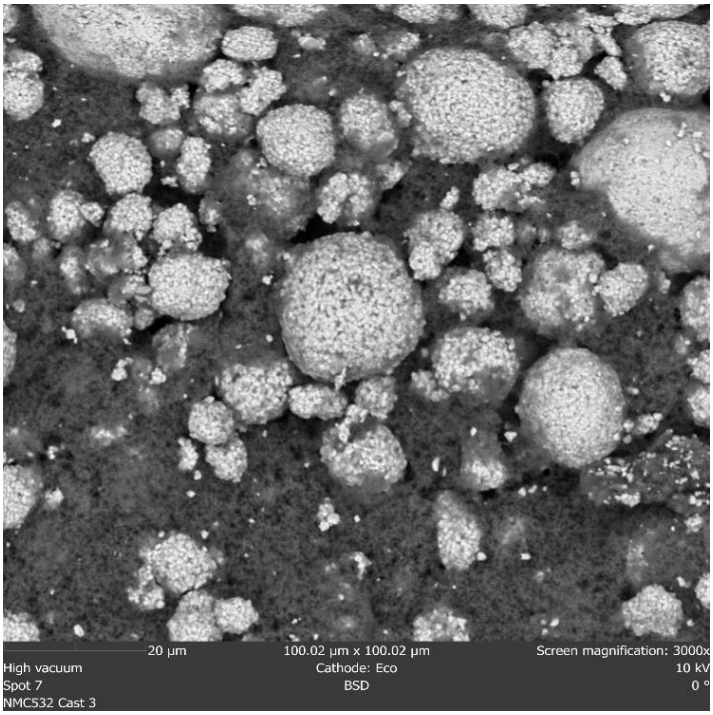


Figure 7-3 NMC532

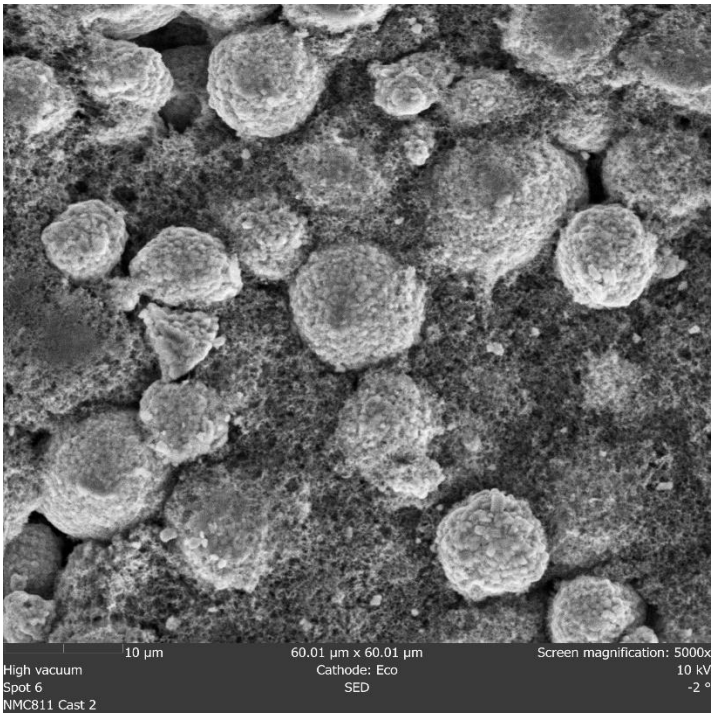


Figure 7-4 NMC811

7.2.2 XRD results of the commercial electrodes

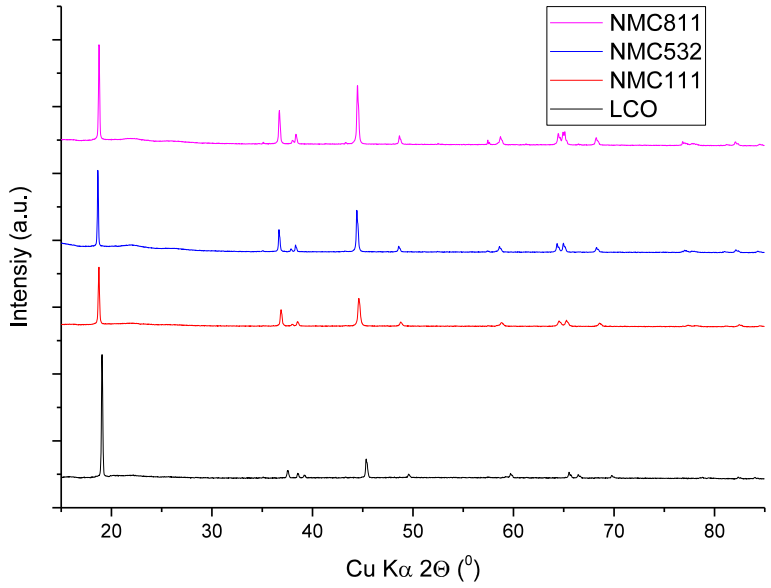


Figure 7-5 XRD of the commercial electrodes